



THE HONG KONG
POLYTECHNIC UNIVERSITY

香港理工大學

Pao Yue-kong Library

包玉剛圖書館

Copyright Undertaking

This thesis is protected by copyright, with all rights reserved.

By reading and using the thesis, the reader understands and agrees to the following terms:

1. The reader will abide by the rules and legal ordinances governing copyright regarding the use of the thesis.
2. The reader will use the thesis for the purpose of research or private study only and not for distribution or further reproduction or any other purpose.
3. The reader agrees to indemnify and hold the University harmless from and against any loss, damage, cost, liability or expenses arising from copyright infringement or unauthorized usage.

If you have reasons to believe that any materials in this thesis are deemed not suitable to be distributed in this form, or a copyright owner having difficulty with the material being included in our database, please contact lbsys@polyu.edu.hk providing details. The Library will look into your claim and consider taking remedial action upon receipt of the written requests.

The Hong Kong Polytechnic University
Department of Mechanical Engineering

Model-Independent Control of A Class of
Uncertain Systems

by

WU Wei

A thesis submitted in partial fulfillment of the requirements
for the degree of
Master of Philosophy

August 2005



Pao Yue-kong Library
PolyU · Hong Kong

CERTIFICATE OF ORIGINALITY

I hereby declare that this thesis is my own work and that, to the best of my knowledge and belief, it reproduces no material previously published or written, nor material that has been accepted for the award of any other degree or diploma, except where due acknowledgment has been made in the text.

_____(Signed)

Wu Wei _____(Name of student)

ABSTRACT

This research aims to develop a new control approach for a class of uncertain systems. Despite intensive research efforts of many researchers, system uncertainty in model parameters is still an existing problem in controller design. It is necessary to carry out research for a new controller, which is able to keep a stable closed-loop system and optimize the performance while requiring plant information as little as possible.

The new control scheme is inspired by the idea of a PID self-tuning controller in the literature, which is able to maintain stable closed-loop regulation for a linear time invariant (LTI) system subject to unanticipated jumps of plant parameters and external disturbances. The controller depends on an assumption that the plant is open-loop stable with a full-row rank for the DC-feedback gain. The plant parameters are not required in the controller design. In this work, an extended high-order self-tuning controller is developed based on the same technique. Two typical versions are studied rigorously. One is called multi-absorber tuning control, which extends PID control by adding multiple resonator-absorbers. The other is called tuning control with a pseudo observer, which uses filter states to approximate the plant states within a user-defined bandwidth. Besides the stability issue, this work also addresses online optimization of the control performance. When the plant parameters are unknown, adaptive optimal control is the only available option. In this work, the simultaneous perturbation method (SPM) is adopted as an additional method to optimize the controller when the plant parameters are unknown. The integration of the stabilization algorithm and optimization control without plant parameters is the main contribution of this work, since this integration forms an independent

module that is suitable to collaborate with any other available adaptive methods.

The proposed control scheme is tested in both simulation and experimental examples. As far as simulation is concerned, within the assumption, all testing plant models are selected arbitrarily for the purpose of testing the controllers without knowing plant parameters. As for experiment, the control problem of flow induced vibration is used to test the practical applicability of proposed control method. The improved results in each example show the validation of the new control scheme.

When studying the control example of flow induced vibration, this work also makes contributions on the understanding of coupled dynamics between flow vortex shedding and structure motion. At the preliminary stage, traditional model-independent methods are tested, such as resonator and variable structure control. However, the performance of these schemes is not effective enough. Besides the above-mentioned new controller, another control scheme is found to be effective, which uses a phenomenological low-order vortex oscillating model as guidance. The key idea is to effectively increase the nonlinear damping term in the model. A new multi-frequency perturbation method is developed, which is unique among all present control laws in fluid dynamics. Experimental results under resonant wind condition have shown its best performance in reducing flow-induced vibration when compared with other controllers. The robustness under different wind speed conditions has also been studied. All the findings have not only shown the effectiveness of proposed new scheme, but also validated the phenomenological model used to describe the complex interaction between vortex shedding and structure motion.

PUBLICATIONS FROM THE THESIS

- Conference Paper
 - Wu,W., Yuan,J., and Cheng,L. (2005). Self-Tuning Sub-Optimal Control Of Time-Invariant Systems With Bounded Disturbance. *Proceedings of American Control Conference, Portland, OR, pp.876-882.*
 - Wu,W., Yuan,J., and Cheng, L. (2005). A Feedback Control Scheme Of Flow-Induced Vibration From A High-Frequency Perturbation Approach. *Symposium on Flows, Structural Vibration, Their Interactions and Control, Guelph, Canada, July 29-31, 2005.* (Also to appear in *Dynamics of Continuous, Discrete and Impulsive Systems, Series A, special volume*)
- Journal Paper
 - Wu,W., Yuan,J., and Cheng,L. (2005). An Extra Stabilization Module For Optimal Control of Uncertain Linear Systems. *Automatica, under review.*

ACKNOWLEDGMENTS

I would like to express my deepest gratitude to Dr. Yuan Jing and Prof. Cheng Li, who served as my chief supervisor and co-supervisor during last two years. Without their great enthusiasm, insightful advice, and respectable patience, this research work could not be achieved. Certainly, the gratitude should also be delivered to the researchers, whose literature inspires me for creative ideas.

Also, my sincere thanks are deserved for my colleagues: Mr.J.C.Hu, Mr.J.F.Huang, Dr.X.Q.Wang, Dr.S.J.Xu, and Dr.M.M.Zhang. Thanks for their kind and patient help with research problems and experiment.

Besides, I wish to acknowledge Hong Kong polytechnic University and Department of Mechanical Engineering for the financial support to me in the form of research studentship and conference funding.

Last but not least, my grateful thanks are dedicated to my family and my girlfriend, for their endless love and support during my research study.

List of Figures

1.1	Two typical adaptive control systems, \hat{a} is estimated parameters	2
1.2	Phase-plane portraits of variable structures	5
1.3	Proposed control scheme	11
1.4	Self-tuning optimal control scheme	14
1.5	The layout of control technique (Cheng et al., 2003)	15
1.6	Concept of flow induced vibration control	15
2.1	Scheme of PID controller	19
2.2	Block interval and sampling interval	32
2.3	An example of ordinary control loop with both disturbance and ref- erence signals	40
2.4	Optimizing PID tuning: trajectory tracking comparison	41
2.5	Optimizing PID tuning: Bode diagram comparison	42
2.6	Optimizing tuning control with pseudo-observer: trajectory tracking comparison	43
2.7	Optimizing tuning control with pseudo-observer: Bode diagram com- parison	43
2.8	Optimizing nonminimum-phase plant control: initial 20s	44
2.9	Optimizing nonminimum-phase plant control: after tuning	45
3.1	Model of cylinder vibration and wake oscillator for FIV	47
3.2	Open-loop control experiment setup	49
3.3	Power spectrum density plot of wake velocity ($St_p \in [0.07, 2.8]$)	51

3.4	RMS reduction values (percentage): structure velocity and wake velocity	52
3.5	Closed-loop control experiment setup	53
3.6	Block diagram of closed-loop control	55
3.7	Bode diagrams of $P(s)$ by no control and active resonator control	56
3.8	Proposed control method: multi-high-frequency perturbation	56
3.9	Experimental setup for validation of control module: PID tuning case	58
3.10	Power spectrum density of vibration signals for cases of no control, original PID control and proposed PID tuning control	59
3.11	Experimental setup for PIV measurement	60
3.12	Technique outline of cross-correlation	61
3.13	Experimental results of structure vibration by no control and variable structure control	63
3.14	Contour of spanwise vorticity from PIV measurement: without control, "-" positive, "--" negative	64
3.15	Contour of spanwise vorticity from PIV measurement: with variable structure control, "-" positive, "--" negative	64
3.16	Experimental results of structure vibration by no control and active resonator control	66
3.17	Contour of spanwise vorticity from PIV measurement: with active resonator control, "-" positive, "--" negative	67
3.18	k_D effect on control performance with $St_\omega = 0.02$ and $b = 0.095$: RMS reduction values (percentage)	68
3.19	ω effect on control performance with $k_D = 3500$ and $b = 0.095$: RMS reduction values (percentage)	68

3.20	b effect on control performance with $k_D = 3500$ and $St_\omega = 0.02$: RMS reduction values (percentage)	69
3.21	Experimental results of structure vibration by no control and proposed control	70
3.22	Contour of spanwise vorticity from PIV measurement: with multi-high-frequency perturbation method, "-" positive, "--" negative . .	71
3.23	Power Spectrum Density (PSD) comparison of structure vibration under conditions without control and with proposed control (Re=1000)	71
3.24	Power Spectrum Density (PSD) comparison of structure vibration under conditions without control and with proposed control (Re=2500)	72
3.25	Power Spectrum Density (PSD) comparison of structure vibration under conditions without control and with proposed control (Re=3400)	72
3.26	Power Spectrum Density (PSD) comparison of structure vibration under conditions without control and with proposed control (Re=4100)	73
3.27	Contours of spanwise vorticity from PIV measurement, "-" positive, "--" negative (Re=1000)	75
3.28	Contours of spanwise vorticity from PIV measurement, "-" positive, "--" negative (Re=2500)	76
3.29	Contours of spanwise vorticity from PIV measurement, "-" positive, "--" negative (Re=3400)	77
3.30	Contours of spanwise vorticity from PIV measurement, "-" positive, "--" negative (Re=4100)	78

Contents

1	INTRODUCTION	1
1.1	Adaptive Control Motif	1
1.1.1	Background	2
1.1.2	Model-Independent Motivation	6
1.2	Flow-Induced Vibration (FIV) Control	8
1.3	Problem Statement	9
1.3.1	Model-Independent Control Module	10
1.3.2	FIV Control Implementation	14
1.4	Outline of Thesis	15
2	CONTROL MODULE DESIGN	17
2.1	Stabilization Mechanism Design	17
2.1.1	Singular Perturbation Technique	17
2.1.2	PID Extended Tuning Controller	19
2.1.3	Tuning Controller with a Pseudo Observer	28
2.1.4	Generalized Tuning Controller	30
2.2	Optimization Mechanism Design	31
2.2.1	Simultaneous Perturbation Gradient Searching	31
2.2.2	Optimization on PID and its Extended Tuning Controllers	34
2.2.3	Optimization on Tuning Controller with a Pseudo Observer	35
2.2.4	Comparison with H_2 Control	39
2.3	Simulation Validation of Control Module	40

2.3.1	PID Tuning	41
2.3.2	Pseudo Observer Tuning	41
3	CASE STUDY: FLOW-INDUCED VIBRATION	46
3.1	Preliminary Study	46
3.1.1	Phenomenological Model	47
3.1.2	Pre-design: High Frequency Perturbation Effect	48
3.2	Active Control	53
3.2.1	Traditional Control Methods	53
3.2.2	Proposed Control Method: multi-high-frequency perturbation	55
3.3	Experimental Validation	57
3.3.1	FIV Control by Control Module: PID Tuning	57
3.3.2	FIV and Vortex Control by Traditional Methods	58
3.3.3	Multi-High-Frequency Perturbation Method	65
4	CONCLUSIONS AND FUTURE WORKS	79
4.1	Controller Development	79
4.1.1	Self-Tuning Design	79
4.1.2	High-Frequency Perturbation Effect	80
4.2	Design Rationale: one useful 'model'	80
4.3	Comments on Future Works	81

CHAPTER 1

INTRODUCTION

The collaboration of multidisciplinary areas has brought control and optimization efforts on related research activities to an increasingly complex level, which emerges from the enhancement of more unknown factors in system models. Conventionally, effectiveness of controller design depends on the availability of plant information beforehand. However, in most practical cases, a perfectly matching model can rarely be constructed as a result of the lack of cognition ability for human beings. In such cases, some model-dependent design schemes may not be applicable, and meanwhile, some efforts should be made on the condition of the information scarcity of plant dynamics.

1.1 Adaptive Control Motif

It is a challenge to design and implement a stable controller when the plant parameters are not fully available. Åström and Haggund (1984) first gave the automatic tuning method for adaptive control of LTI plants. Petersen (1987) proposed a Riccati approach for linear systems with time-varying-but-bounded uncertainties in system state equations, which requires the availability of plant states. Yeh and Youcef-Toumi (1995) designed an adaptation law by using Taylor's expansion for the local expansion of nonlinear systems to cancel the uncertain vector in the state-equation and ensure controlled state to follow the reference trajectory. Adaptive control has

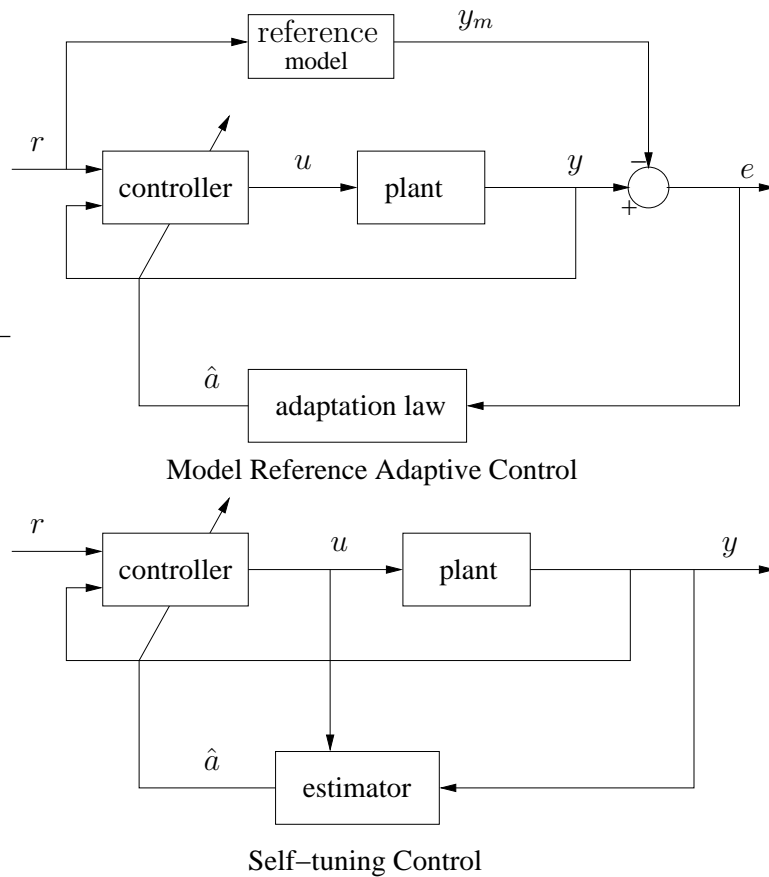


Figure 1.1: Two typical adaptive control systems, \hat{a} is estimated parameters

been proven a very effective method to control uncertain or time varying plants, whose basic idea is to estimate uncertain system parameters online based on measured signals and then use this estimation to calculate controller input parameters. Figure 1.1 shows two typical kinds of adaptive control schemes.

1.1.1 Background

Research in adaptive control started in the early 1950's in connection with the design of autopilots for high-performance aircraft, which operate at a wide range of speeds and altitudes and thus experience large parameter variations (Slotine and Li, 1991). Unfortunately, credit in this subject soon diminished due to the lack of sights and the crash of test flight. Nevertheless, the development of adaptive control theory has never been stalled. With the increasing matureness of control theory during last

decade, various tools have been explored for adaptive control purpose.

One popular design tool is called *adaptive backstepping*, which is developed by Ioannis Kanellakopoulos in collaboration with Petar Kokotović and further improved by Miroslav Krstić with the invention of *tuning functions* (Krstić et al., 1995). Considering a third order pure-feedback system with unknown parameters θ ,

$$\begin{aligned} \dot{x}_1 &= x_2 + \varphi_1^T(x_1, x_2)\theta \\ \dot{x}_2 &= x_3 + \varphi_2^T(x_1, x_2, x_3)\theta \\ \dot{x}_3 &= u + \varphi_3^T(x_1, x_2, x_3)\theta, \end{aligned} \tag{1.1}$$

the idea of backstepping is to design a controller recursively by recognizing some of the state variables as 'virtual controls'. For instance, the first step is to design intermediate control law of first equation of (1.1) and its virtual control is x_2 . Since θ is unknown, this can be solved with an adaptive controller consisting of the control law $\alpha_1(x_1)$ and the update law $\dot{\hat{\theta}} = \tau(x_1)$ from Lyapunov-based design. Then, the first two equations of (1.1) are considered, and at this time x_3 is virtual control. Adaptive backstepping treats θ in the second equation of (1.1) as a new parameter and gives another new estimate with another new update law, which causes the *overparametrization*. This can also be avoided if $\dot{\hat{\theta}} = \tau(x_1)$ in the first step is considered as a function $\tau(x_1)$ rather than an update law. Thus, tuning function is used in subsequent steps to compensate $\dot{\hat{\theta}} - \tau(x_1)$. Whenever $\ddot{\hat{\theta}}$ appears in the next step, it will be replaced by the first derivative of $\tau(x_1)$.

In virtue of backstepping's simplicity and flexibility, many research works have been carried out on its applications and improvement. One prerequisite by Krstić et al. (1995) is that the controlled linearizable system must be transformable into a specified pure feedback form. Wu and Chou (1999) developed a recursive control design method based on backstepping, which does not have previous requirement but

needs a new restrictive condition with a constant relative degree. Furthermore, they combined the feedforward control scheme with the backstepping design in order to prevent unbounded signals due to parameter estimation and ensure solution's feasibility. Kim and Kim (2003) analyzed the tracking function selecting problem of backstepping design procedure for slew maneuver control. Their proposed method using nonlinear tracking function reduces both the settling time and the peak control torque simultaneously, compared with traditional controller with linear tracking function. Recently, the backstepping design method has also been combined with other control methods in practice. Benaskeur and Desbiens (2002) made some efforts on using backstepping algorithm to design robust adaptive PID controller. Stotsky et al. (1997) simplified backstepping control by sliding modes. Wai et al. (2002); Lin et al. (2002) also described backstepping's combinations with fuzzy control and neural network technique.

As mentioned above, another famous control method for uncertain systems is called variable structure control (or called sliding mode control), which is first introduced in Vadim I.Utkin's discontinuous control systems (Utkin, 1992). The variable structure system is such a dynamic system whose structure changes according to the current value of its state. It can be viewed as a system composed of independent structures together with a switching logic between each structure. With appropriate switching logic, a variable structure system can exploit the desirable properties such that any original structure of the system does not own. For instance, considering a dynamic model

$$\begin{aligned} \dot{x}_1 &= x_2 \\ \dot{x}_2 &= -ux_1, \end{aligned} \tag{1.2}$$

there are two structures with $u = 1/a$ and $u = a$, where a is positive. The phase-

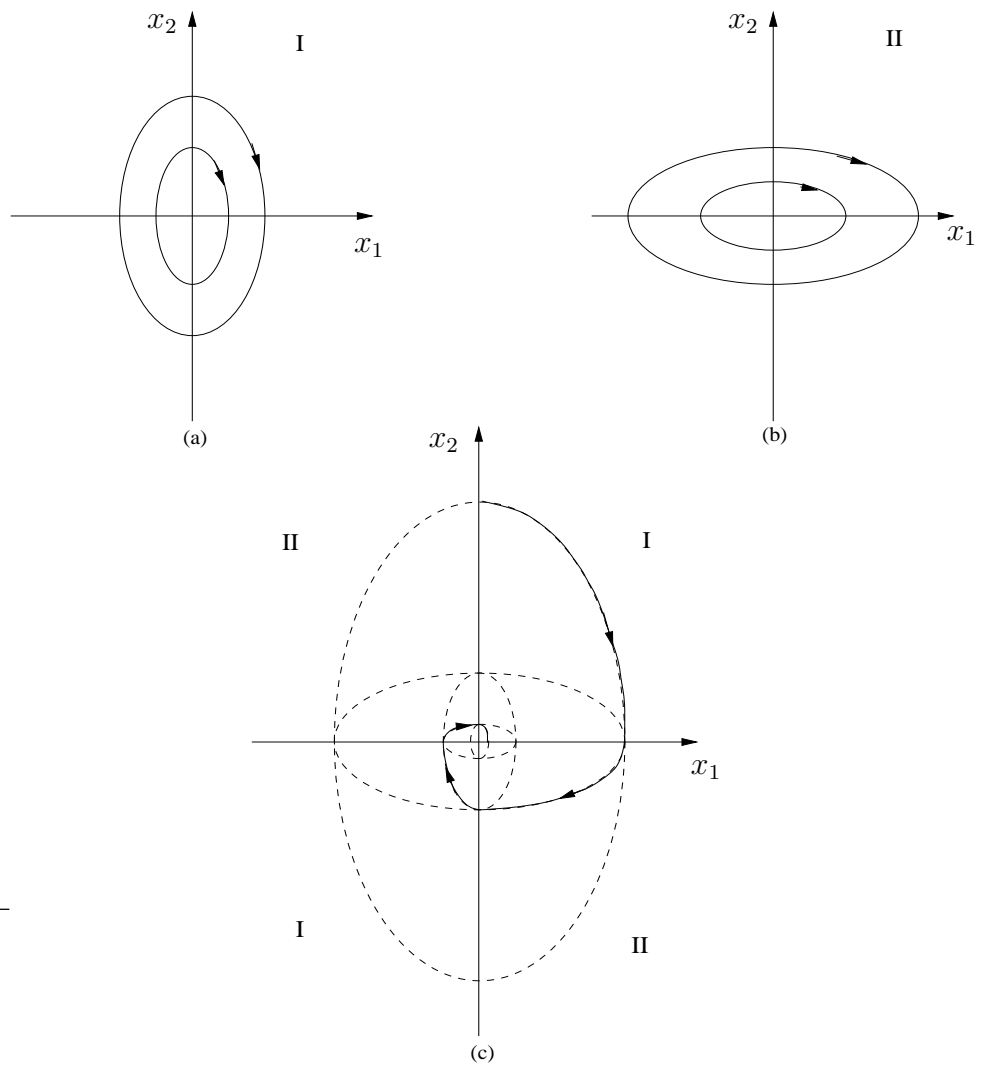


Figure 1.2: Phase-plane portraits of variable structures

plane portraits of individual structure are shown in Figure 1.2 (a) and (b). Obviously, neither of them are asymptotically stable but only stable. However, if a is chosen as

$$u = \begin{cases} 1/a & \text{if } x_1x_2 < 0 \\ a & \text{if } x_1x_2 > 0, \end{cases} \quad (1.3)$$

the system's trajectory will be changed to be asymptotically stable as shown in Figure 1.2 (c). Because of this interesting property, variable structure control has been used in lots of applications to decouple complicated system dynamics. Park et al. (2001) proposed the sliding mode controller with perturbation observer for a 6-DOF parallel manipulator. In order to ensure estimation errors' convergence, a fuzzy adaptive network was also combined with the Lyapunov-based sliding mode design. Park and Tsuji (1999) studied a terminal sliding mode control scheme for second-order nonlinear uncertain systems.

Indeed, there also exists other various adaptive control design schemes. Taking PID control as an example, Ho et al. (2003) proposed a relay auto-tuning scheme with specified bandwidth and phase margin, whose main idea results from iterative feedback tuning. Due to two specifications, only two of the three PID parameters (P, I) can be tuned independently. Having applied the similar preload relay in series with a PID controller, Tan et al. (2002) studied the robustness of their proposed tuning algorithm, which changed all three parameters of PID. Furthermore, Chang et al. (2002) described another PID online updating method for a class of nonlinear systems. The stability of closed-loop PID control system is guaranteed by using Lyapunov approach with a supervisory control and a modified adaptation law with projection.

1.1.2 Model-Independent Motivation

Available adaptive controllers may be generally divided into two groups: the direct and indirect approaches. A common feature of direct adaptive controllers is the use of some closed-loop poles to cancel plant zeros (Feuer and Morse, 1978), which is only applicable to minimum-phase plants. Indirect adaptive control is not subject to such a limitation and the control law may be optimized according to online identification results. These features are favored in many practical applications (Costa et al., 1999; Milliken et al., 1999; Kawamura et al., 2004). A drawback of the indirect adaptive control, however, is its heavy dependence on an adaptive model obtained by online identification. The accuracy of the adaptive model may be poor in at least three situations:

- an initial period before the convergence of the adaptive model;
- a period immediately after an unanticipated jump of plant parameters;
- the disturbance exceeds an unpredictable tolerance level.

Since these situations depend more on plant structures and noise levels than on identification algorithms, it is more reliable to introduce an extra stabilization control module for indirect adaptive controllers in case online identification is inaccurate.

The approach of this research work is based on the second type of adaptive control scheme in Figure 1.1. A PID self-tuning controller, proposed by Chang and Davison (2003), is able to guarantee stable closed-loop regulation while requiring neither information on the plant model nor online identification. It can be improved substantially to a general n -th order switching controller with an additional online optimization mechanism (Wu et al., 2005). The n -th order switching controller does

not require model information nor online identification to achieve sub-optimal control performance. This important feature is used to compensate for the weakness of indirect adaptive controllers in case of poor identification results. A new control scheme therefore has been developed here to combine this switching controller with an indirect adaptive controller and achieve optimal linear quadratic control performance.

1.2 Flow-Induced Vibration (FIV) Control

Flow-induced vibration (FIV) has been regarded as an interesting research topic because of its significant interest in engineering applications, such as construction of bridges and skyscrapers in civil engineering, design of oil-supplier tubes in ocean engineering, and design of aircrafts and land vehicles in mechanical engineering. Numerous fundamental research results on FIV have been reported, which can be found from the comprehensive reviews of Sarpkaya (1979); Bearman (1984); Blevins (1990); Williamson and Govardhan (2004). Moreover, the development of control technique for suppressing FIV has also attracted attentions from many researchers. In order to suppress both vortex shedding and structure vibration, active control method may be adopted due to its effective applicability. Acoustic excitation (Peterka and Richardson, 1969; Hsiao et al., 1990; Liu and Brodie, 2000) and rotational oscillating cylinder (Berger, 1967; Warui and Fujisawa, 1996; Fujisawa et al., 2001) are recognized as precursory methods for active flow control. Recently, Cheng et al. (2003) have developed a novel perturbation technique using embedded piezoelectric actuators for elastically mounted cylinder, which is able to decouple the interaction between flow and structure. Zhang et al. (2003) further extend the idea to feedback control using a PID controller.

As mentioned before, in order to design a stable and effective controller, a dynamic model should be available. There are several analytical works on control problems with regard to the typical Navier-Stokes equation in fluid dynamics field (Bands and Ito, 1994; Christofides and Armaou, 1998; Min and Choi, 1999; Agrachev and Sarychev, 2003). However, for FIV, the full enclosure of model requires the full solution of Navier-Stokes equations with a moving structure as boundary conditions. Although the development of computing technology brings the possibility to direct numerical simulation (DNS) of fluid dynamics, DNS is still a painstaking and compensating computational task that is not suitable for real-time control applications. The search for a simple but representative model for FIV was quite popular in the 1970s (Sarpkaya, 1979). A phenomenological model based on a wake oscillator idea (Bishop and Hassan, 1964) is commonly adopted. The van der pol equation is first introduced by Hartlen and Currie (1970) to represent the wake oscillator. The idea is improved by several researchers later (Skop and Griffin, 1973; Iwan and Blevins, 1974; Skop and Balasubramanian, 1997; Krenk and Nielsen, 1999; Facchinetti et al., 2004). Unfortunately, considering the difficulty of identifying all unknown properties of FIV, most available models are based on a qualitative perception. There has been a lack of a satisfactory FIV model for controller design. Consequently, there is seldom research work employing available models for practical real-time control purpose.

The challenge of active control is due to insufficient knowledge of the FIV model. This research work takes this difficult problem as a testing example for model-independent control scheme developed in the project. Furthermore, according to the model available in the literature, another feedback closed-loop control scheme is proposed by using high frequency perturbations. It is the first attempt to link

a qualitatively developed model to practical controller design for FIV. Since the model is not physically developed, such an additional controller is also regarded as model-independent according to the traditional meaning of plant dynamic model.

1.3 Problem Statement

Due to the collective efforts of numerous researchers, the automatic control theory has been impressively developed to propose a wide coverage of solutions to many applications in books and scientific journals. Considering the practical procedures to implement the control application (Emelyanov and Korovin, 2000),

- the elaboration of a mathematical model of an object
- the investigation and identification of the model parameters
- the formulation of requirements to the properties of the system
- the choice of the law of control and performance of imitation experiment
- the technological realization of the system and the conduction of a natural or seminatural experiment
- the adjustment of the system

however, we must realize that each step requires creative efforts and most of them involve uncertain characters. Therefore, this work mainly makes contributions on the development of the control module design for the model-independent problem. It should also be noticed that plant parameters are only used in the stability analysis but not in any controller parameters. Moreover, flow-induced vibration (FIV) control is used as the experimental object.

1.3.1 Model-Independent Control Module

In modern control theory, a generalized plant is mathematically described by a state-space model,

$$\begin{aligned} \dot{x} &= Ax + Bu + Ew \\ y &= Cx + Fw \\ e &= y_{ref} - y \end{aligned} \tag{1.4}$$

where $x \in \mathbb{R}^n$ is the state, $w \in \mathbb{R}^r$ is disturbance, $u \in \mathbb{R}^m$ is the control signal, $e \in \mathbb{R}^q$ is the error between reference $y_{ref} \in \mathbb{R}^q$ and plant output $y \in \mathbb{R}^q$. Both w and y_{ref} are bounded signals. A , B , C , E , and F are parameter matrices of the plant model. The exact values of these matrices are not available in many practical applications. The common objective is to design a feedback control device given by

$$\begin{aligned} \dot{\phi} &= A_u \phi + B_u e \\ u &= C_u \phi + D_u e \end{aligned} \tag{1.5}$$

where $\phi \in \mathbb{R}^j$ is the controller state, A_u , B_u , C_u , and D_u are parameter matrices of the controller. The controller must stabilize the closed-loop system and provide optimal control performance. The focus of this thesis is how to design A_u , B_u , C_u and D_u without the parameter knowledge of A , B , C , E and F . Taking account of plant uncertainty and disturbance, a new control scheme (as in Figure 1.3) is introduced in this work.

In control practice, when plant model parameter matrices A , B , C , E and F are unknown, a proper online identification algorithm can be applied to estimate A , B and C from the feedback signal y and control input u . In Figure 1.3, the time scale is divided into consecutive epochs. Depending on the accuracy of online identification, each epoch has three or two time slots with equal durations. These time slots are

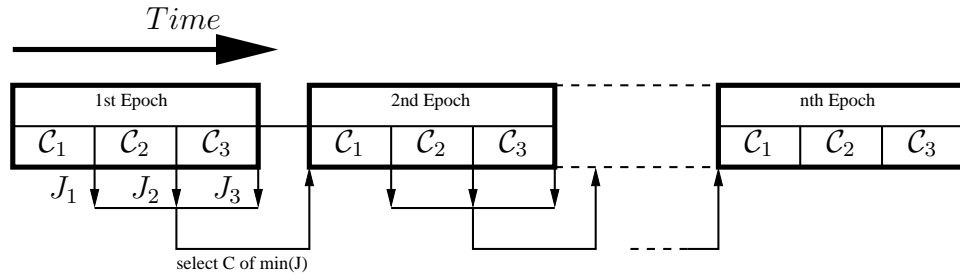


Figure 1.3: Proposed control scheme

allocated to controllers \mathcal{C}_1 , \mathcal{C}_2 and, optionally, \mathcal{C}_3 respectively. The performance of controller \mathcal{C}_i is numerically evaluated by an index function J_i . A possible J_i is the cost function, used in linear quadratic control, obtained by numerical integration over time slot i , i.e. $\lim_{T \rightarrow \infty} E \left\{ \frac{1}{T} \int_0^T e^{T-t} e^T dt \right\}$. At the end of an epoch, the controllers are compared in terms of J_i and the best controller is chosen to be controller \mathcal{C}_1 in the next epoch.

In the first epoch, the controller has minimum plant information compared with other time epochs. A new switching controller is chosen to be \mathcal{C}_1 . This controller is able to stabilize the closed-loop quickly without depending on the plant model or identification results, as to be detailed in section 2.1 of Chapter 2. Besides the first epoch, there are inevitable worst cases when controllers in other epochs may be unstable due to the inaccurate identification results or unanticipated parameter jumps in the plant. The new switching controller will be \mathcal{C}_1 in all worst cases to stabilize the closed-loop quickly. Controller \mathcal{C}_2 is always a randomly-perturbed version of \mathcal{C}_1 in each epoch. The random perturbation is intended to optimize the control performance without online identification, which will be explained in section 2.2 of Chapter 2. Controller \mathcal{C}_3 can be an indirect adaptive controller since the plant may be non-minimum-phase and optimal control performance is expected. This controller depends on an adaptive model available by online identification. It consists of an observer and a state-feedback gain solved from the algebraic Riccati

equation. The observer is open-loop stable if the adaptive model is accurate enough. Although controller \mathcal{C}_3 is allocated to time slot 3, its observer is always tested. If the observer error diverges, it indicates an inaccurate adaptive model and the corresponding epoch only has two time slots for \mathcal{C}_1 and \mathcal{C}_2 . If the observer error of \mathcal{C}_3 converges to a small level, the corresponding epoch will have three time slots for \mathcal{C}_1 , \mathcal{C}_2 and \mathcal{C}_3 respectively. As long as the adaptive model is accurate enough in one epoch, controller \mathcal{C}_3 will be optimal and then become controller \mathcal{C}_1 in the following epochs until the next unanticipated jump of plant parameters.

The stabilization mechanism is always on alert in case of unanticipated jumps of plant parameters as explained in Chang and Davison (2003). Another reason for the stabilization mechanism is the possibility of inaccurate online identification due to an excessive but still bounded disturbance w . Available identification algorithms may tolerate small levels of disturbance w . The exact tolerance level, however, is unknown since it depends more on plant structures than on identification algorithms. Even when the observer error of controller \mathcal{C}_3 converges in open-loop tests, there is still no guarantee that \mathcal{C}_3 will be stable in the closed-loop. It is important to stabilize the closed-loop quickly in case of inaccurate identification results. This is made possible by improving the PID self-tuning controller (Chang and Davison, 2003) to n -th order switching controllers. The stabilization mechanism works if both (1.4) and (1.5) are open-loop stable. This is not a problem because the observer of \mathcal{C}_3 must be stable before \mathcal{C}_3 is allocated a time slot. The worst case controller \mathcal{C}_1 is also open-loop stable to be explained in section 2.1 of Chapter 2.

Since the control module does not need online identification, the stability requirement on the adaptive controller is relaxed significantly. The new control scheme works even in the worst case when the adaptive model never converges due to a

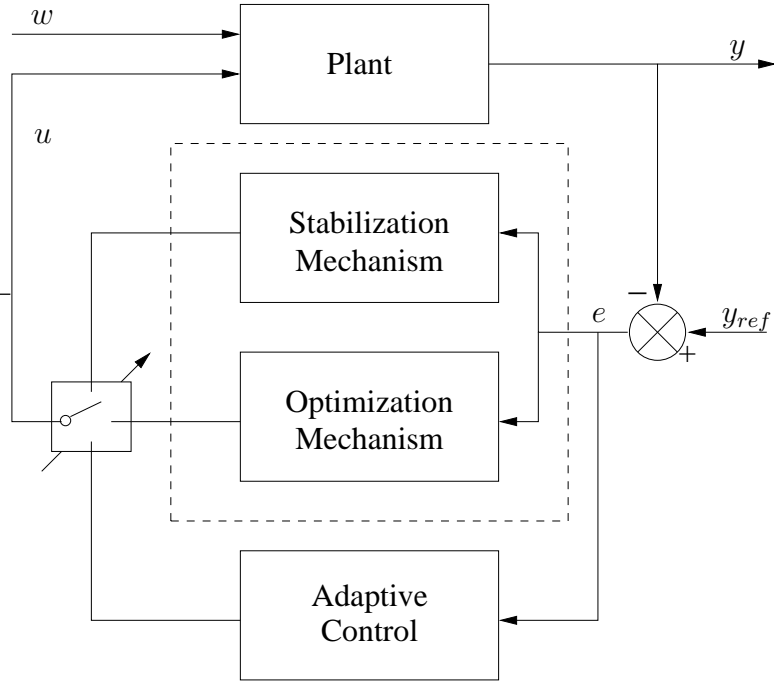


Figure 1.4: Self-tuning optimal control scheme

severe disturbance w and a sensitive plant structure. In that case, all epochs will have two time slots for \mathcal{C}_1 and \mathcal{C}_2 only. For best focus, this study only concentrates on the design of \mathcal{C}_1 and \mathcal{C}_2 . Figure 1.4 shows the functional block diagram of the new control scheme, in which the stabilization module is in the dash-line block.

Before going further, we need to make following general assumptions as discussed by Chang and Davison (2003).

(A1) Plant (1.4) is open-loop stable, which implies the invertibility of A .

(A2) DC steady-state gain matrix $\mathcal{T} = -CA^{-1}B$ has full-row rank q and $m \geq q$, which implies the existence of solution $-\mathcal{T}K$, where $K \in \mathbb{R}^{m \times q}$.

These assumptions match the practical situations for the design of active controller of many engineering applications, such as control of electro-servomechanism system, and the flow-induced vibration.

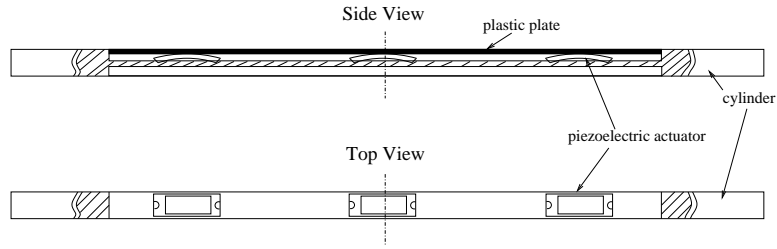


Figure 1.5: The layout of control technique (Cheng et al., 2003)

1.3.2 FIV Control Implementation

Considering a typical FIV phenomenon, when flow is passing through immersed body, the vortex shedding is formed in the wake and excites the body to vibrate. The motion of the body will further affect vortex, and in turn the force acting on the body itself. Especially, when vortex shedding frequency lies in certain range near the resonant frequency of body structure, energy in both wake and structure vibration will be magnified. This phenomenon usually occurs at the *lock-in* regime. An elastically mounted square cylinder immersed in a closed-loop wind tunnel is used as the testing object, to which case the perturbation technique of Cheng et al. (2003) is also applicable here with some newly developed controllers. The upper surface of the cylinder is movable and driven by embedded piezoelectric actuators, which is shown in Figure 1.5. The surface motion transfers control actions to the FIV system, which creates local perturbation on the flow around cylinder. Figure 1.6 shows the concept of FIV control, where M_s is upper slide mass and M_c is cylinder mass. The objective is to suppress both structure vibration and wake vortex shedding at lock-in regime by applying effective control methods. Due to modeling difficulty for real-time use of control design for FIV as introduced in section 1.2, model-independent controllers can be considered to achieve the desired objectives. The primary motivation is therefore to prompt the investigation of suitable model-

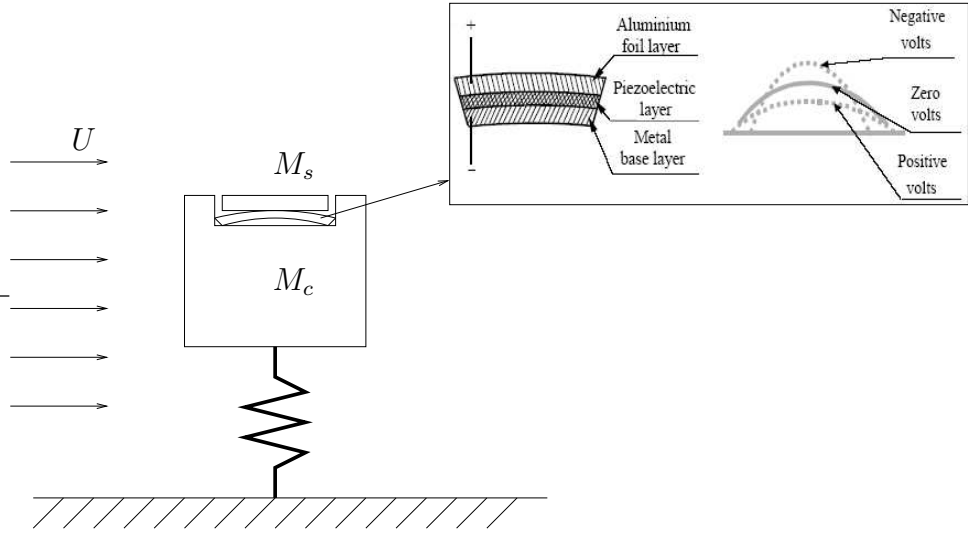


Figure 1.6: Concept of flow induced vibration control

independent control methods that are tested in this practical example.

1.4 Outline of Thesis

This research is carried out in two stages. Basically, it gives the mathematical development of a novel model-independent control module for uncertain systems. Furthermore, due to the uncertain dynamics, experiment of FIV control is adopted as the testing object for the practical validation of developed control module. In addition, several control studies for this practical example are also involved. The organization of this thesis is as follows. Chapter 2 describes the control module design, which consists of the stabilization mechanism design and the optimization mechanism design. Chapter 3 is dedicated to the case study of FIV, which gives preliminary knowledge of its control problem and one additional feedback scheme. Based on the methodologies developed, both simulation and experimental results for specific controllers are shown in respective Chapter. After that, several highlights are drawn and useful comments for future works are addressed in Chapter 4.

CHAPTER 2

CONTROL MODULE DESIGN

2.1 Stabilization Mechanism Design

The first and most important part of the problem is how to stabilize the closed-loop system of plant and controller under disturbance when A , B , C are not available and the adaptive model is inaccurate. The solution of this problem enables the controller to optimize the performance index while maintaining a stable closed-loop. Chang and Davison (2003) propose a self-tuning algorithm for PID 3-term controller. The stability of their algorithm is proven by using singular perturbation method. Inspired from this idea, an extended tuning version is developed by Wu et al. (2005). In this section, based on the work in Wu et al. (2005), we would like to give a broader consideration about the stabilization algorithm design¹. First, a brief introduction of singular perturbation technique is given.

2.1.1 Singular Perturbation Technique

One important tool in the analysis of controller stability is singular perturbation technique, which is commonly used in model reduction for complex dynamics by control engineers. Generally, the plant can be decomposed into two-time-scale systems, a fast manifold and a slow quasi-steady-state, which correspond to extraneous

¹Most technical expressions in this Chapter require the basic knowledge in control engineering, which can be referred to textbook by Ogata (1997).

uncertainties and real plant dynamics respectively. How to achieve a satisfactory degree of robustness and insensitivity to inevitable uncertainties is one application of singular perturbation technique. The detailed analysis of this technique in control can be found in Kokotović et al. (1986). Here, we only apply the technique to the analysis of system eigenvalue properties. Consider the standard singularly perturbed system,

$$\begin{aligned}\dot{x} &= (A_{11} + \varepsilon^{\beta_1} \overline{A_{11}})x + (A_{12} + \varepsilon^{\beta_2} \overline{A_{12}})z \\ \varepsilon \dot{z} &= (A_{21} + \varepsilon^{\beta_3} \overline{A_{21}})x + (A_{22} + \varepsilon^{\beta_4} \overline{A_{22}})z\end{aligned}\tag{2.1}$$

where $\beta_i \geq 1$ are fixed finite constants for $i \in \{1, 2, 3, 4\}$, and $(x, z, \varepsilon) \in \mathbb{R}^{n_1} \times \mathbb{R}^{n_2} \times \mathbb{R}^+$. The first equation represents the slow time-scale system and the second one is for the fast time-scale system. What is the relationship between the eigenvalues for system (2.1) and the small scalar ε ? The following Lemma in Kokotović et al. (1986, p.57) gives the answer.

Lemma 2.1.1. *For the singularly perturbed system (2.1), if A_{22}^{-1} exists, then as $\varepsilon \rightarrow 0$, n_1 eigenvalues of (2.1) tend to $\text{eig}(A_0) := \text{eig}(A_{11} - A_{12}A_{22}^{-1}A_{21})$, while the remaining n_2 eigenvalues of (2.1) tend to infinity, with a rate of $1/\varepsilon$, along the asymptotes defined by $\text{eig}(A_{22})/\varepsilon$.*

It reveals the disjoint of eigenvalues for system (2.1), which are of order $\mathcal{O}(1)$ and $\mathcal{O}(1/\varepsilon)$ respectively. The smaller value of ε gives larger gap between these two sets of eigenvalues. It is an inherent character of singular perturbed system. Furthermore, since eigenvalue is an important indicator of system stability, Lemma 2.1.1 hereby provides a very powerful stability analysis tool. It can be found that there exists an $\varepsilon^* > 0$ such that for $\varepsilon \in (0, \varepsilon^*]$ system (2.1) is asymptotically stable, if $\text{eig}(A_0)$ and $\text{eig}(A_{22}) \subset \mathbb{C}^-$.

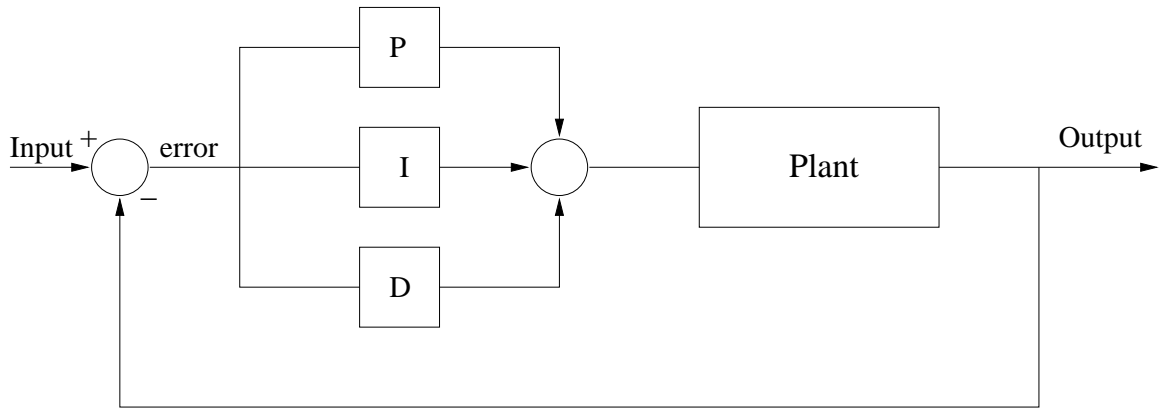


Figure 2.1: Scheme of PID controller

2.1.2 PID Extended Tuning Controller

Brief Introduction to PID Controller

Figure 2.1 shows a PID control of a plant. $P = K_p$ gives a proportion of the system error to the plant, which introduces an offset error. $I = K_i \frac{1}{s}$ accumulates error throughout the control period, which removes the offset given by P action but introduces a phase lag into the plant. $D = K_d s$ describes the rate of error change, which is used to reduce overshoot and introduces a phase lead to remove the phase lag from I action. Usually, in practical implementation, an alternative form of $D = K_d \frac{sN}{s + N}$ is used, where $N \in \mathbb{R}^+$. One typical experimental approach of tuning method is called Ziegler-Nichols rules (Ogata, 1997), which are based on experimental step responses or based on the value of K_p that results in marginal stability when only the proportional control action is used. However, none of them can be designed analytically except manually when system model is not known.

Tuning Method Extended by Multiple 1st Order Terms

There have been a lot of automatic tuning methods for PID in the literature. However, for plant with uncertain parameters, it is a challenge to design a self-tuning

rule for PID to maintain closed-loop stability, especially with disturbance participating. (Chang and Davison, 2003) propose a solution for this problem, however, it cannot provide an optimal solution. It is an intuitive guess that only 3-term low order controller may not be able to achieve high performance when the uncertain plant is a higher order one. As a result, it is desired to have a high order optimizing controller, which is stable when applied to control an uncertain plant with only (A1) and (A2) assumptions made in section 1.3.1.

Inspired from the PID switching idea from Chang and Davison (2003), we consider an extended tuning control as shown in Equation (2.2), where $(\beta_\varepsilon, \beta_\rho, \bar{\varepsilon}_2, N, \bar{\rho}) \in \mathbb{R}^+ \times \mathbb{R}^+ \times \mathbb{R}^+ \times \mathbb{R}^+ \times \mathbb{R}^+$ as fixed constants, $\varepsilon_1 = \varepsilon_0/\tau^k$ with $(\varepsilon_0, k, \tau - 1) \in \mathbb{R}^+ \times \mathbb{Z}^+ \times \mathbb{R}^+$ as tuning function, $K = \bar{k}(k)$ as K tuning function ², $(a_1, a_2, \dots, a_h) \in \mathbb{C}^+$ and $(c_1, c_2, \dots, c_h) = (\bar{c}_1 \varepsilon_1^{\beta_{c_1}+1}, \bar{c}_2 \varepsilon_1^{\beta_{c_2}+1}, \dots, \bar{c}_h \varepsilon_1^{\beta_{c_h}+1}) \in \mathbb{R}$. The updating time for tuning functions is set at the time when u hits the pre-defined input constraint boundary.

$$u(s) = K \left\{ \underbrace{\left[\frac{\varepsilon_1 I}{s} + \bar{\rho} \varepsilon_1^{\beta_\rho+1} I + \bar{\varepsilon}_2 \varepsilon_1^{\beta_\varepsilon+1} \frac{sNI}{s+N} \right]}_{PID \text{ switching}} + \underbrace{\left[\frac{c_1 I}{s+a_1} + \frac{c_2 I}{s+a_2} + \dots + \frac{c_h I}{s+a_h} \right]}_{added \text{ items}} \right\} \times e(s). \quad (2.2)$$

If one a_k is complex number, then another a_{k+1} must exist to act as a conjugate of a_k . The corresponding c_k and c_{k+1} form one conjugate pair. Define the PID control input state as $[\eta^T \ \xi^T]^T$, and the additional state as $\Psi \in \mathbb{R}^h$. The state-space expression for (2.2) can be written as (2.3) in partial diagonal form, which means if a_k and a_{k+1} are complex conjugate with each other, then values $-a_k$ and $-a_{k+1}$ can be replaced by a 2×2 real matrix in the diagonal direction.

²reference (Chang and Davison, 2003, p.1977) gives definitions for tuning and K tuning functions. One example for updating of tuning function, $\varepsilon'_1 = \varepsilon_1/\tau = \varepsilon_0/\tau^{k+1}$.

$$\begin{aligned}
\begin{bmatrix} \dot{\eta} \\ \dot{\xi} \\ \dot{\Psi} \end{bmatrix} &= \begin{bmatrix} 0 & 0 & \vdots & 0 & 0 & \cdots & 0 \\ 0 & -NI & 0 & 0 & \cdots & 0 \\ \hline 0 & 0 & -a_1 & & & 0 \\ 0 & 0 & & -a_2 & & \\ \vdots & \vdots & & & \ddots & \\ 0 & 0 & 0 & & & -a_h \end{bmatrix} \begin{bmatrix} \eta \\ \xi \\ \psi_1 \\ \psi_2 \\ \vdots \\ \psi_h \end{bmatrix} + \begin{bmatrix} \varepsilon_1 I \\ I \\ I \\ I \\ \vdots \\ I \end{bmatrix} e \\
u &= K \begin{bmatrix} 1 & -\bar{\varepsilon}_2 \varepsilon_1^{\beta_\varepsilon+1} N^2 & \vdots & \bar{c}_1 \varepsilon_1^{\beta_{c_1}+1} & \bar{c}_2 \varepsilon_1^{\beta_{c_2}+1} & \cdots & \bar{c}_h \varepsilon_1^{\beta_{c_h}+1} \end{bmatrix} \begin{bmatrix} \eta \\ \xi \\ \vdots \\ \psi_1 \\ \psi_2 \\ \vdots \\ \psi_h \end{bmatrix} \\
&+ \left[K \bar{\rho} \varepsilon_1^{\beta_\rho+1} + K \bar{\varepsilon}_2 \varepsilon_1^{\beta_\varepsilon+1} N \right] e.
\end{aligned} \tag{2.3}$$

Following the same routine as Wu et al. (2005), the closed-loop system described by (1.4) and (2.2) is written as

$$\begin{aligned}
\dot{\tilde{x}} &= \hat{A} \tilde{x} + \hat{B} v \\
\tilde{y} &= \hat{C} \tilde{x} + \hat{D} v,
\end{aligned} \tag{2.4}$$

$$\begin{aligned}
\begin{bmatrix} \hat{A} & \hat{B} \\ \hat{C} & \hat{D} \end{bmatrix} &= \\
\begin{bmatrix} A - (\rho + \varepsilon_2 N) B K C & B K & -\varepsilon_2 N^2 B K & B H K & | & (\rho + \varepsilon_2 N) B K & E - (\rho + \varepsilon_2 N) B K F \\ -\varepsilon_1 C & 0 & 0 & 0 & | & \varepsilon_1 I & -\varepsilon_1 F \\ -C & 0 & -NI & 0 & | & I & -F \\ -GC & 0 & 0 & -\Omega & | & G & -GF \\ \hline C & 0 & 0 & 0 & | & 0 & F \\ -(\rho + \varepsilon_2 N) K C & K & -\varepsilon_2 N^2 K & H K & | & (\rho + \varepsilon_2 N) K & -(\rho + \varepsilon_2 N) K F \end{bmatrix}
\end{aligned} \tag{2.4a}$$

where $\tilde{x} = [x^T \ \eta^T \ \xi^T \ \Phi^T]^T$, $v = [y_{ref}^T \ w^T]^T$, $\hat{y} = [y^T \ u^T]^T$, $\Omega = \text{diag}\{a_1, a_2, \dots, a_h\}$, $G = [I, I, \dots, I]^T$, $H = [\bar{c}_1 \varepsilon_1^{\beta_{c_1}+1}, \bar{c}_2 \varepsilon_1^{\beta_{c_2}+1}, \dots, \bar{c}_h \varepsilon_1^{\beta_{c_h}+1}]$, $(\rho, \varepsilon_2) = (\bar{\rho} \varepsilon_1^{\beta_\rho+1}, \bar{\varepsilon}_2 \varepsilon_1^{\beta_\varepsilon+1})$.

Now, we apply Lemma 2.1.1 to prove the following Theorem of stability condition of closed-loop system (2.4).

Theorem 2.1.1. *If plant (1.4) is open-loop stable with $\text{eig}(A) \in \mathbb{C}^-$ and its DC steady-state gain matrix \mathcal{T} has full-row rank, then the extended controller (2.2) guarantees the stability of the closed-loop system (2.4) if ε_1 is sufficiently small.*

Proof. By applying similarity transformation, matrix \hat{A} is rewritten as (2.5).

$$\hat{A}^* = \left[\begin{array}{c|ccc} 0 & -\varepsilon_1 C & 0 & 0 \\ BK & A - (\varepsilon_1^{\beta_\rho+1} \bar{\rho} + \varepsilon_1^{\beta_\varepsilon+1} \bar{\varepsilon}_2 N) BKC & -\varepsilon_1^{\beta_\varepsilon+1} \bar{\varepsilon}_2 N^2 BK & BHK \\ 0 & -C & -NI & 0 \\ 0 & -GC & 0 & -\Omega \end{array} \right]. \quad (2.5)$$

The equivalence of this proof is to verify $\text{eig}(\hat{A}^*/\varepsilon_1) \subset \mathbb{C}^-$. Notice that B is one $m \times 1$ matrix and H is one $1 \times h$ matrix, and for the i -th column of H there is an $\varepsilon_1^{\beta_{c_i}+1}$ control action. Therefore, the resultant matrix for BHK must be a $m \times h$ matrix with the control action $\varepsilon_1^{\beta_{c_i}+1}$ in its i -th column. Let $(bhk)_{ij}$ be element of BHK without the $\varepsilon_1^{\beta_{c_i}+1}$ multiple, then BHK is written as,

$$\begin{bmatrix} \varepsilon_1^{\beta_{c_1}+1} (bhk)_{11} & \varepsilon_1^{\beta_{c_2}+1} (bhk)_{12} & \cdots & \varepsilon_1^{\beta_{c_h}+1} (bhk)_{1h} \\ \varepsilon_1^{\beta_{c_1}+1} (bhk)_{21} & \varepsilon_1^{\beta_{c_2}+1} (bhk)_{22} & \cdots & \varepsilon_1^{\beta_{c_h}+1} (bhk)_{2h} \\ \vdots & \vdots & \ddots & \vdots \\ \varepsilon_1^{\beta_{c_1}+1} (bhk)_{m1} & \varepsilon_1^{\beta_{c_2}+1} (bhk)_{m2} & \cdots & \varepsilon_1^{\beta_{c_h}+1} (bhk)_{mh} \end{bmatrix} \quad (2.6)$$

$$BHK := \left[\begin{array}{ccc} \varepsilon_1^{\beta_{c_1}+1} \overrightarrow{bhk}_1 & \varepsilon_1^{\beta_{c_2}+1} \overrightarrow{bhk}_2 & \cdots & \varepsilon_1^{\beta_{c_h}+1} \overrightarrow{bhk}_h \end{array} \right].$$

Now, we define the following sub-matrix,

$$A_{11} = \begin{bmatrix} 0 \end{bmatrix}, \quad (2.7a)$$

$$A_{12} = - \begin{bmatrix} C & 0 & 0 \end{bmatrix}, \quad (2.7b)$$

$$A_{21} = \begin{bmatrix} BK \\ 0 \\ 0 \end{bmatrix}, \quad (2.7c)$$

$$A_{22} = \begin{bmatrix} A & 0 & 0 \\ -C & -NI & 0 \\ -GC & 0 & -\Omega \end{bmatrix}, \quad (2.7d)$$

$$\overline{A}_{22}^1 = - \begin{bmatrix} -\bar{\rho}BKC & 0 & 0 \\ 0 & 0 & 0 \\ 0 & 0 & 0 \end{bmatrix}, \quad (2.7e)$$

$$\overline{A}_{22}^2 = - \begin{bmatrix} \bar{\varepsilon}_2 NBKC & \bar{\varepsilon}_2 N^2 BK & 0 \\ 0 & 0 & 0 \\ 0 & 0 & 0 \end{bmatrix}, \quad (2.7f)$$

$$\overline{A}_{22}^{h1} = \begin{bmatrix} 0 & 0 & \overrightarrow{bhk_1} & 0 & \cdots & 0 \\ 0 & 0 & 0 & 0 & \cdots & 0 \\ 0 & 0 & 0 & 0 & \cdots & 0 \end{bmatrix}, \quad (2.7h1)$$

$$\overline{A}_{22}^{h2} = \begin{bmatrix} 0 & 0 & 0 & \overrightarrow{bhk_2} & \cdots & 0 \\ 0 & 0 & 0 & 0 & \cdots & 0 \\ 0 & 0 & 0 & 0 & \cdots & 0 \end{bmatrix}, \quad (2.7h2)$$

\vdots

$$\overline{A}_{22}^{hh} = \begin{bmatrix} 0 & 0 & 0 & 0 & \cdots & \overrightarrow{bhk_h} \\ 0 & 0 & 0 & 0 & \cdots & 0 \\ 0 & 0 & 0 & 0 & \cdots & 0 \end{bmatrix}, \quad (2.7hh)$$

$$\begin{bmatrix} A_{11} & & & & & & A_{12} \\ A_{21} & A_{22} + \varepsilon_1^{\beta_\rho+1} \overline{A}_{22}^1 + \varepsilon_1^{\beta_\varepsilon+1} \overline{A}_{22}^2 + \varepsilon_1^{\beta_{c_1}+1} \overline{A}_{22}^{h1} + \varepsilon_1^{\beta_{c_2}+1} \overline{A}_{22}^{h2} + \cdots + \varepsilon_1^{\beta_{c_h}+1} \overline{A}_{22}^{hh} \end{bmatrix}, \quad (2.8)$$

and one singularly perturbed system matrix is written as (2.8). Obviously, from Lemma 2.1.1, the eigenvalues of system (2.8) will tend to

$$\left\{ \frac{eig(A)}{\varepsilon_1} \cup \frac{-N}{\varepsilon_1} \cup \frac{eig(-\Omega)}{\varepsilon_1} \cup eig(-\mathcal{T}K) \right\}.$$

Since $eig(A) \subset \mathbb{C}^-$ and the full-row rank condition of \mathcal{T} are assumed, and for $-\Omega = -diag\{a_1, a_2, \dots, a_h\} \subset \mathbb{C}^-$, the system matrix of (2.8) is stable, which

exactly refers to the stability of \hat{A}^*/ε_1 , e.g. $\text{eig}(\hat{A}^*/\varepsilon_1) \subset \mathbb{C}^-$. Thus, the closed-loop system (2.4) is also stable with $\text{eig}(\hat{A}) \subset \mathbb{C}^-$. \square

According to Theorem 2.1.1, the PID extended tuning controller (2.2) is applicable to system (1.4) as long as tuning function ε_1 is kept in a value-descending tuning direction.

Tuning Method Extended by Multiple 2nd Order Terms (Multi-Absorber Tuning)

Alternatively, 2nd order terms can be used to extend the above tuning controller, which is regarded as absorber tuning and more flexible in design. Here, we explain how 2nd order absorbers can be added in the stabilization algorithm. In order to keep the simplicity in analysis, we neglect differences in tuning parameter assignment for PID terms, i.e. $\beta_\rho = \beta_\varepsilon = \beta - 1$ in (2.2). Consider a transfer function,

$$u(s) = K \begin{bmatrix} \varepsilon_1 F \\ I \end{bmatrix} \begin{bmatrix} sI \\ I \end{bmatrix} (s^2 I + \Omega)^{-1} G_0 + \varepsilon_1^\beta \left(\bar{\rho} + \bar{\varepsilon}_2 \frac{sN}{s+N} \right) I \times e(s) \quad (2.9)$$

where $\beta - 1 \in \mathbb{R}^+$, $\Omega = \text{diag}\{0, \omega_1^2, \dots, \omega_r^2\}$ and $F = [F_0 \quad F_1]$.

Theorem 2.1.2. *If plant (1.4) is under assumptions (A1) and (A2), and $G_0 = D_1 F_1^T$ and $F_0 = D_0 G_0^T$, where D_0 and D_1 are diagonal matrices with positive values, then the extended controller (2.9) guarantees the stability of the closed-loop system (2.4) when ε_1 is sufficiently small.*

Proof. The $\varepsilon_1 F \begin{bmatrix} sI \\ I \end{bmatrix} (s^2 I + \Omega)^{-1} G_0$ term in Equation (2.9) is in fact a set of multiple absorbers. Excluding F , it can be expressed as $\dot{\vartheta} = A_{11}\vartheta + \varepsilon_1 G e = A_{11}\vartheta - \varepsilon_1 G C x +$

$\varepsilon_1 G y_{ref}$, where $\vartheta = [\vartheta_1^T \ \dot{\vartheta}_1^T]^T$, $G = \begin{bmatrix} 0 \\ G_0 \end{bmatrix}$, and $A_{11} = \begin{bmatrix} 0 & I \\ -\Omega & 0 \end{bmatrix}$. The derivative term $\frac{sN}{s+N}$ can be expressed as $\dot{\zeta} = -N\zeta + e = -N\zeta - Cx + y_{ref}$ in state-space form. Thus, control signal u (2.9) is rewritten as

$$u = K \left[F\vartheta - \varepsilon_1^\beta (\bar{\rho} + \bar{\varepsilon}_2 N)y - \varepsilon_1^\beta \bar{\varepsilon}_2 N^2 \zeta + \varepsilon_1^\beta (\bar{\rho} + \bar{\varepsilon}_2 N)y_{ref} \right]. \quad (2.10)$$

Since the reference trajectory y_{ref} and disturbance w are uniformly bounded, the closed-loop system's stability only depends on $\{\vartheta, \zeta, x\}$. To simplify the analysis, let y_{ref} and w be zero, and (2.10) becomes

$$u = K \left[F\vartheta - \varepsilon_1^\beta (\bar{\rho} + \bar{\varepsilon}_2 N)Cx - \varepsilon_1^\beta \bar{\varepsilon}_2 N^2 \zeta \right]. \quad (2.11)$$

We simply substitute equation (2.11) into $\dot{x} = Ax + Bu$ and get

$$\begin{aligned} \dot{\vartheta} &= A'_{11}\vartheta - \varepsilon_1 GCx \\ \dot{\zeta} &= -N\zeta - Cx \\ \dot{x} &= BKF\vartheta + \left[A - \varepsilon_1^\beta (\bar{\rho} + \bar{\varepsilon}_2 N)BKC \right] x - \varepsilon_1^\beta \bar{\varepsilon}_2 N^2 BK\zeta. \end{aligned} \quad (2.12)$$

Again, the problem results in the analysis of the stability of closed-loop system matrix \hat{A} in $\dot{\nu} = \hat{A}\nu$, where $\nu = [\vartheta^T, x^T, \zeta^T]^T$ and

$$\begin{aligned} \hat{A} &= \begin{bmatrix} A'_{11} & -\varepsilon_1 GC & 0 \\ BKF & A - \varepsilon_1^\beta (\bar{\rho} + \bar{\varepsilon}_2 N)BKC & -\varepsilon_1^\beta \bar{\varepsilon}_2 N^2 BK \\ 0 & -C & -NI \end{bmatrix} \\ &= \begin{bmatrix} A'_{11} & \varepsilon_1 A_{12} \\ A_{21} & A_{22} + \varepsilon_1^\beta \overline{A_{22}} \end{bmatrix} \end{aligned} \quad (2.13)$$

with $A'_{11} = \begin{bmatrix} 0 & I \\ -\Omega & 0 \end{bmatrix}$, $A_{12} = [-GC \ 0]$, $A_{21} = \begin{bmatrix} BKF \\ 0 \end{bmatrix}$, $A_{22} = \begin{bmatrix} A & 0 \\ -C & -NI \end{bmatrix}$ and $\overline{A_{22}} = - \begin{bmatrix} (\bar{\rho} + \bar{\varepsilon}_2 N)BKC & \bar{\varepsilon}_2 N^2 BK \\ 0 & 0 \end{bmatrix}$. These matrices can be deduced further to

$$\text{get } A_{22}^{-1} = \begin{bmatrix} A^{-1} & 0 \\ -N^{-1}CA^{-1} & -N^{-1}I \end{bmatrix}, A_{12}A_{22}^{-1}A_{21} = -GCA^{-1}BKF = \begin{bmatrix} 0 & 0 \\ G_0TKF_0 & G_0TKF_1 \end{bmatrix},$$

$$\text{and } A'_{11} - \varepsilon_1 A_{12}A_{22}^{-1}A_{21} = \begin{bmatrix} 0 & I \\ -\Omega - \varepsilon_1 G_0TKF_0 & -\varepsilon_1 G_0TKF_1 \end{bmatrix}.$$

Consider following singularly perturbed system,

$$\begin{aligned} \dot{x}_1 &= A_{11}x_1 + A_{12}x_2 \\ \varepsilon_1 \dot{x}_2 &= A_{21}x_1 + (A_{22} + \varepsilon_1^{\beta} \overline{A_{22}})x_2 \end{aligned} \tag{2.14}$$

where $A_{11} = \frac{A'_{11}}{\varepsilon_1}$, according to Lemma 2.1.1, $\text{eig}(\hat{A}/\varepsilon_1) \rightarrow \text{eig}(A_{11} - A_{12}A_{22}^{-1}A_{21}) \cup \frac{\text{eig}(A_{22})}{\varepsilon_1}$ as $\varepsilon_1 \rightarrow 0$, i.e. eigenvalues tend to

$$\text{eig} \left(\begin{bmatrix} 0 & I \\ -\Omega - \varepsilon_1 G_0TKF_0 & -\varepsilon_1 G_0TKF_1 \end{bmatrix} \right) \cup \frac{\text{eig}(A)}{\varepsilon_1} \cup \frac{-N}{\varepsilon_1}.$$

From assumptions (A1) and (A2), TK is well defined and A is stable. \hat{A}/ε_1 must be stable as long as $G_0TKF_1 > 0$, where G_0 and F_1 are our design factors. Obviously, if both of them are chosen as those values in Theorem 2.1.2, the stability of \hat{A}/ε_1 will be assured. Since $G_0 = D_1F_1^T$, then $G_0TKF_1 = D_1F_1^T TKF_1$. Due to Assumption (A2) and D_1 is diagonal matrix with positive values, therefore, $G_0TKF_1 > 0$. Consequently closed-loop system matrix \hat{A} is stable with $\varepsilon_1 \rightarrow 0$. \square

Following the proof, we present the extended 2nd order absorber tuning implementation of controller (2.9) for a SISO plant as an example. Let $F = [f_{00} \ f_{01} \ 0 \ f_{11}]$,

$G_0 = [g_0 \ g_1]^T$, and $\Omega = \text{diag}\{0, \omega_1^2\}$, then

$$F \begin{bmatrix} SI \\ I \end{bmatrix} (S^2I + \Omega)^{-1}G_0 = \begin{bmatrix} f_{00} & f_{01} & 0 & f_{11} \end{bmatrix} \begin{bmatrix} \frac{g_0}{s} \\ \frac{sg_1}{s^2 + \omega_1^2} \\ \frac{g_0}{s^2} \\ \frac{g_1}{s^2 + \omega_1^2} \end{bmatrix} \quad (2.15)$$

$$= \frac{g_0 f_{00}}{s} + \frac{s f_{01} + f_{11}}{s^2 + \omega_1^2} g_1.$$

Together with proportional and derivative terms in (2.9), the tuning controller with an absorber of resonant frequency ω_1 is found as

$$u(s) = K \left\{ \overbrace{\left[\varepsilon_1 \frac{g_0 f_{00}}{s} + \bar{\rho} \varepsilon_1^\beta + \bar{\varepsilon}_2 \varepsilon_1^\beta \frac{sN}{s+N} \right]}^{\text{PID switching}} + \overbrace{\varepsilon_1 \frac{s f_{01} + f_{11}}{s^2 + \omega_1^2} g_1}_{\text{single absorber}} \right\} \times e(s). \quad (2.16)$$

If $f_{00}g_0 > 0$, $g_1 f_{01} > 0$, and $f_{11}g_1 > 0$, from Theorem 2.1.2, the closed-loop system of (1.4) and (2.16) is stable with sufficiently small $\varepsilon_1 > 0$.

Remark 2.1.1. A damping matrix Ξ can also be added to relax the absorber design,

which only modifies A_{11} to $\begin{bmatrix} 0 & I \\ -\Omega & -\Xi \end{bmatrix}$. Then, $\text{eig}(\varepsilon_1^{-1}A_{11} - A_{12}A_{22}^{-1}A_{21})$ tends to

$\text{eig} \left(\begin{bmatrix} 0 & I \\ -\Omega - \varepsilon_1 G_0 T K F_0 & -\Xi - \varepsilon_1 G_0 T K F_1 \end{bmatrix} \right)$. On the complex plane, the damp-

ing effect is represented by the additional positive definite matrix Ξ , which shifts

open-loop poles away from imaginary axis without affecting the stability proof. The

merit is to relax the requirement of $G_0 T K F_1 > 0$ when $\text{eig}(\Xi)_{\min}$ is sufficiently large.

◇

2.1.3 Tuning Controller with a Pseudo Observer

The extended tuning controller may be further modified to the one with a pseudo observer. We notice that for controller (2.2), the first three terms for PID switching can be omitted while the added items still keep the stabilizability of closed-loop system. The controller may then be expressed in a transfer function form with fixed poles in the negative complex plane and a tunable numerator.

Corollary 2.1.1. *Under assumptions (A1) and (A2), the plant (1.4) can be stabilized by a tuning controller*

$$\begin{aligned} u(s) &= K \frac{b_1 s^{h-1} I + b_2 s^{h-2} I + \dots + b_h I}{(s + a_1)(s + a_2) \dots (s + a_h)} e(s) \\ &= K \frac{b_1 s^{h-1} I + b_2 s^{h-2} I + \dots + b_h I}{s^h + a_1^* s^{h-1} + a_2^* s^{h-2} + \dots + a_h^*} e(s) \end{aligned} \quad (2.17)$$

where $\{a_1^*, a_2^*, \dots, a_h^*\}$ are fixed initial constants which ensure eigenvalues of denominator all on the negative complex plane, and $\{b_1, b_2, \dots, b_h\} = \{\bar{b}_1 \varepsilon_1^{\beta_{b_1}+1}, \bar{b}_2 \varepsilon_1^{\beta_{b_2}+1}, \dots, \bar{b}_h \varepsilon_1^{\beta_{b_h}+1}\} \subset \mathbb{R}$.

Proof. The proof is omitted since it is a special case of Theorem 2.1.1. □

One key design point remains on how to choose suitable coefficients $\{a_1^*, a_2^*, \dots, a_h^*\}$ for the denominator of (2.17). We start the discussion from the steady-state observer viewpoint. Usually, even in the control problem of the plant with a model, it is still difficult to determine all plant states for controller implementation. Instead, only plant output is available to measure in a more practical sense. A useful approach is to employ the steady-state observer method to recover plant initial states by using output y and its initial $(n - 1)$ derivatives. If the plant is observable, then there

exists a map (Σ) such that

$$\Sigma : \mathbb{R}^{n-1} \longrightarrow \mathbb{R}^{n-1}$$

$$\begin{pmatrix} x_2 \\ x_3 \\ \vdots \\ x_{n-1} \\ x_n \end{pmatrix} \longrightarrow \begin{pmatrix} \dot{y} \\ \ddot{y} \\ \vdots \\ y_{n-2} \\ y_{n-1} \end{pmatrix} .$$

It is quite straightforward to implement such an observer-controller design with plant parameters in hands. One may refer the methods to traditional state observer design (Ogata, 1997) or suitable regressive observers, such as Kalman-Bucy filter (Kokotović et al., 1986). However, for this project, we analyze the model-independent control without plant model parameters. Therefore, if we want to use the state-recovery idea, it is more appropriate to name such an observer as the *pseudo observer* since we do not use any plant model, which differs from the design origin of a real observer.

We assume that there exists such a map Σ for state-recovery using derivatives of y , namely derivatives of e . Then, the design problem remains in twofold. First, we use suitable filter to obtain derivatives of e within the filter bandwidth. Second, tuning method takes effects on the stabilization of such a map. Considering the

controllable canonical form of the controller,

$$\dot{\Psi} = \begin{bmatrix} -a_1^* & -a_2^* & \cdots & -a_h^* \\ 1 & 0 & \cdots & 0 \\ 0 & 1 & \cdots & 0 \\ \vdots & \vdots & \vdots & \vdots \\ 0 & \cdots & 1 & 0 \end{bmatrix} \Psi + \begin{bmatrix} I \\ 0 \\ 0 \\ 0 \\ 0 \end{bmatrix} e \quad (2.18)$$

$$u = [b_1 I \quad b_2 I \quad \cdots \quad b_h I] \Psi + b_{h+1} e,$$

a set of Butterworth filter coefficients can be used as the values of \vec{a}^* . Consequently,

$\frac{s^k}{s^h + a_1 s^{h-1} + \cdots + a_h} e(s)$ gives a reasonably accurate approximation of $s^k e(s)$ in a certain bandwidth. Meanwhile, the stabilizability of closed-loop system will be maintained by the tunable parameters $\{b_1, b_2, \dots, b_{h+1}\}$ as mentioned in Corollary 2.1.1.

2.1.4 Generalized Tuning Controller

After considering above special cases, we now give a more generalized view on tuning controller in the stabilization mechanism development. Still, since y_{ref} and w are uniformly bounded, it can give us a better focus on the closed-loop stability analysis if we let them be zero. Define A_u , B_u , C_u and D_u as the state-space parameter matrix for the dynamic feedback controller u . We find the closed-loop system matrix as

$$\hat{A} = \begin{bmatrix} A - BD_u C & BC_u \\ -CB_u & A_u \end{bmatrix}. \quad (2.19)$$

To ensure its stability, we impose tuning function ε_1^β into C_u and D_u , and the closed-loop matrix becomes

$$\hat{A}^* = \begin{bmatrix} A - \varepsilon_1^\beta B D_u C & \varepsilon_1^\beta B C_u \\ -C B_u & A_u \end{bmatrix}. \quad (2.20)$$

We can simply construct the same singular perturbed system as in Lemma 2.1.1 with $A_{11} = A$, $\overline{A_{11}} = -BD_uC$, $A_{12} = 0$, $\overline{A_{12}} = BC_u$, $A_{21} = -\varepsilon_1CB_u$, $\overline{A_{21}} = 0$, $A_{22} = \varepsilon_1A_u$, and $\overline{A_{22}} = 0$. Thus, eigenvalues for this perturbed system tend to

$$\text{eig}(A) \cup \text{eig}(\varepsilon_1A_u),$$

when $\varepsilon_1 \rightarrow 0$ and A_u^{-1} exists. Obviously, the requirement for the stability is that both A and A_u are stable, which can be satisfied from assumption (A1) and controller design.

2.2 Optimization Mechanism Design

2.2.1 Simultaneous Perturbation Gradient Searching

Now, we come to the optimization problem. An important objective of this research work is to find an optimization controller without using plant parameters in practical implementation process while only using some properties of these parameters to predict closed-loop stability. Thus, special optimization algorithm, which is regarded as plant parameter independent, must be useful to accomplish our goal. Simultaneous Perturbation Method (SPM) based on gradient searching is such a method in the literature (Spall, 1992; Maeda and Yoshida, 1999; Maeda and Figueiredo, 1997). Considering an unknown objective function $J(\chi)$, where $\chi \in R^n$ is a set of parameters of J , the algorithm is described as follows (Maeda and Yoshida, 1999)

$$\begin{aligned} \chi_{t+1} &= \chi_t - \alpha \Delta \chi_t \\ \Delta \chi_t^i &= \frac{J(\chi_t + p \varrho_t) - J(\chi_t)}{p} \varrho_t^i \end{aligned} \tag{2.21}$$

where α is a design parameter, p is the perturbation magnitude for one searching step, χ^i represents the i -th element of vector χ , and ϱ^i denotes the i -th element of

the sign vector ϱ , which is assigned randomly and independent with each other. For the second equation of (2.21), we expand $J(\chi_t + p\varrho_t)$ with respect to χ_t ,

$$J(\chi_t + p\varrho_t) = J(\chi_t) + p\varrho_t^T \frac{\partial J(\chi_t)}{\partial \chi} + \frac{p^2 \varrho_t^T}{2} \frac{\partial^2 J(\chi_{\varrho 1})}{\partial \chi^2} \varrho_t, \quad (2.22)$$

then substitute into (2.21),

$$\Delta \chi_t^i = \varrho_t^i \varrho_t^T \frac{\partial J(\chi_t)}{\partial \chi} + \frac{p \varrho_t^i}{2} \varrho_t^T \frac{\partial^2 J(\chi_{\varrho 1})}{\partial \chi^2} \varrho_t, \quad (2.23)$$

the expectation of above equation is (Maeda and Figueiredo, 1997)

$$E(\Delta \chi_t^i) = \frac{\partial J(\chi_t)}{\partial \chi_t^i} + E \left\{ \frac{p \varrho_t^i}{2} \varrho_t^T \frac{\partial^2 J(\chi_{\varrho 1})}{\partial \chi^2} \varrho_t \right\} \quad (2.24)$$

which means that if p is sufficiently small, the second term of the right-hand side of (2.24) is small. Then $\Delta \chi_t^i \approx \partial J(\chi_t) / \partial \chi_t^i$. The precious point of this method is that objective function's gradients can be evaluated approximately by two estimations $J(\chi + p\varrho)$ and $J(\chi)$.

For a typical selection of $J(\chi)$ in practice, the error ³ function is usually used

$$J(\chi_t) = \sum_{k=1}^{\lambda} e^2(k) \quad (2.25)$$

where k is the sampling number in a block interval, and λ is the total sampling number for one block interval as illustrated in Figure 2.2. The performance index in SPM looks exactly the same as H_2 norm. However, for available H_2 design methods, e.g. LMI design or Riccati equation approach, at least the nominal values of A , B and C are required. While in SPM, little knowledge about A , B and C is used during the optimizing process.

Mostly random search algorithm was proposed for feedforward controller with FIR transfer function $R(z)$. The perturbation of $R(z) + \delta R(z)$ is always stable in

³Here, error is the difference between reference output signal y_{ref} and output signal y , which is similar as the definition in section 1.3.

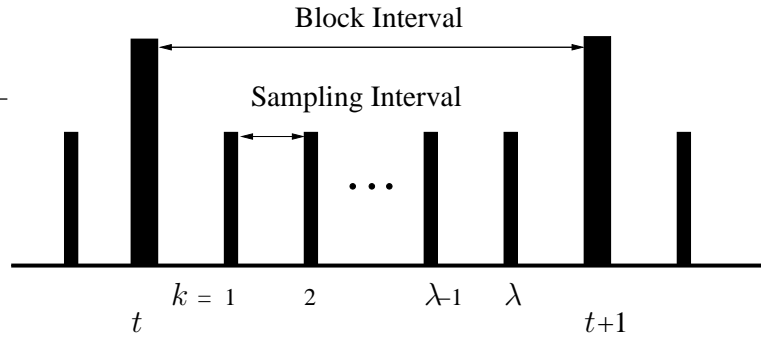


Figure 2.2: Block interval and sampling interval

feedforward system. When applied to feedback control, however, $R(s) + \delta R(s)$ may destabilize the closed-loop system even $\delta R(s)$ is sufficiently small and $R(s) + \delta R(s)$ is open-loop stable. For this reason, an additional algorithm must be designed to safe-guard the online optimization process. To simplify the problem, we assume disturbance w in optimization problem to be ergodic while not necessarily to be bounded by a *very small* constant compared with reference signals. We concentrate on how stabilization algorithms discussed in section 2.1 can be integrated with SPM to achieve the optimization purpose. It should be noticed that there are two types of perturbations:

singular perturbation It is used in stabilization algorithm development. Actually, it is the tuning action of the term ε_1 .

simultaneous perturbation It is used in optimization algorithm as the term p , which gives a varying effect on the parameters that affect performance index during gradient searching.

Remark 2.2.1. *The key point is that we can consider **simultaneous perturbation** in optimization process as interference in stabilization process. Once the stability of system has been threatened due to optimizing, **singular perturbation** will then take effects in the tuning term ε_1 to drag controller parameters back to the*

stabilization region for the closed-loop system. \diamond

2.2.2 Optimization on PID and its Extended Tuning Controllers

$$\left\{ \begin{array}{l}
 \text{(1) PID tuning (Chang and Davison, 2003)} \\
 u(s) = K \left[\frac{\varepsilon_1 I}{s} + \bar{\rho} \varepsilon_1^{\beta_\rho+1} I + \bar{\varepsilon}_2 \varepsilon_1^{\beta_\varepsilon+1} \frac{sNI}{s+N} \right] \times e(s) \\
 \text{(2) extended by 1st order terms} \\
 u(s) = \\
 K \left\{ \left[\frac{\varepsilon_1 I}{s} + \bar{\rho} \varepsilon_1^{\beta_\rho+1} I + \bar{\varepsilon}_2 \varepsilon_1^{\beta_\varepsilon+1} \frac{sNI}{s+N} \right] + \frac{\bar{c}_1 \varepsilon_1^{\beta_{c_1}+1} I}{s+a_1} + \frac{\bar{c}_2 \varepsilon_1^{\beta_{c_2}+1} I}{s+a_2} + \dots + \frac{\bar{c}_h \varepsilon_1^{\beta_{c_h}+1} I}{s+a_h} \right\} \times e(s) \\
 \text{(3) extended by 2nd order terms} \\
 u(s) = K \left\{ \varepsilon_1 F \begin{bmatrix} sI \\ I \end{bmatrix} (s^2 I + \Omega)^{-1} G_0 + \varepsilon_1^\beta \left(\bar{\rho} + \bar{\varepsilon}_2 \frac{sN}{s+N} \right) I \right\} \times e(s)
 \end{array} \right. \quad (2.26)$$

We first recall and consider PID and its extended tuning controllers (2.26) as candidates for optimization. For each controller, there exist crucial parameters to affect its performance acting on the closed-loop system. For PID tuning, they are $\{\varepsilon_0, \bar{\rho}, \bar{\varepsilon}_2\}$. For 1st order extended version, other more parameters $\{\bar{c}_1, \bar{c}_2, \dots, \bar{c}_h\}$ are accounted. While for 2nd order extended version, each elements in the remaining matrix from FG_0 multiplication must also be accounted in addition to $\{\varepsilon_0, \bar{\rho}, \bar{\varepsilon}_2\}$. Define the crucial parameter set as Π , we now enumerate how to optimize controller performance with regard to Π by SPM and tuning stabilization algorithm.

Algorithm 2.2.1. 1. arbitrarily set initial values of Π

2. examine the control input u for the corresponding initial values of Π^0
 - (a) if u is on the boundary or outside of the constraint region, apply one corresponding controller in (2.26) to the system and get Π^i
 - (b) if u is inside of the constraint region, then go on
3. define the total sampling number λ , and calculate $J(\Pi^i) = \sum_{k=1}^{\lambda} e^2(k)$
4. perform SPM of Π^i to get Π^{i+1} , examine their corresponding control input u'
 - (a) if u' is on the boundary or outside of the constraint region, apply one corresponding controller (2.26) to the system and get another set of Π^{i+1}
 - (b) if u' is inside of the constraint region, then go on
5. calculate $J(\Pi^{i+1}) = \sum_{k=1}^{\lambda} e^2(k)$
6. evaluate the gradient of J for the tuning of Π^i
7. start from the latest tuned Π^i , and go to step 3.

It should be noticed that throughout this procedure, A, B, C matrix of plant are not used any more but assumptions (A1) and (A2) should be assured.

2.2.3 Optimization on Tuning Controller with a Pseudo Observer

Furthermore, we can also implement optimization on tuning controller with a pseudo observer discussed in section 2.1.3. We recall the general type controller in Corollary 2.1.1,

$$u(s) = K \frac{\bar{b}_1 \varepsilon_1^{\beta_{b_1}+1} s^{h-1} I + \bar{b}_2 \varepsilon_1^{\beta_{b_2}+1} s^{h-2} I + \dots + \bar{b}_h \varepsilon_1^{\beta_{b_h}+1} I}{s^h + a_1^* s^{h-1} + a_2^* s^{h-2} + \dots + a_h^*} e(s).$$

For $\{a_1^*, a_2^*, \dots, a_h^*\}$, we can use the states of an all-pole filter, say a Butterworth filter, to approximate the plant states in a certain bandwidth. Thus, the remaining crucial parameters are $\{\bar{b}_1, \bar{b}_2, \dots, \bar{b}_h\}$ and \bar{b}_{h+1} when using the pseudo observer idea. We notice that when stability is threatened by tuning, stabilization algorithm will drag parameters of controller greatly back to stable region. In turn, optimization effort in previous epoches could be 'ruined'. Considering the optimization with Π^i must have followed a stable routine, we can use previous latest stable parameter set of Π^i instead of using stabilization algorithms in section 2.1. The steps are written as follows.

Algorithm 2.2.2. (*Option to Algorithm 2.2.1*)

4. perform SPM of Π^i to get Π^{i+1} , examine their corresponding control input u'
 - (a) if u' is on the boundary or outside of the constraint region, drag Π^{i+1} back to Π^i , and re-implement step 4
 - (b) if u' is inside of the constraint region, then go on

Global Optimization Possibility

Traditionally, a state-observer based controller can achieve optimal control performance if it minimizes a linear quadratic (LQ) function. Such a controller is known as a linear quadratic regulator (LQR). Its gain vector K can be solved from the algebraic Riccati equation (ARE), as quoted from Ogata (1997),

$$A^T P + PA + [TK - (T^T)^{-1} B^T P]^T [TK - (T^T)^{-1} B^T P] - PBR^{-1} B^T P + Q = 0$$

where Q is a positive-definite (or semipositive-definite) matrix, R is a positive-definite matrix, and $R = T^T T$. The minimization of performance index with respect

to K is the same as the minimization of

$$x^T [TK - (T^T)B^T P]^T [TK - (T^T)^{-1}B^T P]x.$$

If the closed-loop matrix is stable, then there always exists a positive-definite matrix P . Obviously, the solution of K is found optimal by letting $TK = (T^T)^{-1}B^T P$. Therefore, a state-observer plus a gradient searching method of suitable performance index can solve the Linear Quadratic Gaussian (LQG) controller for a plant with known parameter matrices A , B and C . When A , B and C are not available, the proposed tuning controller has to be applied. It is quite interesting to analyze whether the pseudo observer tuning method can also achieve a global optimization solution. Considering the Laplace transform for the highest order derivative approximation $\tilde{y}_{n-1}(t)$ by passing $y(t)$ through a filter, whose denominator can be used in the pseudo observer,

$$s^{(n-1)}\tilde{Y}(s) = \frac{s^{(n-1)} \prod_{i=1}^{n-1} r_i}{\sigma^{(n-1)} \prod_{i=1}^{n-1} (s + r_i/\sigma)} Y(s) = \frac{s^{(n-1)} R}{\prod_{i=1}^{n-1} (\sigma s + r_i)} Y(s) \quad (2.27)$$

where $\sigma \in \mathbb{R}^+$, $\{r_i\}$ are stable poles and $R = \prod_{i=1}^{n-1} r_i$. Other lower order derivative approximations of $y(t)$ can also be found through the same filter within its bandwidth. Here, we give a rough consideration about the relationship between the approximation error of $y - \tilde{y}$ and the positive scalar σ . For the approximation error of 1st order derivative, $E_1(s) = Y_1(s) - \tilde{Y}_1(s) = \left(1 - \frac{\prod_{i=1}^{n-1} r_i}{\prod_{i=1}^{n-1} (\sigma s + r_i)} \right) Y_1(s)$. It is obvious that when $\sigma \rightarrow 0$, $E_1(s) \rightarrow 0$ with the stabilization mechanism for $y(t)$ developed in section 2.1. In other words, the more stable poles of r_i the filter has, the more accurate approximation is obtained. As for other higher order derivatives,

the conclusion also holds. If the plant dynamics can be defined by

$$\begin{aligned} \dot{x} &= A_p x + B_p u \\ y &= C_p x, \end{aligned} \tag{2.28}$$

there exists an optimal control law $u = K^*x$ to achieve the LQ solution. Considering the existence of the map Σ for states x obtained from derivatives of y , we define the transform matrix as T . Then, a controller $u = K^*T\vec{y}$ with $\vec{y} = \{y, \dot{y}, \dots, y_{n-1}\}$ can be obtained. Furthermore, for a sufficient small σ , \vec{y} filtered by $y(t)$ can be used to approximate the derivatives of y . Therefore, the control law $u = K^*T\vec{y}$ can be used to approximate the optimal controller solution if the plant is observable. In fact, for the practical implementation, σ does not need to be very small and a set of Butterworth low-pass filter coefficients can be used to achieve LQG solution within its bandwidth, which covers that of the plant.

optional proof of global optimization We can also use singular perturbation approach to prove this finding, since it is common in the literature when proving parameter convergence for observer-like output feedback controller, such as the high-gain observer (Khalil, 1996).

Proof. For a traditional observer design, the expression for the state estimation is (Ogata, 1997)

$$\dot{\hat{x}} = (A - K_e C)\hat{x} + Bu + K_e y \tag{2.29}$$

where K_e is the weighting matrix, and A, B need to be the same as the plant A, B matrix, which may not be possible in practice. However, in the pseudo observer case, it does not use the plant A, B but uses \tilde{A}, \tilde{B} , and the state estimation is

$$\dot{\hat{x}} = (\tilde{A} - K_e C)\hat{x} + \tilde{B}u + K_e y. \tag{2.30}$$

Therefore, a control input $u = K\tilde{x}$ can be obtained. Define the error between real state x and estimated state \tilde{x} to be e . Then subtracting $\dot{x} = Ax + Bu = Ax + BK\tilde{x}$ by (2.30), we get

$$\dot{e} = (A - \tilde{A} + BK - \tilde{B}K)x + (\tilde{A} - K_e C - BK + \tilde{B}K)e. \quad (2.31)$$

Define a transform T such that $T\tilde{A}T^{-1} = \Lambda_A$, where Λ_A is the diagonal matrix with r_i as eigenvalues. Then, $\tilde{A} = T^{-1}\Lambda_A T$. The error state derivatives can be deduced as

$$T\dot{e} = (-\Lambda_A T + TA + TBK - T\tilde{B}K)x + (\Lambda_A - TK_e CT^{-1} - TBKT^{-1} + T\tilde{B}KT^{-1})Te. \quad (2.32)$$

Define $\zeta = Te$ and $\Lambda_A = \Lambda/\sigma$. We get following expressions,

$$\begin{aligned} \dot{x} &= (A + BK)x + BKT^{-1}\zeta \\ \sigma\dot{\zeta} &= [-\Lambda T + \sigma(TA + TBK - T\tilde{B}K)]x + [\Lambda + \sigma(T\tilde{B}KT^{-1} - TK_e CT^{-1} - TBKT^{-1})]\zeta, \end{aligned} \quad (2.33)$$

which compose a new singularly perturbed system with $A_{11} = A + BK$, $A_{12} = BKT^{-1}$, $A_{21} = -\Lambda T$, and $A_{22} = \Lambda$. Since Λ is the diagonal form of filter's \tilde{A} , then Λ^{-1} must exist. Therefore, from singular perturbation Lemma 2.1.1, for sufficiently small $\sigma \rightarrow 0$, the eigenvalues of system (2.33) tends to

$$\text{eig}(A_{11} - A_{12}A_{22}^{-1}A_{21}) \cup \text{eig}\left(\frac{A_{22}}{\sigma}\right), \quad (2.34)$$

which are $\text{eig}(A + 2BK)$ and $\text{eig}\left(\frac{\Lambda}{\sigma}\right)$ respectively. For original plant $\dot{x} = Ax + Bu$ and $y = Cx$, one K^* can be found to keep the closed-loop stability $\text{eig}(A + BK^*) \subset \mathbb{C}^-$ and also give an optimal controller solution $u = K^*x$ by solving the algebraic Riccati Equation. Then, if the controller law to be $u = K\tilde{x} = \frac{1}{2}K^*\tilde{x}$, then $\text{eig}(A + 2BK) = \text{eig}(A + BK^*)$, which is on the stable complex plane. \square

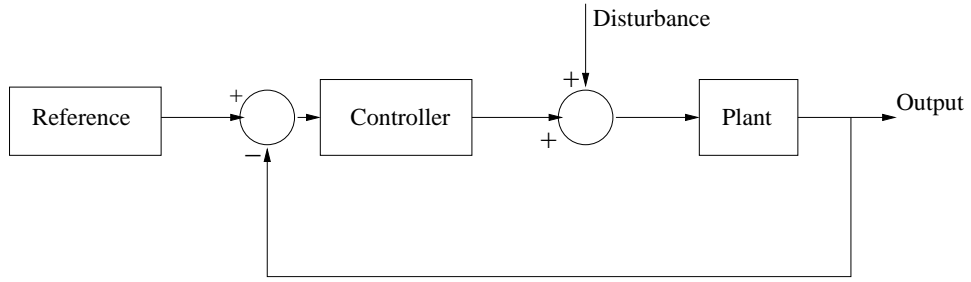


Figure 2.3: An example of ordinary control loop with both disturbance and reference signals

2.2.4 Comparison with H_2 Control

Since our performance index J is equivalent to the H_2 norm when $\frac{1}{T} \int_0^T w^2 dT = \text{const}$ for sufficiently large T , we give the comparison between our method and typical H_2 optimization control.

For H_2 optimization control, there are many methods to design a controller when plant parameters are available. The Riccati and LMI are the most popular tools for this purpose. A common feature of the two methods is to bound the H_2 norm of the closed-loop system by a conservative upper bound v and then minimize v subjected to some linear constraints. The offline optimization depends on parameters of the plant.

For proposed method, it minimizes the H_2 norm of the closed-loop system directly without requiring the knowledge of plant parameters. It is an online optimization based on a different principle under a more relaxed requirements.

2.3 Simulation Validation of Control Module

The ordinary control loop with both disturbance and reference signals is shown in Figure 2.3. In this study, we consider a trajectory tracking problem subject to the disturbance of bounded white noise. The purpose of the demonstrations is

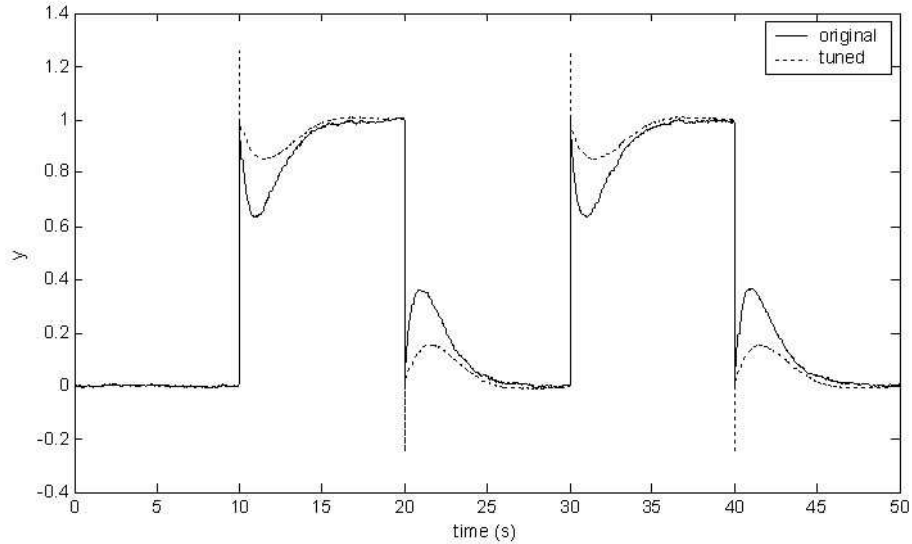


Figure 2.4: Optimizing PID tuning: trajectory tracking comparison

to validate the proposed control module's ability to improve the response of the closed-loop system under disturbance. Thus, all the plant parameters are chosen randomly without any intention. Throughout this section, Matlab/Simulink is used to implement the validation purpose.

2.3.1 PID Tuning

Let the reference be a pulse signal with a period of 20s and unit magnitude. The plant has the transfer function

$$H_p(s) = \frac{360}{s^2 + 2s + 360} \quad (2.35)$$

The 1st controller described in (2.26) is tested here. We set the initial coefficients of $\{\epsilon_0, \bar{\rho}, \bar{\epsilon}_2\}$ as $\{1, 1, 1\}$. The parameters are changed to $\{2.286, 3.104, 4.426\}$ after a period of tuning. Figure 2.4 gives comparison of trajectory tracking between original parameters control and optimally tuned parameters control. Figure 2.5 gives the bode diagram comparison of the closed-loop. From the graph, it is evident that the 1st controller in (2.26) can improve control performance as described in this study.

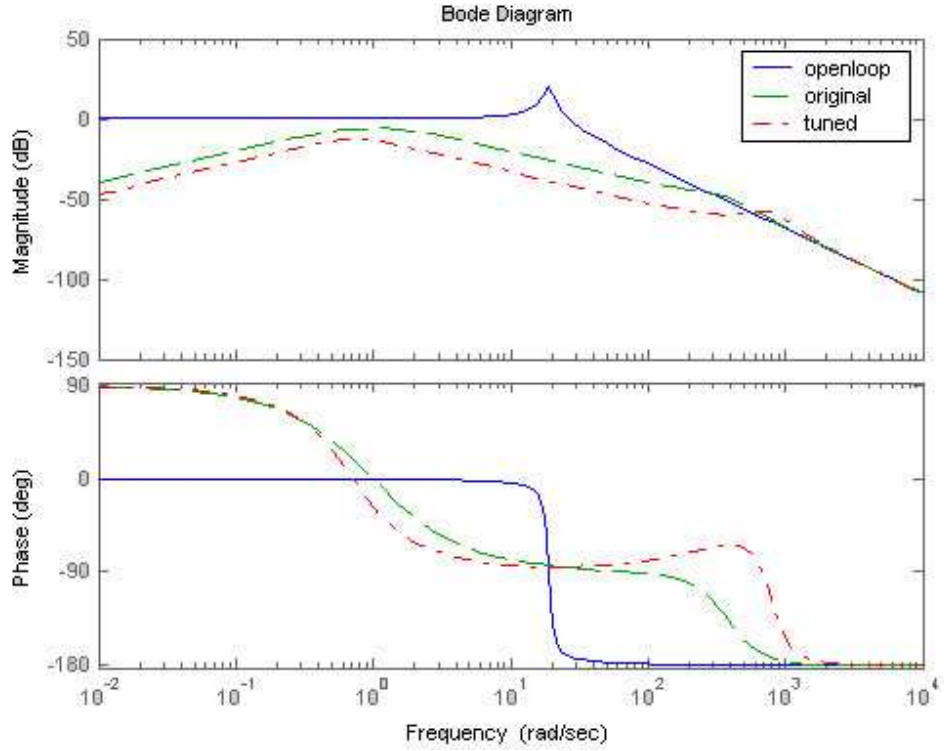


Figure 2.5: Optimizing PID tuning: Bode diagram comparison

2.3.2 Pseudo Observer Tuning

Still let reference be unit pulse signal with a period of 20s. In order to verify the feasibility of the extended tuning controller under more complicated conditions, the transfer function of the plant is changed to

$$H_p(s) = \frac{360}{s^2 + 2s + 360} + \frac{600}{s^2 + 2s + 600} \quad (2.36)$$

with an increased order. We apply controller (2.17) with the coefficients $\{a_1^*, a_2^*, \dots, a_h^*\}$ of a 5-order Butterworth filter. Let the initial values of $\{b_1, b_2, b_3, b_4, b_5\}$ be $\{0, 0, 0, 0, 0\}$.

After optimizing for a while, the 1st tuned set $\{b'\}$ is $\{-0.875, 1.3324, 1.6018, -1.1951, -2.002, 2.02\}$. Then, in order to see its persistence, we keep controller tuning $\{b'\}$ and get the 2nd tuned set $\{-2.1993, 0.7404, 0.8314, -0.5692, -2.1006, 1.8992\}$. From Figure 2.6 and Figure 2.7, the improved results are obtained, which validates such a tuning optimal controller.

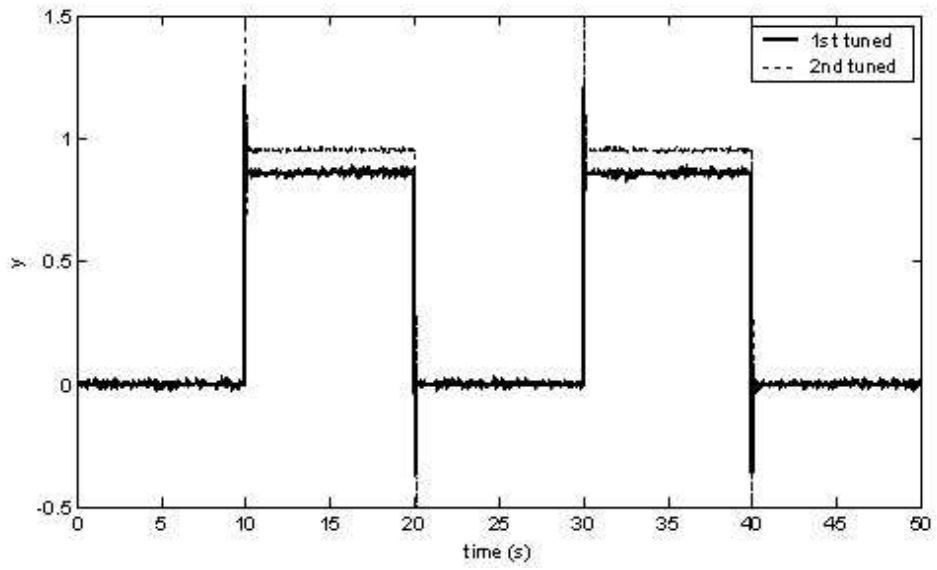


Figure 2.6: Optimizing tuning control with pseudo-observer: trajectory tracking comparison

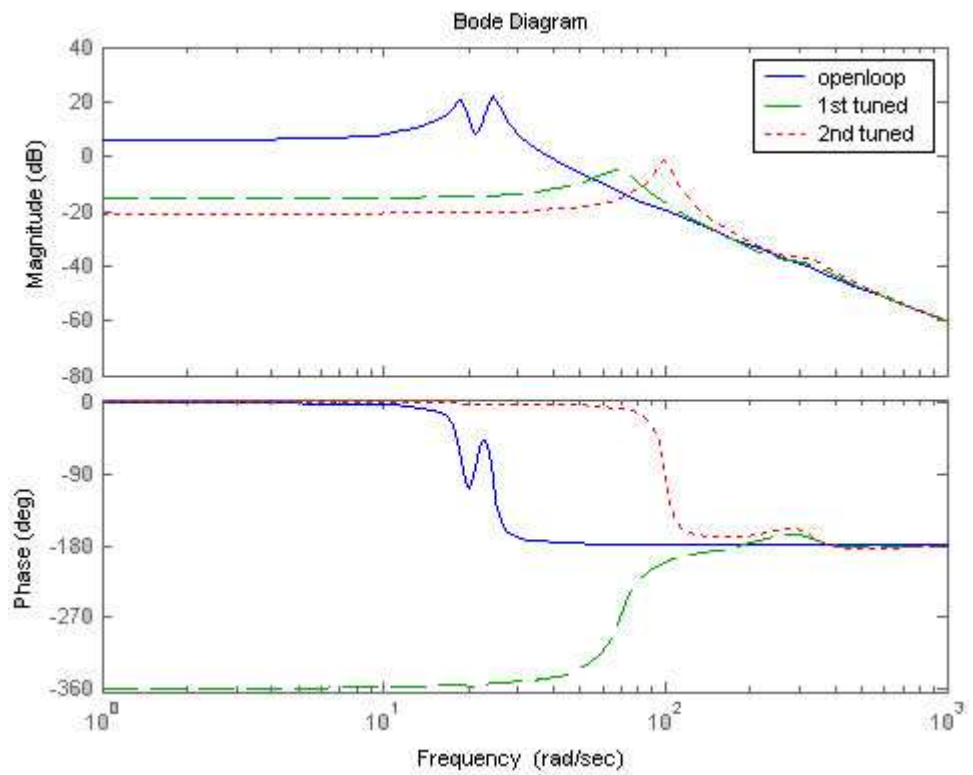


Figure 2.7: Optimizing tuning control with pseudo-observer: Bode diagram comparison

Non-Minimum Phase Plant

It is well-known that nonminimum-phase plant control is always one tough problem when applying adaptive stabilization control. One may notice that throughout the stability analysis in section 2.1, there is no restriction on the selection of zeros of plant (1). That indicates the possibility of applying our suboptimal controllers for nonminimum-phase plant control as long as assumptions (A1) and (A2) are valid. Here, we give an example for it using previous tuning controller with 5 order butterworth filter coefficients. The plant is also chosen randomly without any intension, which is

$$H_p(s) = \frac{s - 360}{s^2 + 2s + 360} + \frac{s - 600}{s^2 + 2s + 600} \quad (2.37)$$

Let unit pulse signals with a period of 20s be reference signals. The initial set of $\{b'\}$ follows from preview example $\{-2.1993, 0.7404, 0.8314, -0.5692, -2.1006, 1.8992\}$. Figure 2.8 shows time response of closed-loop system in the 1st 20s. After optimizing for several hours, the tuned set becomes $\{1.3779, -1.5795, -0.5461, 0.7937, -0.0351, 0.1577\}$. Figure 2.9 shows a much more improved result for trajectory tracking of closed-loop system.

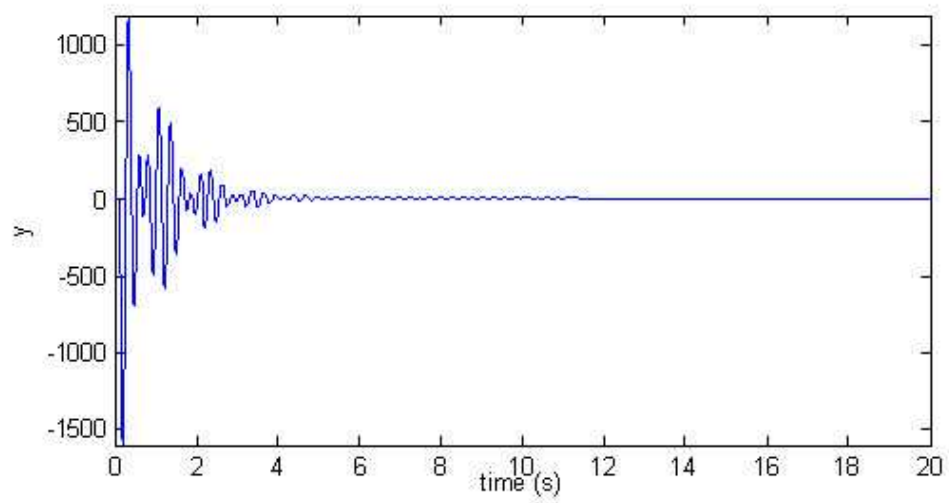


Figure 2.8: Optimizing nonminimum-phase plant control: initial 20s

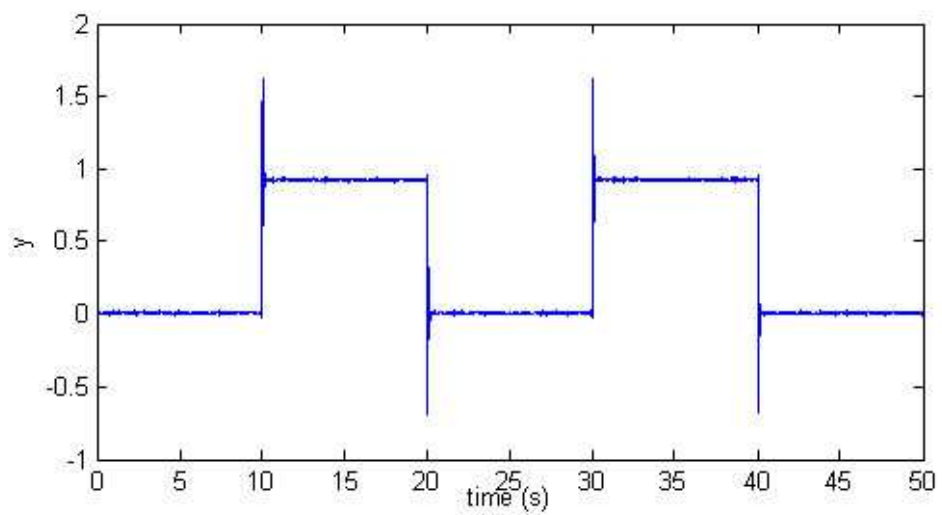


Figure 2.9: Optimizing nonminimum-phase plant control: after tuning

CHAPTER 3

CASE STUDY: FLOW-INDUCED VIBRATION

3.1 Preliminary Study

Most control design problems are based on the availability of plant model. In FIV case, however, the problem is more difficult since the available models are either too analytically complicated or too qualitative and phenomenological to be applicable for the understanding of fluid-structure interaction. Thus, a special design routine has to be followed. Before using the control module developed in Chapter 2, it is preferred to perform a preliminary study on the characteristics of FIV phenomenon and its control problem. In this section, a typical model to represent FIV is introduced briefly. We look for the key characteristics in the model and make initial prediction on the direction of controller design. After that, suitable experiments are conducted to verify the prediction. It should be noticed that the controller only depends on the qualitative information of the model without the knowledge of the exact model parameters since the model is a phenomenological one. For this reason, only experimental validation is adopted here rather than numerical simulations.



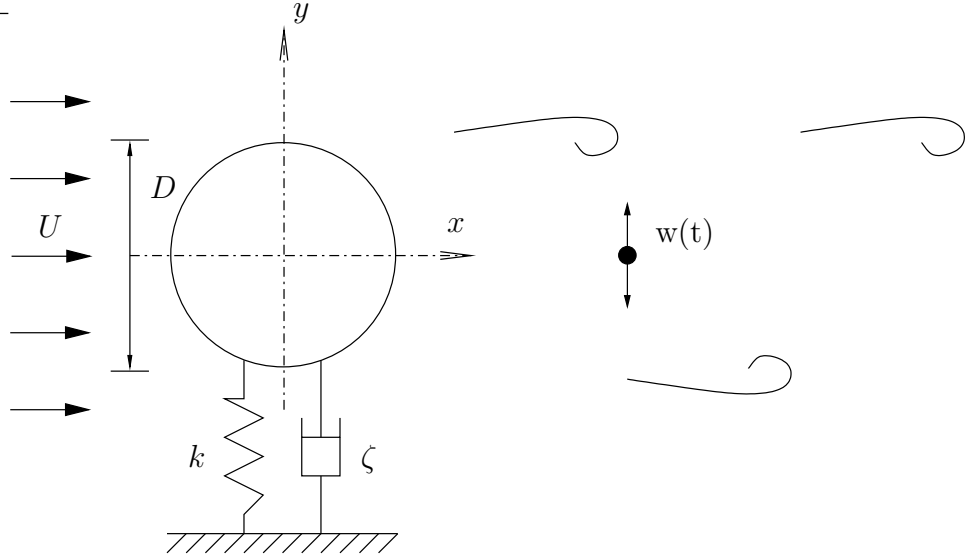


Figure 3.1: Model of cylinder vibration and wake oscillator for FIV

3.1.1 Phenomenological Model

Let us consider a typical 1-dof elastically mounted rigid cylinder with diameter D and length l . The cylinder is restricted to oscillate transversely to the uniform and stationary flow with free stream velocity U as shown in Figure 3.1. The most commonly used model is a double oscillator model to describe FIV, which consists of a structure oscillator $y(t)$ for cylinder transverse motion and a wake oscillator $w(t)$ for vortex shedding. The equation of structure oscillator can be written as

$$m_0(\ddot{y} + 2\zeta\omega_0\dot{y} + \omega_0^2y) = \frac{1}{2}\rho U^2 C_L D l \quad (3.1)$$

where m_0 is the sum of cylinder mass and added fluid mass, ζ is the damping ratio, ω_0 is the undamped natural frequency of cylinder, ρ is the fluid mass density and C_L is the nondimensional lift coefficient of the fluid flow around the cylinder. For the wake oscillator, all available phenomenological models use a van der pol equation with a nonlinear damping term to describe the self-sustainable fluid oscillation. There are different modeling approaches in the literature. Here, we adopt the simplest form

from (Krenk and Nielsen, 1999). The model is written as

$$m_f \left[\ddot{w} - 2\zeta_f \omega_s \left(1 - \frac{w^2 + \dot{w}^2 / \omega_s^2}{w_0^2} \right) \dot{w} + \omega_s^2 w \right] = -\frac{1}{2} \rho U^2 F_C D l \quad (3.2)$$

where F_C is the force term imposed by cylinder, m_f is the equivalent mass of wake oscillator, which is proportional to the fluid mass density ρ and the structure volume Dl , ζ_f is the damping ratio, ω_s is the vortex shedding frequency expressed in terms of $2\pi StU/D$ with St as the Strouhal number. In the vibration interval $(0, w_0)$, the damping term is negative to excite wake oscillation, and outside $(0, w_0)$ it is positive. The reason for choosing this damping model will be discussed in the next section, which is related to the controller design.

The coupling format of these two oscillators is another controversial topic. For equation (3.1) and (3.2), C_L and F_C are usually regarded as coupling candidates in the literature. The substantial research is based on how to choose the combinations of $\{w, \dot{w}, \ddot{w}\}$ or $\{y, \dot{y}, \ddot{y}\}$ to represent C_L and F_C respectively (Hartlen and Currie, 1970; Krenk and Nielsen, 1999; Facchinetti et al., 2004). While in this study, we concentrate on control problem of FIV by using only qualitative information in the model. Therefore, the coupling effects are left open in this study.

3.1.2 Pre-design: High Frequency Perturbation Effect

After the brief introduction of the phenomenological model, we try to find some property of FIV based on an experimental study. Consider the control technique developed by Cheng et al. (2003) as shown in Figure 1.5. A local perturbation¹ effect

¹It should be noticed that the term 'perturbation' used in this Chapter is neither singular perturbation in stabilization mechanism design nor simultaneous perturbation in optimization mechanism design in Chapter 2. It refers to the physical movement created by the control technique introduced by Cheng et al. (2003). In fact, it is the practical implementation method of previous two perturbations.

p is imposed on the flow around the cylinder by the excitation of a movable plastic plate driven by embedded piezoelectric actuators. Suppose p causes a sinusoidal vibration component at frequency ω_p to the wake oscillation signal $w(t) = A_p \sin(\omega_p t)$. Obviously, it should also affect the FIV model given by (3.1) and (3.2). Due to the fact that coupling mechanism is still not clear, we only consider the perturbation effect on the damping term in the wake oscillator. Due to the perturbation, the damping term becomes

$$2\zeta_f \omega_s \left(\frac{A_p^2 \omega_s^2 \sin^2 \omega_p t + A_p^2 \omega_p^2 \cos^2 \omega_p t}{w_0^2 \omega_s^2} - 1 \right) \quad (3.3)$$

with values between $2\zeta_f \omega_s \frac{A_p^2 \omega_s^2 - w_0^2 \omega_s^2}{w_0^2 \omega_s^2}$ and $2\zeta_f \omega_s \frac{A_p^2 \omega_p^2 - w_0^2 \omega_s^2}{w_0^2 \omega_s^2}$. One key point is that if perturbation frequency ω_p is much higher than vortex shedding frequency ω_s , the maximum damping value of wake oscillator will be larger. This helps us make the following conjecture.

Conjecture 3.1.1. *Assume that the flow-induced vibration can be described by a phenomenological model given by equations (3.1) and (3.2). If a control scheme helps to increase the frequency of wake oscillation in the local flow around structure, then this scheme will help to suppress vortex shedding in the wake.*

To avoid using ambiguous findings in formulating a suitable numerical simulation for the verification of this conjecture, we prefer to conduct an experiment for the validation. Based on the perturbation technique in Figure 1.5, an open-loop control is conducted by using sinusoidal signals with a fixed amplitude but different frequencies. The experiment is carried out in a closed circuit wind tunnel with a square test section of $0.6 \times 0.6m^2$ and a length of $2.4m$. One square cylinder of height $h = 15.2mm$, which is supported on springs at both ends, is placed in the downstream of wind tunnel and allowed to vibrate vertically as shown in Figure

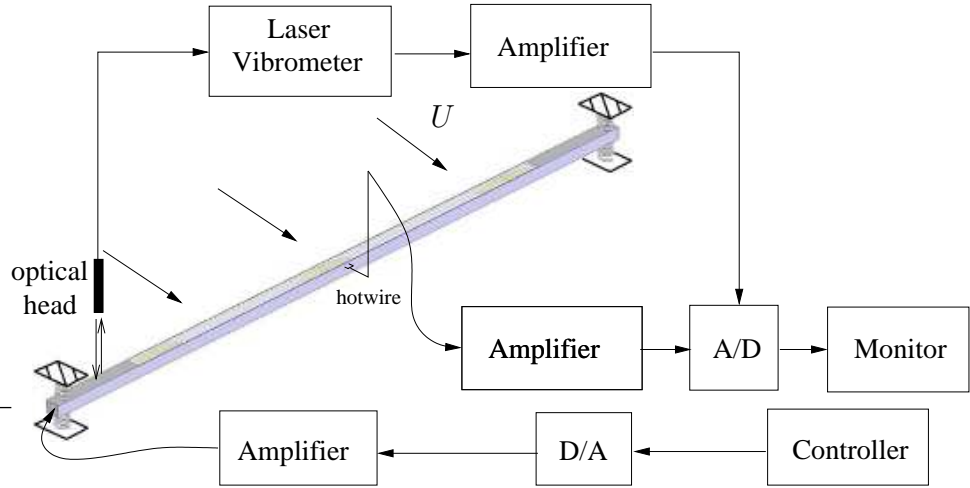
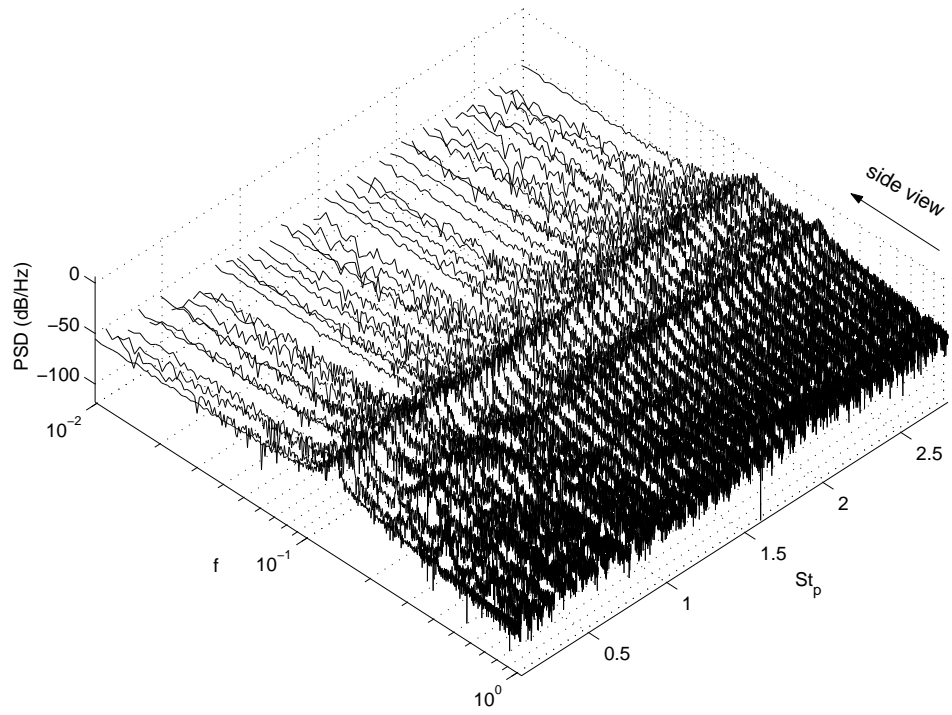


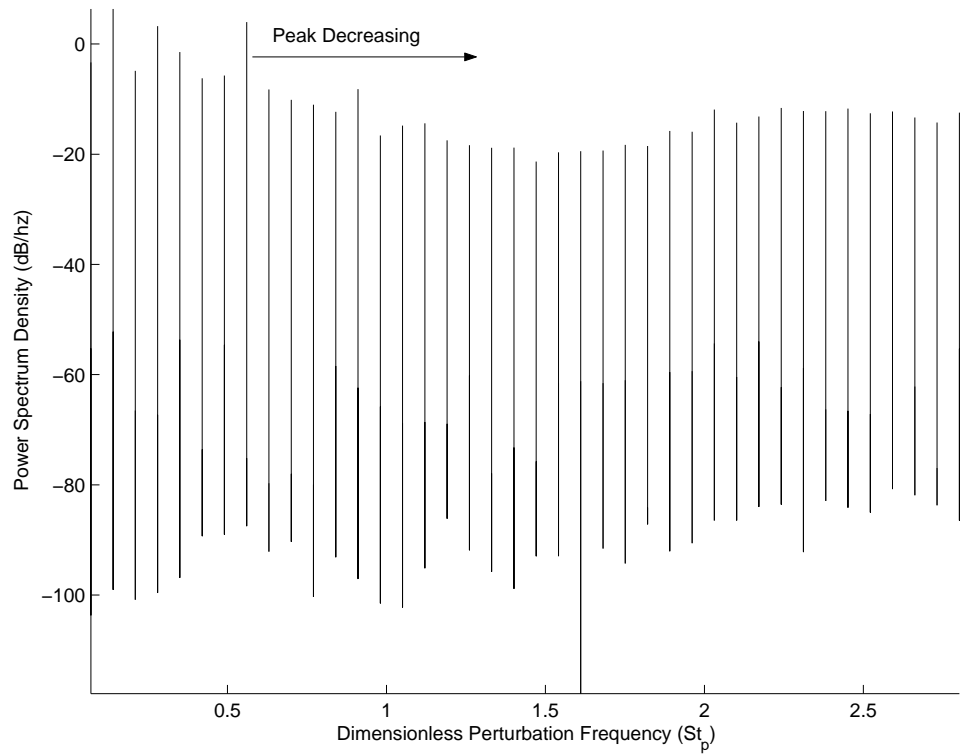
Figure 3.2: Open-loop control experiment setup

3.9. The free-stream velocity $U_\infty = 2.17ms^{-1}$ excites cylinder to vibrate due to the occurrence of vortex shedding. The results are monitored by a laser vibrometer for structure vibration and a hotwire for wake vortex shedding, which are shown in Figure 3.2. The flow condition is set at FIV lock-in regime, where $\omega_s \approx \omega_0$. Define the dimensionless frequency as St_f , the dimensionless shedding frequency as $St_s \approx 0.13$, and the dimensionless perturbation frequency as $St_p = f_p D/U$. In the experiment, power spectrum densities (PSD) of wake velocity signals are obtained under different perturbation frequencies $St_p \in [0.07, 2.80]$. These signals are plotted in Figure 3.3. It is found that for $St_p \geq 0.7$, the peak level of PSD drops significantly and the overall peak level in this St_p region is much lower than that in the region of $St_p < 0.7$. Besides the peak level, the rms (root-mean-square) value reduction of signals between controlled and non-controlled cases is also plotted as in Figure 3.4 to assess the overall control effect. As for wake velocity reduction, the rms reduction level for $St_p \geq 0.7$ is higher than the rms reduction level for smaller St_p . The experimental results matches the description of Conjecture 3.1.1.

This phenomenon also agrees with other findings in flow control using acoustic excitation. Hsiao et al. (1990); Liu and Brodie (2000) find that effective perturbation



(a) overview



(b) side view

Figure 3.3: Power spectrum density plot of wake velocity ($St_p \in [0.07, 2.8]$)

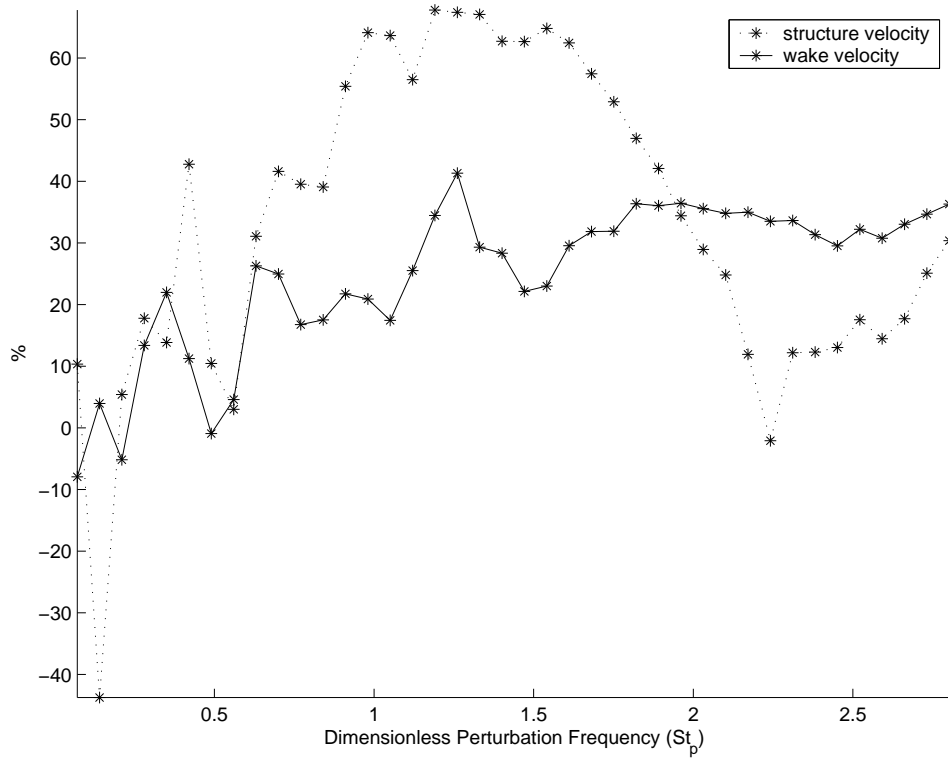


Figure 3.4: RMS reduction values (percentage): structure velocity and wake velocity

frequency range for acoustic excitation is corresponding to shear-layer instability frequency, which is of higher order than vortex shedding frequency and dependent on the Reynolds number (Peterka and Richardson, 1969). When St_p is in the order of 1, as mentioned by Hsiao et al. (1990), another 'lock-in' phenomenon occurs. The instability waves are amplified, and momentum transport and flow mixing are enhanced, which affects wake characteristics significantly when compared to no perturbation condition. In our investigation, the phenomenological model also agrees with this point. In addition, considering the frequency effect of perturbation p on structure vibration, a higher frequency perturbation results in more energy imposed on the structure in the same time interval. Therefore, the control of FIV must balance between counteracting flow energy on structure by increasing damping and imposing perturbation energy on structure by increasing frequency. Indeed, in Figure 3.4, there is an optimal frequency region $St_p \in [0.5, 2]$, where both wake and

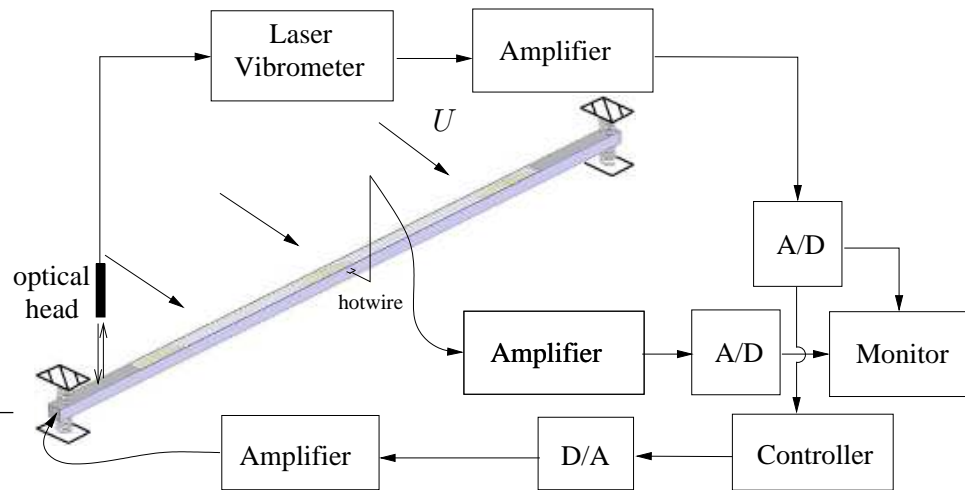


Figure 3.5: Closed-loop control experiment setup

structure velocity have considerable reduction. This finding of high frequency perturbation effect gives one possible control design direction for FIV based on the phenomenological model.

3.2 Active Control

Based on the perturbation technique, we try to find a more effective control scheme for reduction of both structure and wake oscillations in the *lock-in* regime. It is known that closed-loop control usually provides more satisfactory performance than open-loop control (Zhang et al., 2003). Thus, this research pursues a closed-loop control method for FIV by using structure vibration signal as feedback signal as shown in Figure 3.5. We first study traditional control methods, and then give a multi-frequency control scheme by the inspiration from the finding in the pre-design section.

3.2.1 Traditional Control Methods

variable structure control

A possible solution for structure vibration control under unknown disturbance is called variable structure control. For FIV problems, structure vibration is induced by the uncertain but bounded flow excitation. Considering a structure vibration model,

$$\ddot{y} + 2\zeta\omega_0\dot{y} + \omega_0^2y = \frac{d + u}{m_0} \quad (3.4)$$

where d is the bounded fluid force and u is the actuator control input. For a Lyapunov energy function $L = \frac{1}{2}(\dot{y}^2 + \omega_0^2y^2)$, its derivative, evaluated along the trajectory of equation (3.4), can be derived as

$$\dot{L} = \dot{y}(\ddot{y} + \omega_0^2y) = -2\zeta\omega_0\dot{y}^2 + \frac{\dot{y}(d + u)}{m_0}. \quad (3.5)$$

We substitute a typical variable structure control law $u = -sgn(\dot{y})F_u$ into equation (3.5), where sgn is sign function and F_u is peak force generated by actuator. The result becomes

$$\dot{L} = -2\zeta\omega_0\dot{y}^2 + \frac{\dot{y}d - |\dot{y}|F_u}{m_0}. \quad (3.6)$$

Ideally, this control law forces the derivative of L negative definite when $F_u \geq ||d||$. Since L is positive definite, by the direct method of Lyapunov theory, system (3.4) is asymptotically stable at $(\dot{y}, y) = (0, 0)$. The control results will be discussed later in this Chapter.

active resonator control

Considering vibration control in engineering applications, passive resonator method is widely adopted. However, there also exist some limitations:

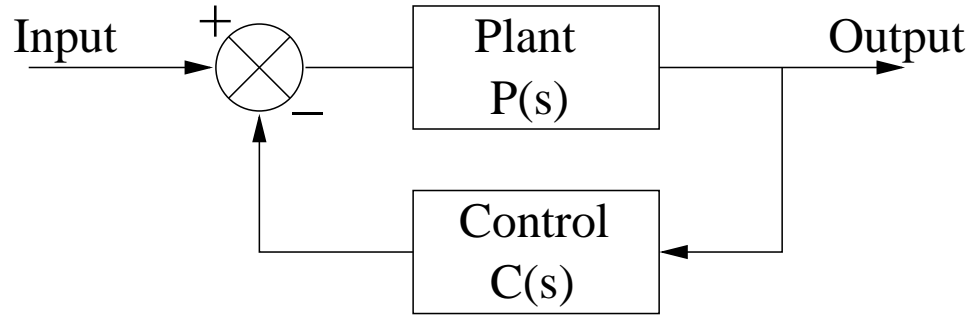


Figure 3.6: Block diagram of closed-loop control

- A passive resonator is very effective in suppressing noise/vibration at a tuned frequency while creating resonances at two other frequencies, which are not desired.
- Although it is possible to improve the control performance of a traditional resonator by fine-tuning the coupling effects between the resonator (active/passive) and the structure, the tuning process requires detailed model parameters of the structure and actuators, which is not practical in this study.

Therefore, active resonator control is adopted to import a virtual resonator in the closed-loop system, which is able to counteract the peak of plant vibration at its natural frequency. This idea is used for structure vibration control in FIV problem. Suppose the cylinder has a transfer function $P(s) = \frac{s}{s^2 + 0.25s + 125^2}$ with undamped natural frequency at $20Hz$, which is the natural frequency of cylinder in Figure 3.5. A possible control law may be $C(s) = \frac{s^2 + 50000s + 125^2}{s^2 + 1000s + 125^2}$ and the block diagram is shown in Figure 3.6. The simulation results are given in Figure 3.7. The experimental results will be given in this Chapter later.

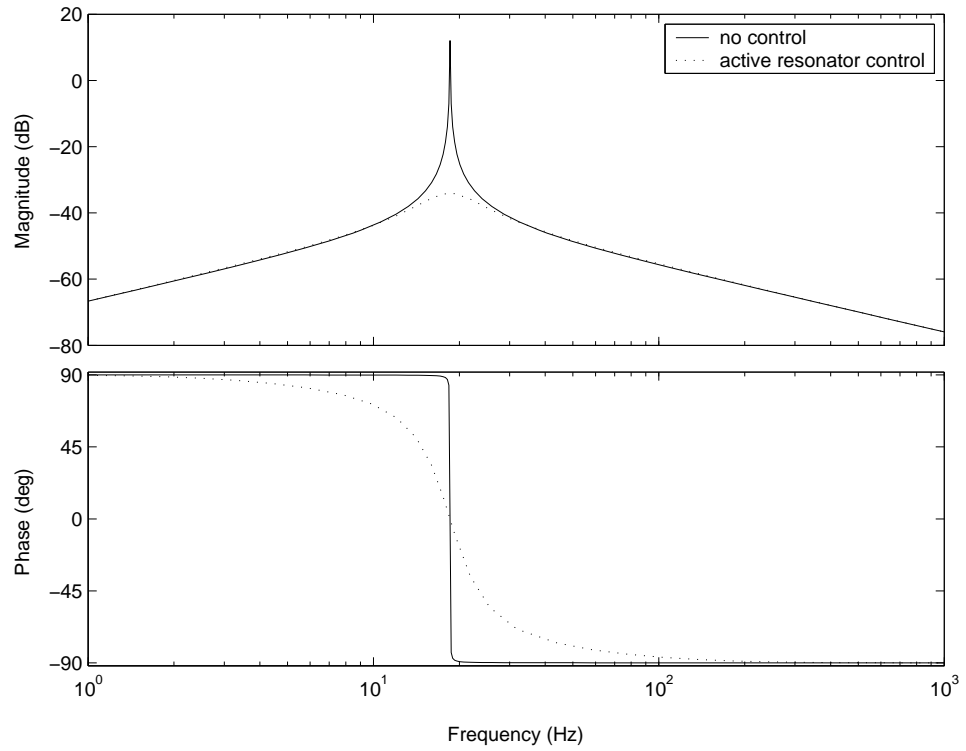


Figure 3.7: Bode diagrams of $P(s)$ by no control and active resonator control

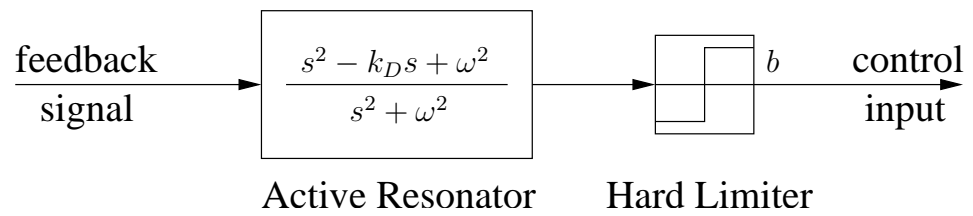


Figure 3.8: Proposed control method: multi-high-frequency perturbation

3.2.2 Proposed Control Method: multi-high-frequency perturbation

Considering the finding in the pre-design section 3.1.2, the high frequency perturbation approach based on the phenomenological model is preferred to design an effective controller for FIV problem in the lock-in regime. One merit of high frequency control is that since St_p is far away from the lock-in regime, the perturbation phase design can be neglected. Recalling the results in Figure 3.4, there is an optimal perturbation frequency region $St_p \in [0.5, 2]$. An active resonator with an optimal frequency St_p can be adopted. However, considering the limitations of active resonator in closed-loop feedback control for FIV, the negative damping term has to be used to keep the perturbation from the controller. This is also reasonable by analyzing the phenomenological model. In the wake oscillator, a nonlinear damping term is used to allow self-sustainable oscillation in the FIV model system. As a result, a similar measure to allow self-sustainable oscillation in the controller should be applied so that the controller can counteract FIV continuously. Furthermore, in order to prevent the controller from diverging due to negative damping, a hard limiter should also be added before feeding control input. In practice, it is possible to use a low-frequency resonator, which actually produces multi-high-frequency perturbation signals when integrated with a hard limiter. The proposed control method is shown in Figure 3.8.

3.3 Experimental Validation

3.3.1 FIV Control by Control Module: PID Tuning

In order to see practical feasibility of control module in Chapter 2, we also give an example for the case of PID tuning of flow induced vibration. The setup is the same as the closed-loop control in Figure 3.5. All the experiment are carried out in a closed circuit wind tunnel with a square test section of $0.6 \times 0.6m^2$ and a length of $2.4m$. A DSpace rapid control prototyping board is used to load control programs (designed in Matlab/Simulink) into the hardware so that it acts as the controller function for different applications. The control difficulty results from the uncertainty about the interaction between flow vortex shedding and structure vibration. However, as mentioned by Zhang et al. (2004), a set of PID parameters can be found to achieve high closed-loop control performance, which indicates satisfaction of the stable assumption. Although nonlinearity is involved when considering fluid dynamics, it is still of interest to see whether the optimal controllers described in this study works all the same.

Here, we test PID tuning controller and set initial PID parameters randomly as $\{1, 2, 3\}$. The estimation of J uses the vibration signal from the laser-vibrometer as shown in Figure 3.9 and reference signal is zero. After applying optimization for several minutes, the tuned parameters are $\{1.478, 1.480, 2.887\}$. The comparison of power spectrum density (PSD) plots for original and tuned parameters is shown in Figure 3.10. It is noticed that the optimal controller really gives improvement on the performance.

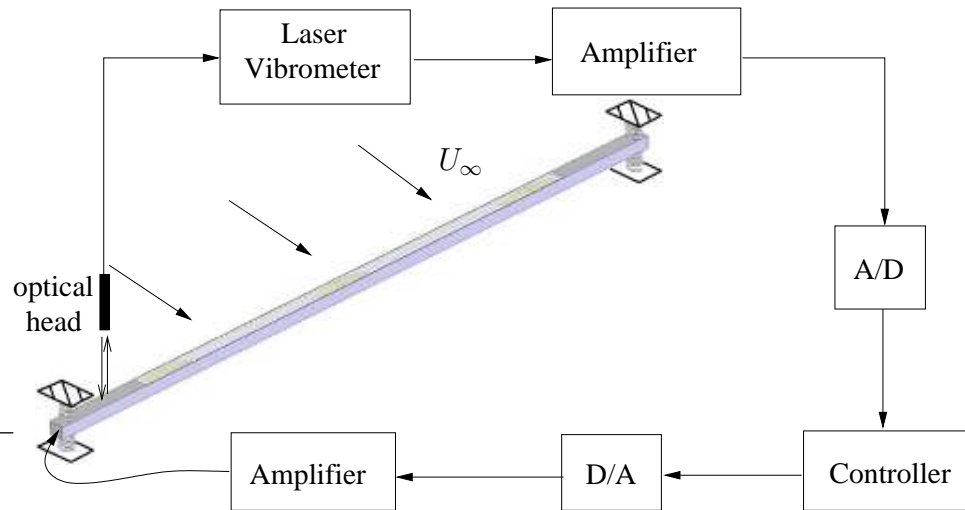


Figure 3.9: Experimental setup for validation of control module: PID tuning case

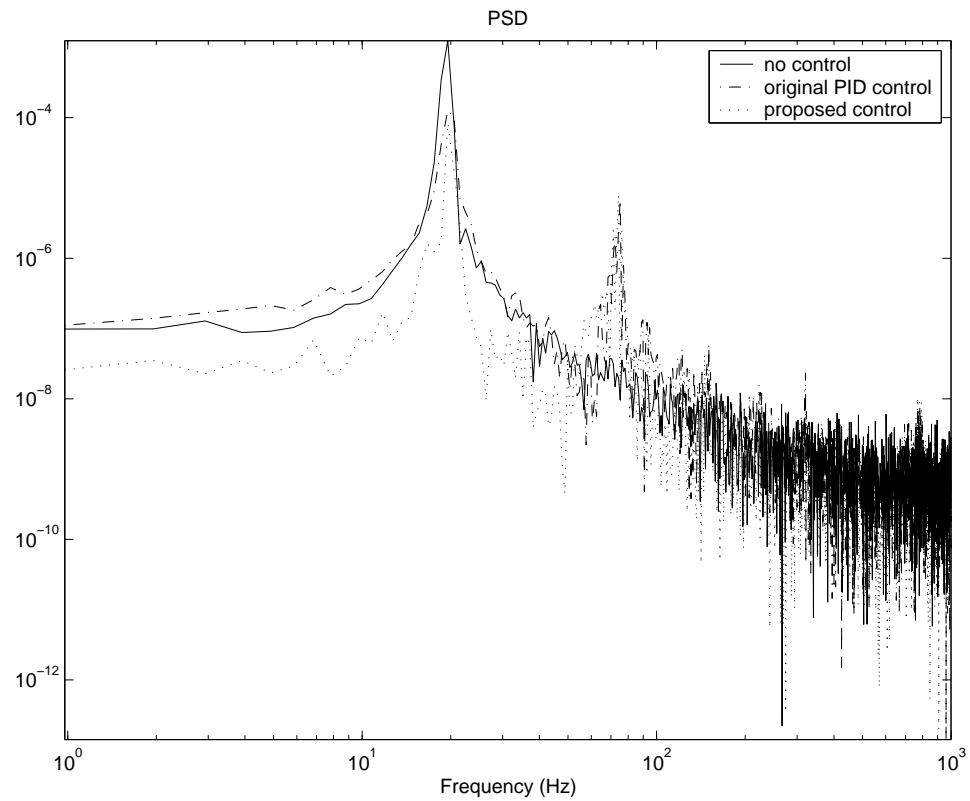


Figure 3.10: Power spectrum density of vibration signals for cases of no control, original PID control and proposed PID tuning control

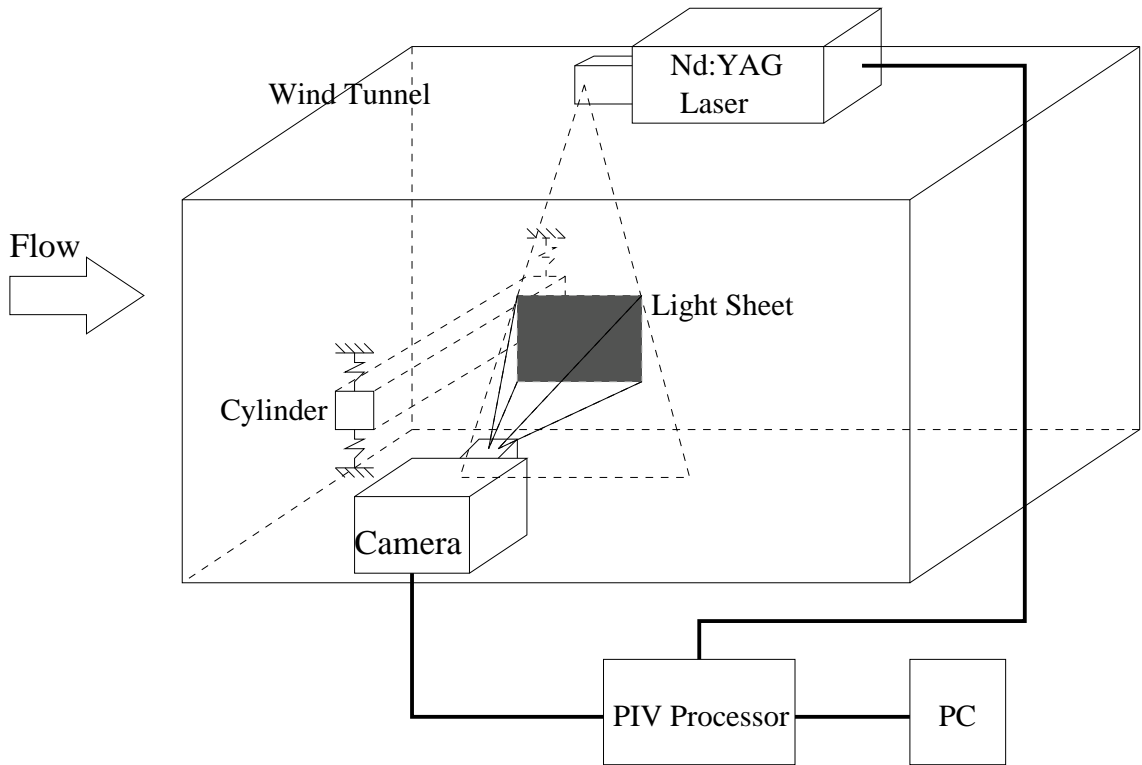


Figure 3.11: Experimental setup for PIV measurement

3.3.2 FIV and Vortex Control by Traditional Methods

Now, we look at the control results of FIV and vortex shedding by the controllers as discussed in Chapter 3. In this section, a new technique called Particle Image Velocimetry (PIV) is adopted to monitor the vortex behavior. Before revealing the results, a brief introduction is given for PIV process.

Particle Image Velocimetry (PIV) for Flow Measurement

The setup for PIV measurement is shown in Figure 3.11. The main advantages of PIV are: (1) non-disturbance on flow; (2) instantaneous velocity distribution for the whole wake field. The detailed theory of PIV measurement can be referred to the guide by Raffel et al. (1998). Here, a brief introduction is drawn based on the literature.

Particles in the fluid are illuminated by a sheet of laser, which is pulsed twice.

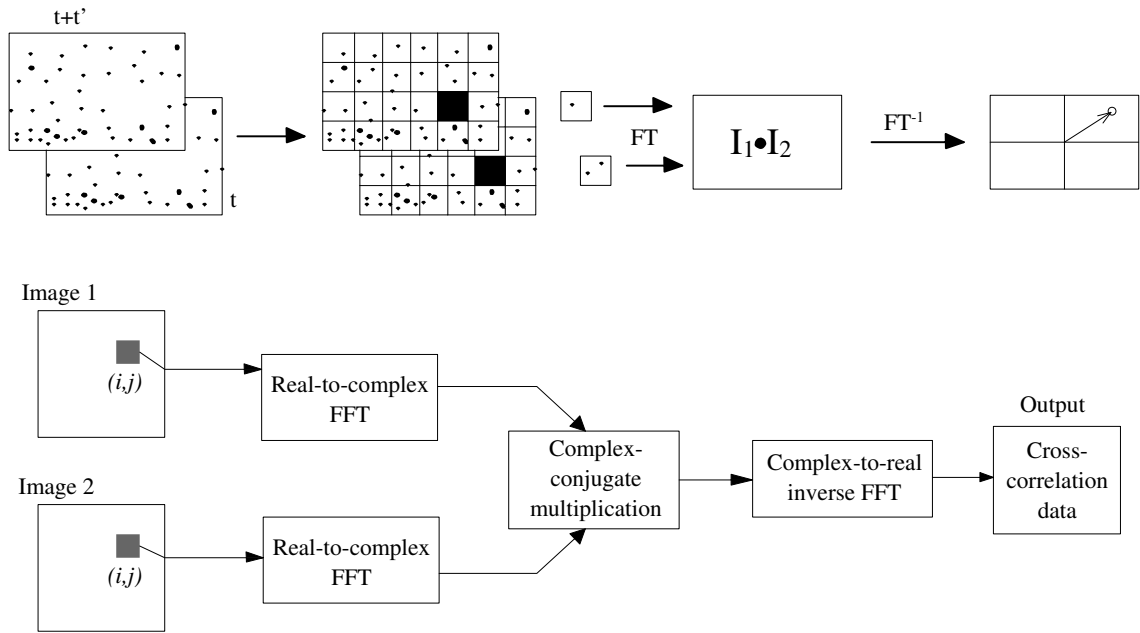


Figure 3.12: Technique outline of cross-correlation

The particles scatter light into a photographic lens of camera located at 90° to the sheet, so that its in-focus object plane coincides with the illuminated slice of fluid. Images are formed on the video array, which are then postprocessed by the computer. Since the fundamental components of velocity are length and time, it is supposed to be a direct method for PIV to measure velocity. However, PIV usually can only trace the particle's movement, which is different from air fluid particle. Mostly, we use a kind of paraffin oil from shell, which will be vaporized and then, mixed with air flow. It requires two properties for the tracing fluid application. On one hand, diameter of vaporized oil particles should be small enough to follow wind flow. On the other hand, the reflection ratio of the particles must be good enough for camera to catch. Instead of measuring the air flow velocity directly, PIV traces the inline moving particles', which indicates that it is an indirect technique. The main technique outline to get velocity vectors is shown in Figure 3.12, which is called cross-correlation process. In practice, some additional processes can also be applied to improve the accuracy, such as validation process and filtering process.

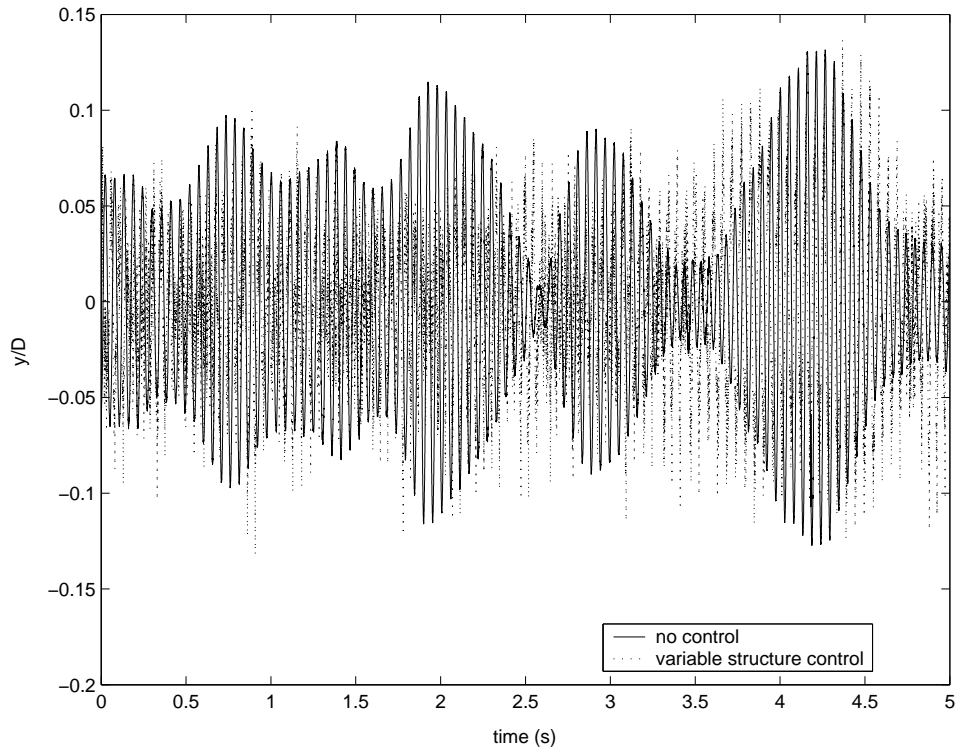
Variable Structure Control

Having been discussed in section 3.2.1 of Chapter 3, one variable structure controller $u = -sgn(\dot{y})F_u$ is theoretically proven to be suitable for FIV problem. We test the controller in the lock-in condition. The experimental results for structure vibration are shown in Figure 3.13. For the wake field, Figure 3.14 and Figure 3.15 show the contours of normalized spanwise vorticity, $\omega_z^* = \omega_z D/U$, under the conditions of no control and with variable structure control respectively. The PIV vorticity contours in this study are all instantaneous, the cutoff level is about 7% of maximum ω_z^* , and the uncertain estimation coefficient is about 9%. Also, the vortex circulation (Γ) is estimated as in (Zhang et al., 2004),

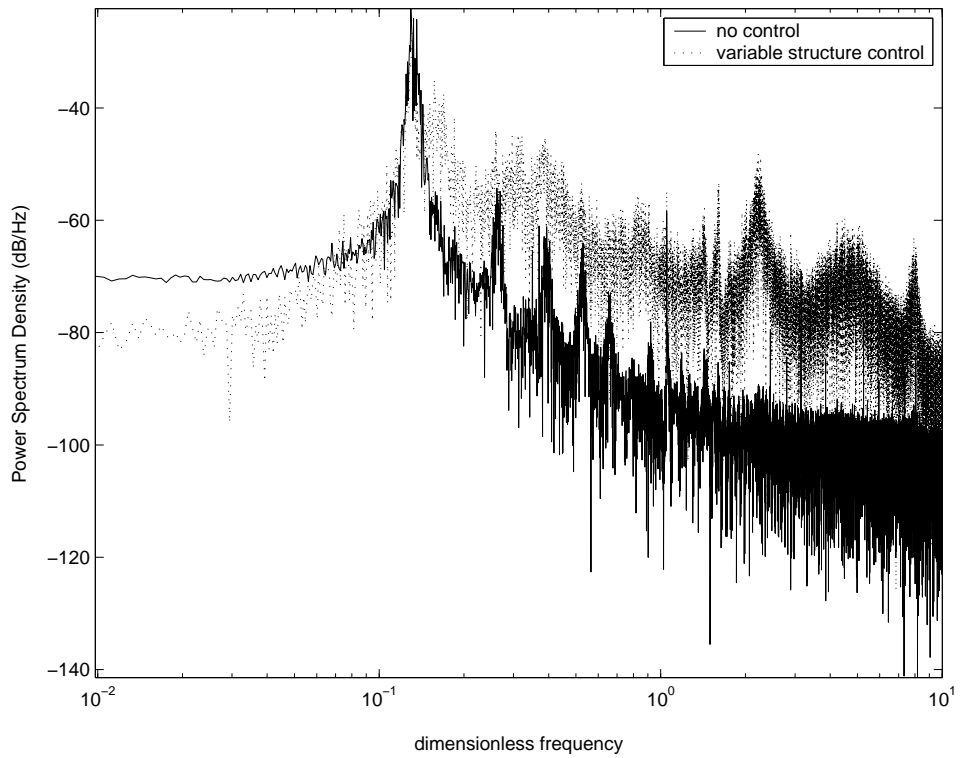
$$\frac{\Gamma}{UD} = \sum_{i,j} (\omega_z^*)_{ij} \frac{\Delta A}{D^2}, \quad (3.7)$$

where $\Delta A = \Delta x \Delta y$.

It is found that this ideal design does not work perfectly. The rms reduction level of structure vibration is only around 24.4%. Considering the peak level in the Figure 3.13(b), unnecessary peaks have overwhelmed the peak in the uncontrolled case. This phenomenon results from a commonly known chattering problem in variable structure control (Guldner and Utkin, 2000). In practical applications, unmodeled dynamics in closed-loop system often prevent the actuator from responding to the control demand instantaneously, and the imperfect control signal will cause oscillations in the system. This effect causes a local unstable condition at the equilibrium point. On accounting of the control effect on the wake field, by comparing Figure 3.14 and Figure 3.15, the spanwise vorticity level has been reduced and the reduction of vortex circulation is around 10%.



(a) time domain response



(b) power spectrum density

Figure 3.13: Experimental results of structure vibration by no control and variable structure control

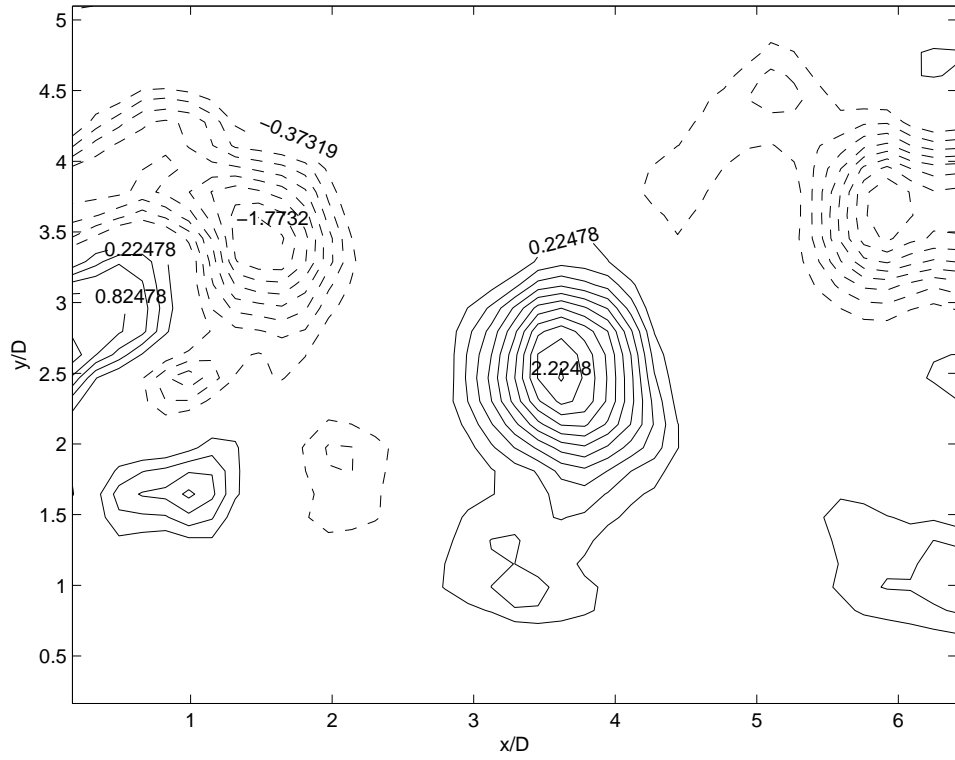


Figure 3.14: Contour of spanwise vorticity from PIV measurement: without control, ”-” positive, ”- -” negative

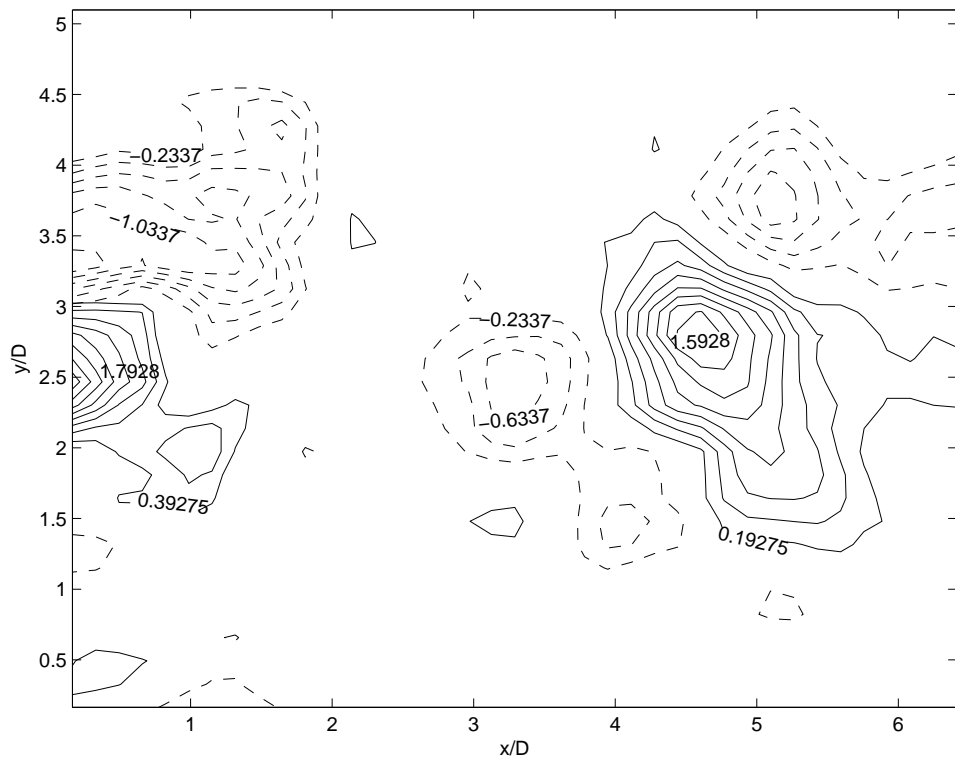


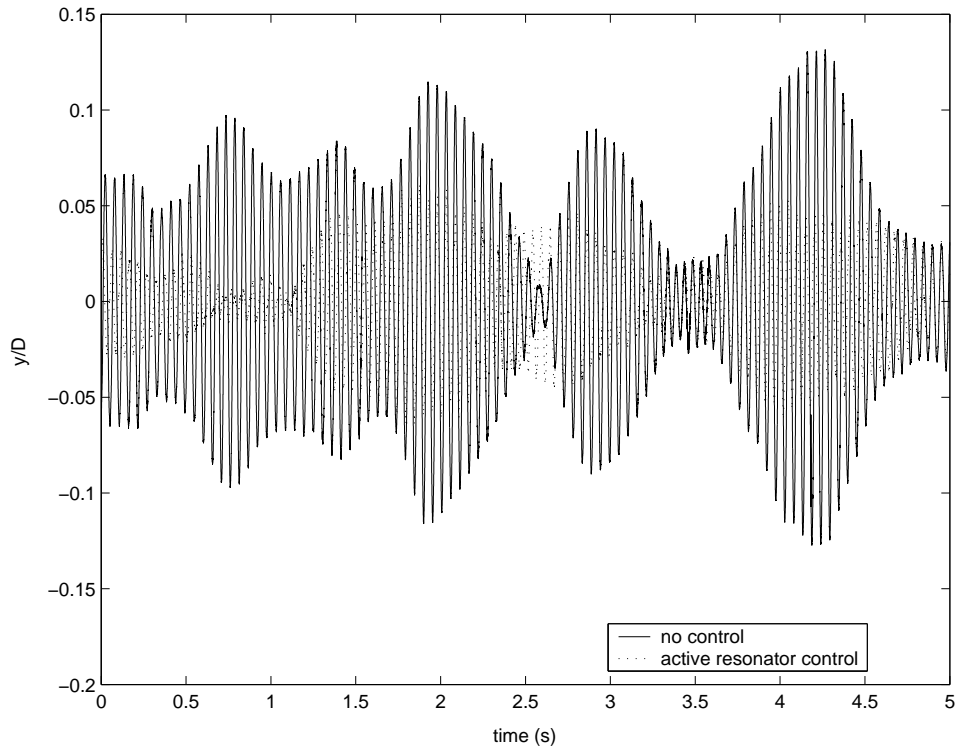
Figure 3.15: Contour of spanwise vorticity from PIV measurement: with variable structure control, ”-” positive, ”- -” negative

Active Resonator Control

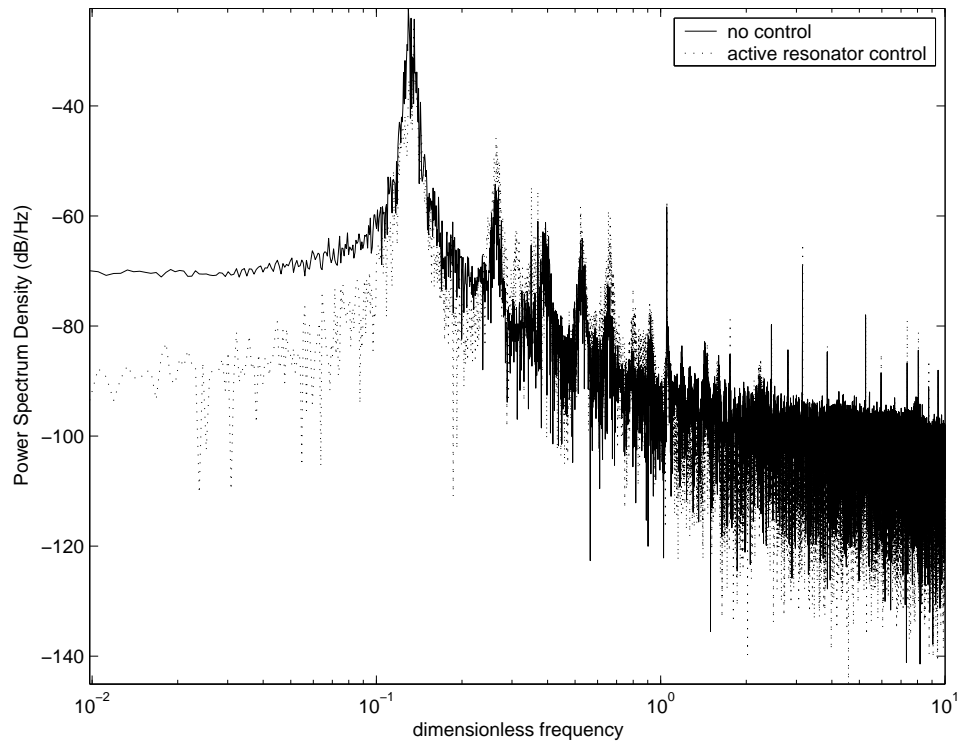
Following the same experiment setup, the active resonator controller designed in section 3.2.1 is also tested. The experimental results for structure vibration are shown in Figure 3.16. The rms reduction value of structure vibration velocity is 49%, which is not quite satisfactory and even worse than those by open-loop control in section 3.1.2. By observation, the resonator frequency matches the natural frequency of structure vibration, but also coincides with shedding frequency of wake vortex. The unknown interaction between the control signal and flow shedding may weaken original control effect on the structure. In this experiment, it is found that control signal even increases the spanwise vorticity level and gives a 7% rise of vortex circulation by comparing Figure 3.14 and Figure 3.17. Furthermore, since the objective of this method is only to suppress structure vibration, flow excitation will always exist. While vibration amplitude is approaching zero, due to feedback control, the active resonator also generates "near zero" control input on the structure. Thus, flow excitation will dominate the control effect again and consequently structure will tend to vibrate. The model uncertainty limits the performance of active resonator control.

3.3.3 Multi-High-Frequency Perturbation Method

In the section, we test the proposed multi-high-frequency perturbation method, which is based on the Conjecture 3.1.1 in section 3.1.2. As in Figure 3.8, the design factors are k_D and ω for the active resonator, and bound b for the hard limiter. Several experiments are conducted to assess the control effect of each parameter. In all the experiments, the testing environment is set at the lock-in regime, where $St_s \approx St_0 = 0.13$ and $Re \approx 1800$. Structure vibration velocity is the feedback signal.



(a) time domain response



(b) power spectrum density

Figure 3.16: Experimental results of structure vibration by no control and active resonator control

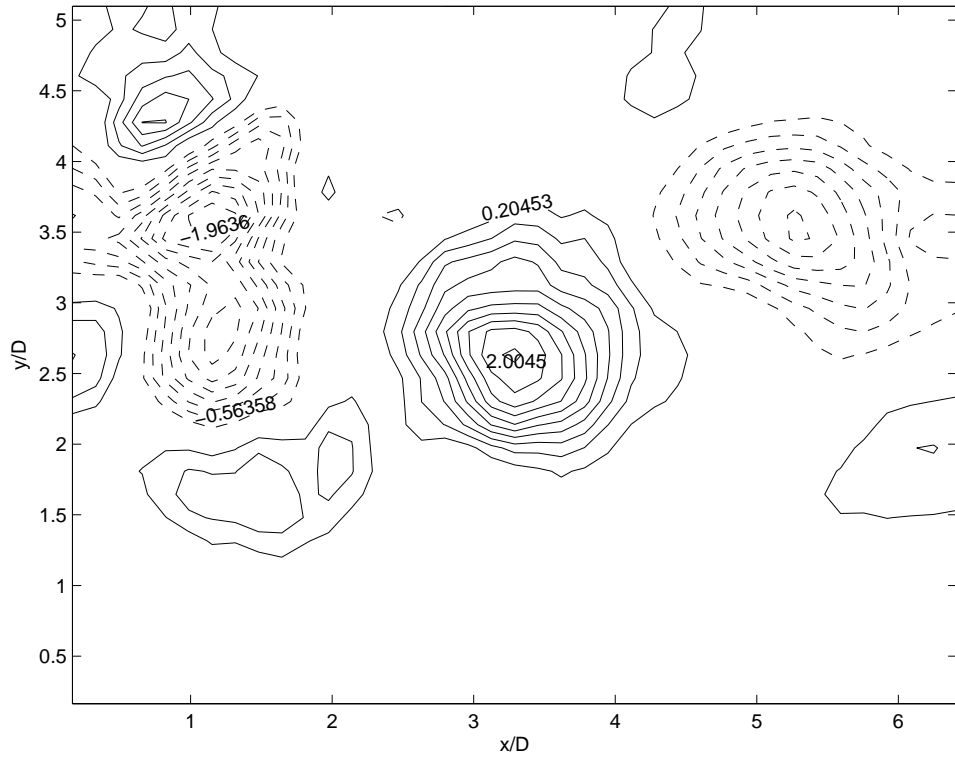


Figure 3.17: Contour of spanwise vorticity from PIV measurement: with active resonator control, "-" positive, "--" negative

We use the rms reduction values of both structure velocity and wake velocity signals, for the cases without control and with the proposed control method, to evaluate control performance as shown in Figure 3.18-3.20. Most results demonstrate better control performance than those achieved by other methods studied in the work. The best performance of suppressing structure vibration is over 70%. Considering individual parameter effects, from Figure 3.18, a larger k_D gives more improved result due to its contribution on increasing controller's damping. From Figure 3.19, there also exists certain optimal region for the selection of ω , which agrees well with the findings on the pre-design testing using open-loop perturbation in section 3.1.2. Closed-loop control is more steady and robust with the variation of ω . From Figure 3.20, it is seen that a larger bound b means more energy can be used to compensate FIV system energy, and in turn better reduced result is found.

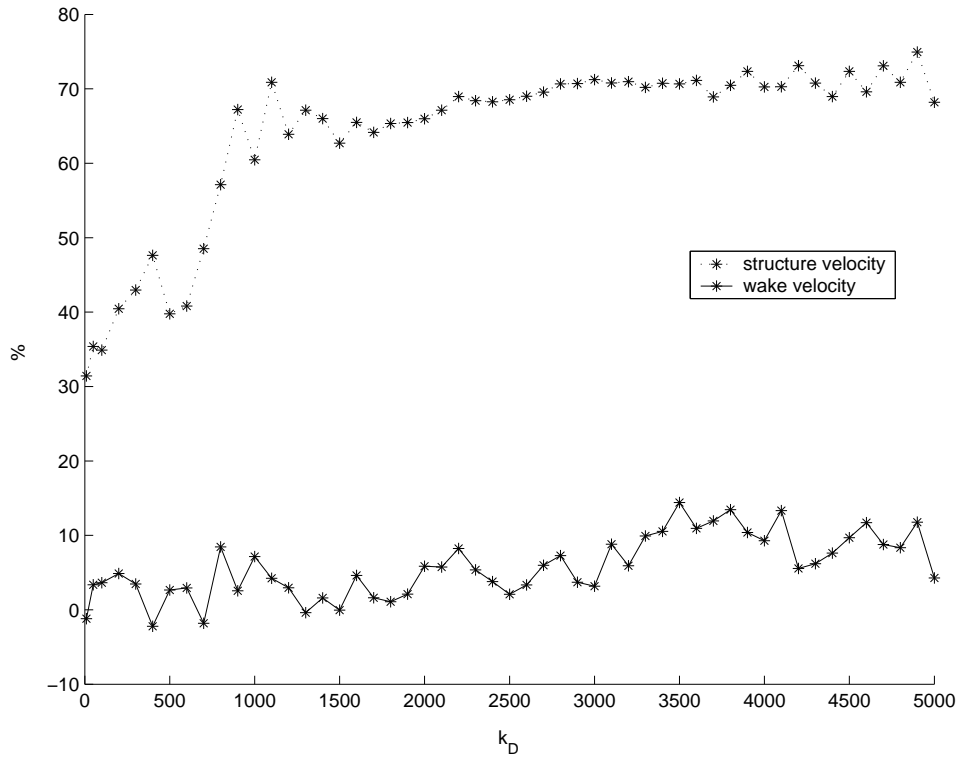


Figure 3.18: k_D effect on control performance with $St_\omega = 0.02$ and $b = 0.095$: RMS reduction values (percentage)

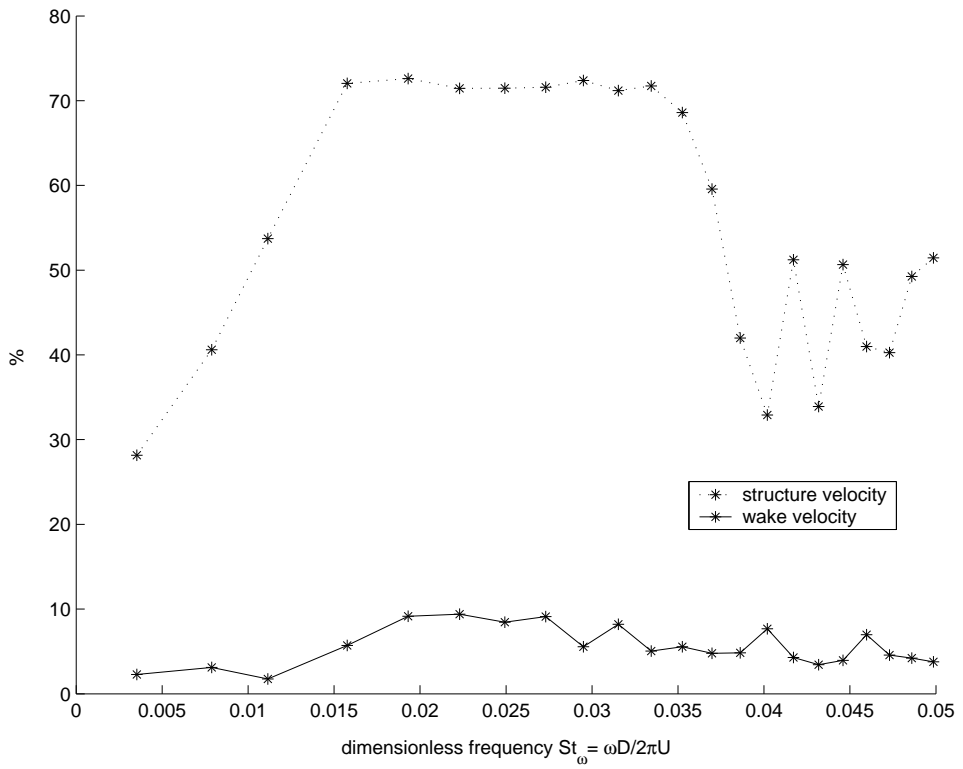


Figure 3.19: ω effect on control performance with $k_D = 3500$ and $b = 0.095$: RMS reduction values (percentage)

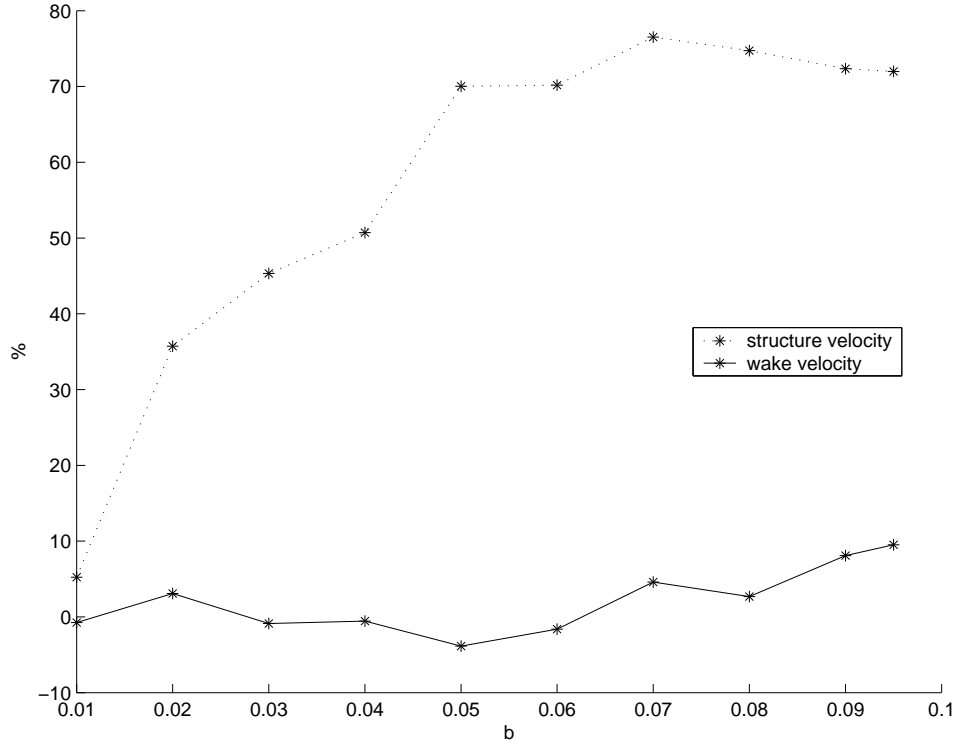
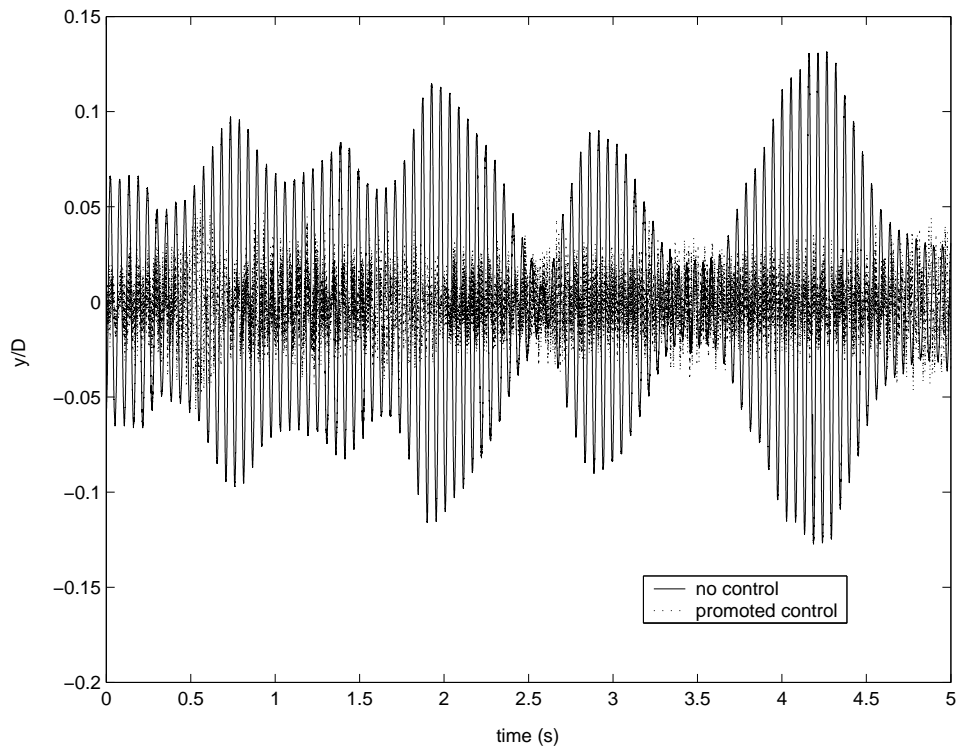


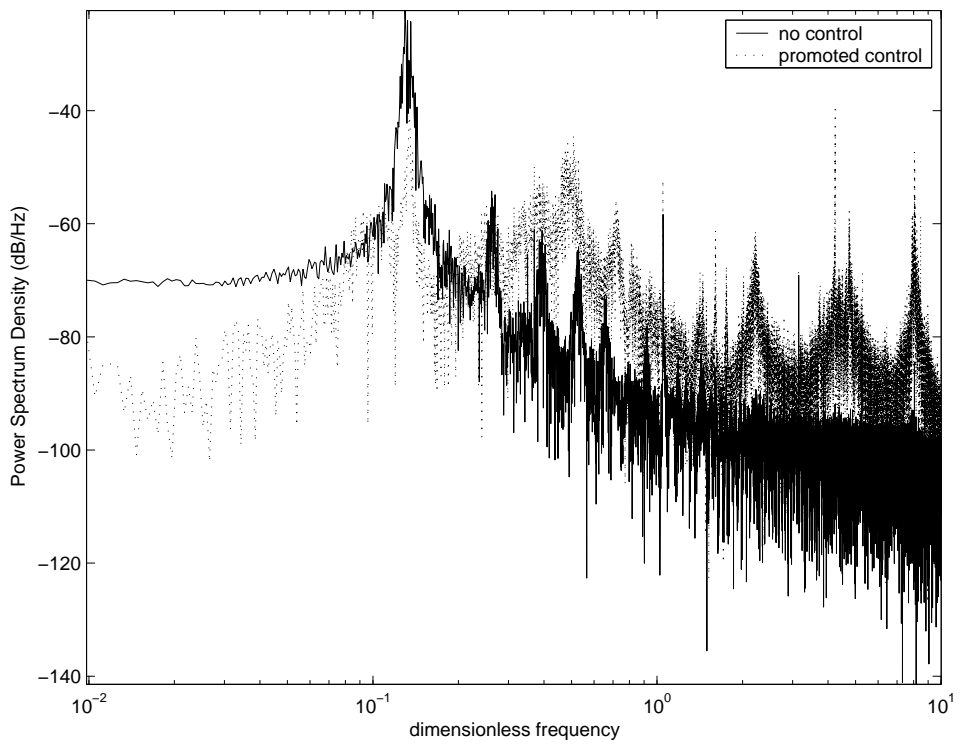
Figure 3.20: b effect on control performance with $k_D = 3500$ and $St_\omega = 0.02$: RMS reduction values (percentage)

Merit: interpretation of phenomenological models

By now, an effective controller has been found by using the phenomenological model as a design guide. Moreover, together with section 3.1.2, this controller also verifies Conjecture 3.1.1 derived from the model study. Take the proposed controller with $(k_D, St_\omega, b) = (3500, 0.02, 0.095)$ as an example. Figure 3.21 gives experimental results of structure vibration. Clearly, in Figure 3.21(b), there are multi-high-frequency responses around the region $St_p \in [0.5, 2]$, which has been considered as optimal perturbation frequency region in Figure 3.4. Furthermore, considering Equation (3.3) for the wake oscillator damping term, if $\omega_p = \omega_s$, which means perturbation frequency is equal to shedding frequency, then this damping term will be $\frac{A_p^2}{w_0^2} - 1$. If perturbation amplitude A_p is moderately small, then $\frac{A_p^2}{w_0^2} < 1$ gives a negative damping term in all situations. This will increase wake oscillation, which



(a) time domain response



(b) power spectrum density

Figure 3.21: Experimental results of structure vibration by no control and proposed control

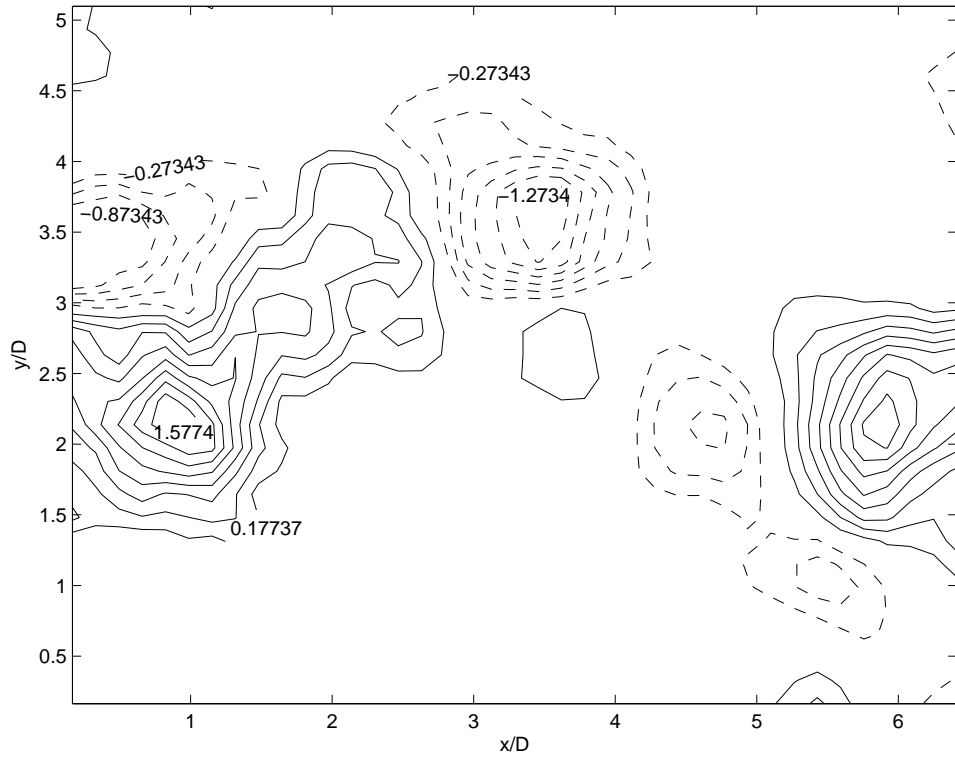


Figure 3.22: Contour of spanwise vorticity from PIV measurement: with multi-high-frequency perturbation method, "-" positive, "--" negative

also agrees with experimental analysis about St_p around St_s by Cheng et al. (2003). As for the wake field, the contour of spanwise vorticity is shown in Figure 3.22. The overall level is reduced by comparing Figure 3.14. The vortex circulation Γ is also reduced by around 25%.

Robustness Study of Proposed Control

It is very difficult to study controller robustness for different flow conditions. Here, we give a general attempt to verify whether the proposed controller is always working within certain flow velocity range. Figure 3.23-3.26 show the power spectrum densities comparison of non-controlled and controlled cases for different Reynolds numbers. In this research work, at the lock-in condition, $Re = 1800$. The tested flow conditions are $Re = 1000, 2500, 3400, 4100$. Improved results are found only for those Reynolds numbers, which are near the resonant condition. The reductions

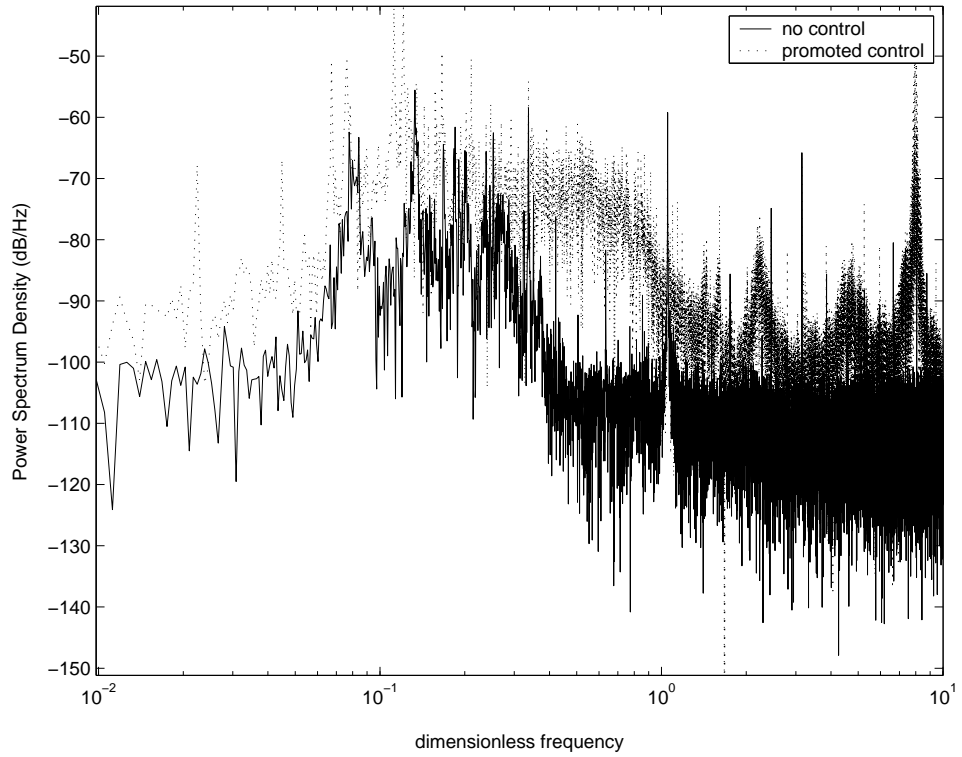


Figure 3.23: Power Spectrum Density (PSD) comparison of structure vibration under conditions without control and with proposed control ($Re=1000$)

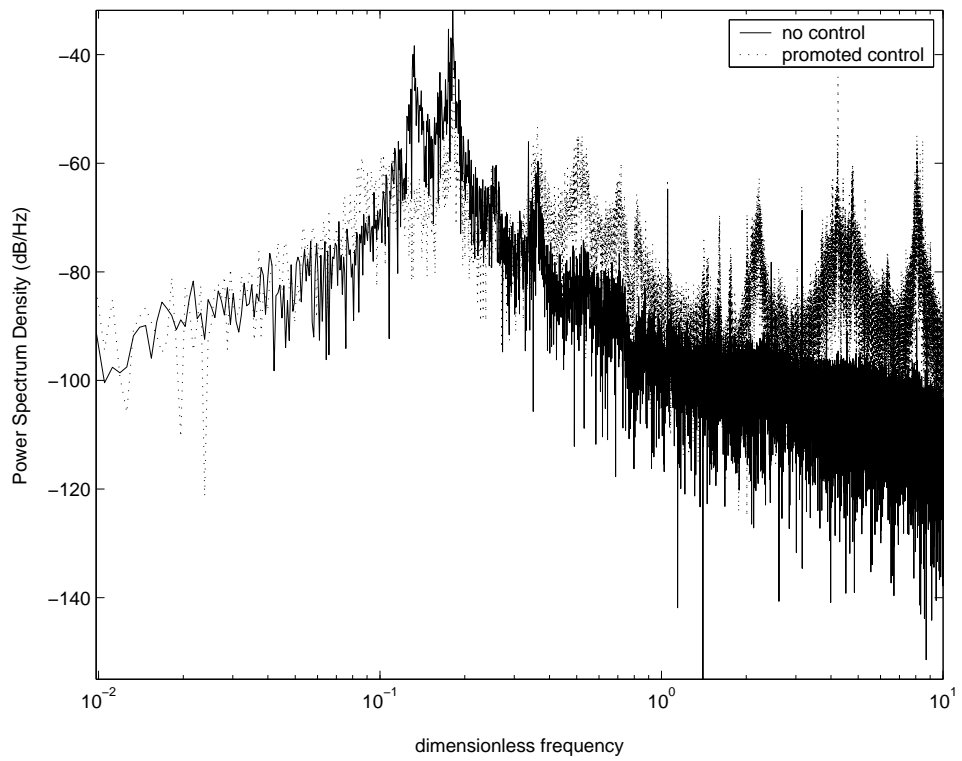


Figure 3.24: Power Spectrum Density (PSD) comparison of structure vibration under conditions without control and with proposed control ($Re=2500$)

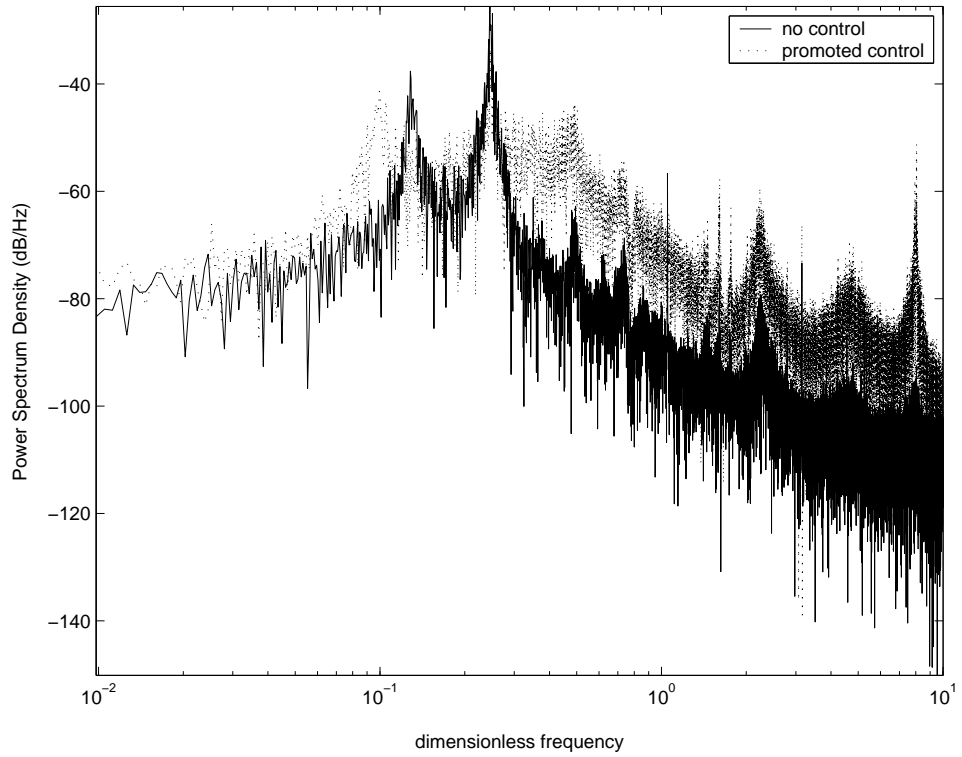


Figure 3.25: Power Spectrum Density (PSD) comparison of structure vibration under conditions without control and with proposed control ($Re=3400$)

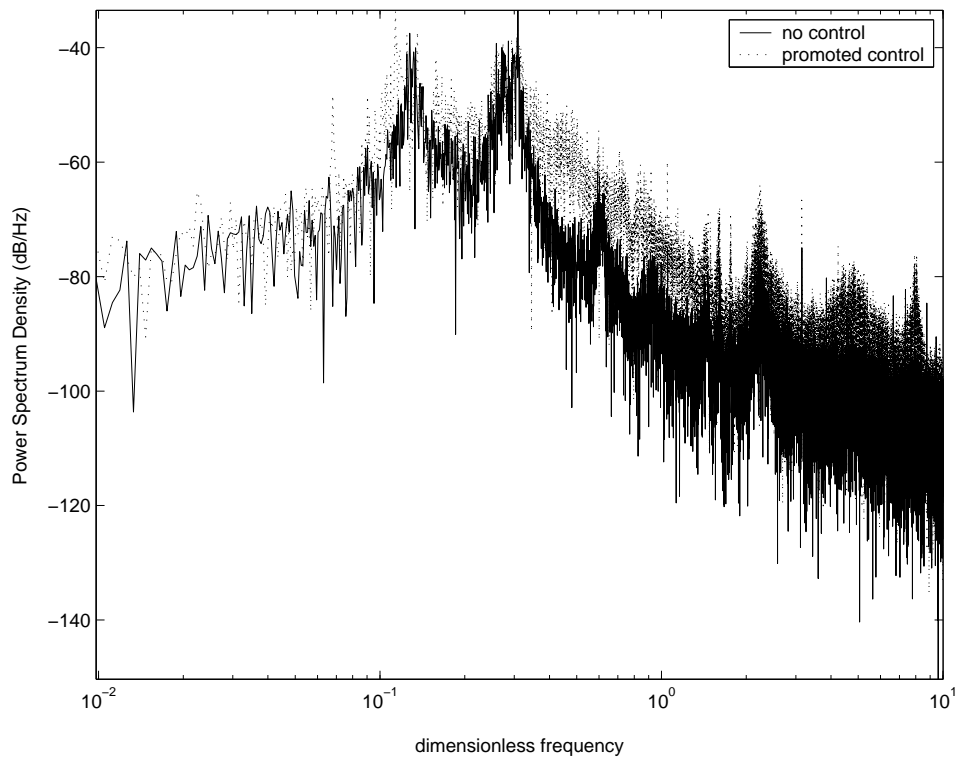
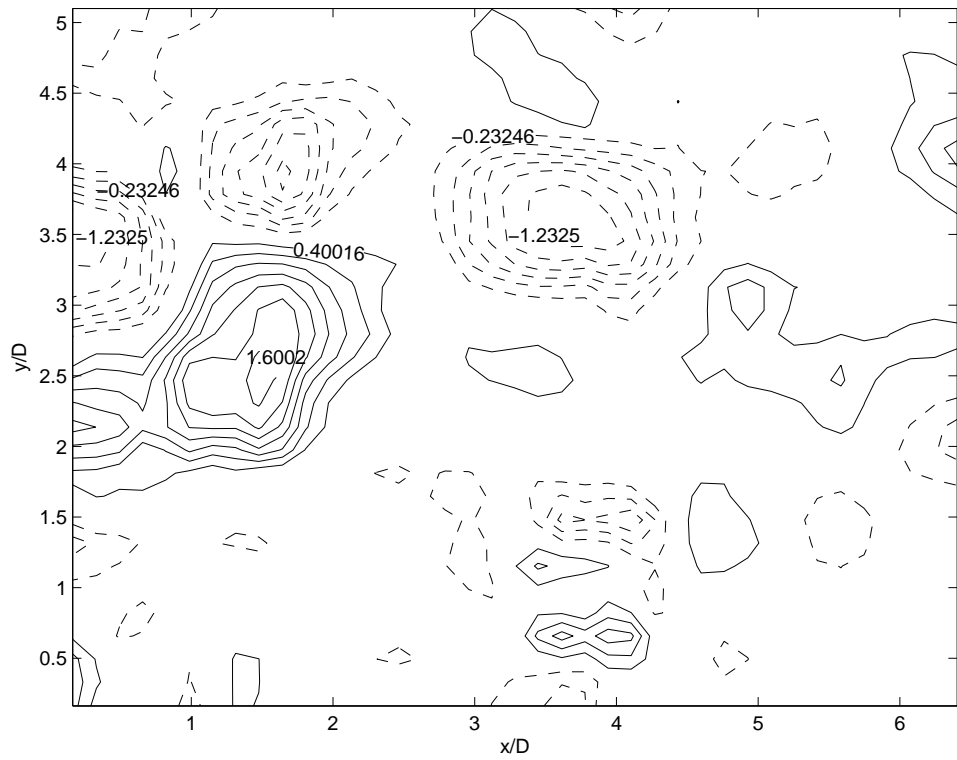


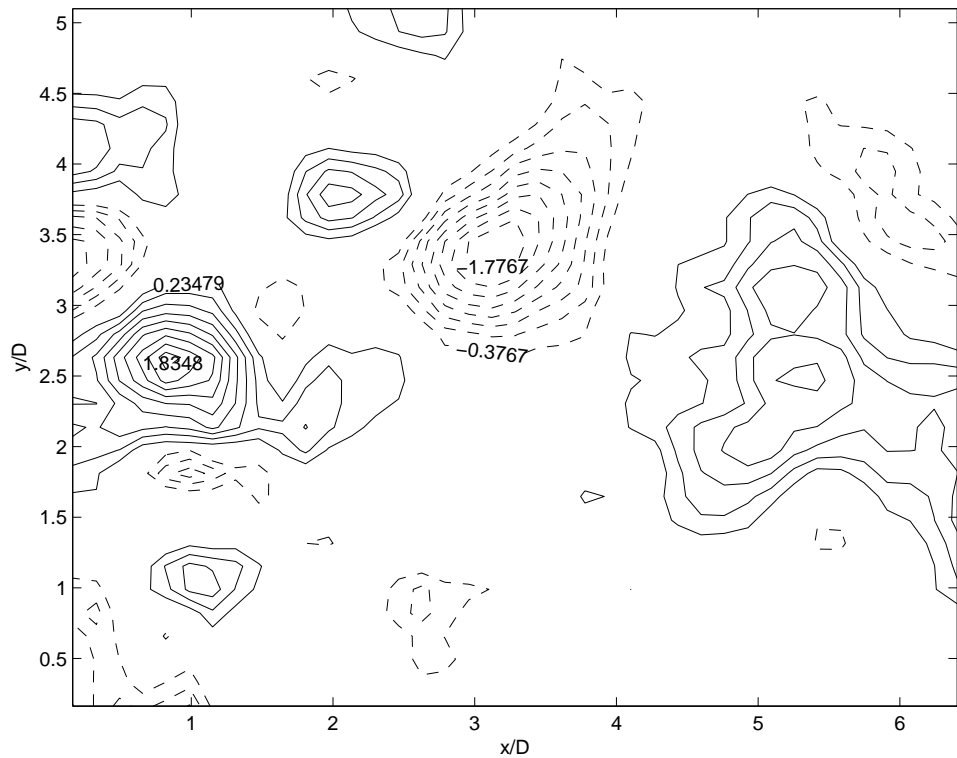
Figure 3.26: Power Spectrum Density (PSD) comparison of structure vibration under conditions without control and with proposed control ($Re=4100$)

of PSD peaks can be found in Figure 3.24 and 3.25. The rms reduction values are around 36% and 38% respectively. The spanwise vorticity contours in Figure 3.28 and 3.29 also give reduced results due to the proposed control. And vortex circulation reductions are 17% and 25% respectively. However, for Figure 3.23 and Figure 3.26, control performances are not satisfactory. The results of Figure 3.23 are obtained at a low Reynolds number, and under that condition, flow energy is not sufficient to be compensated by control input. Thus, the surplus energy of control input generated by the negative damping term will be transferred to cylinder and make it vibrate. Then, the wake response will be more mystery. As shown in Figure 3.27, the spanwise vorticity even increases. On the other hand, the results of Figure 3.26 are obtained at a high Reynolds number. Although perturbation makes some contributions on the reduction of vortex shedding as shown in Figure 3.30, the wake flow is still strong enough to excite cylinder due to the strong wind background. Furthermore, the wake oscillator model is used to represent the flow and structure interaction in near the lock-in regime. For the cases of $Re = 1000$ and $Re = 4100$, the phenomenological model may not be applicable again. Thus, it is reasonable that perturbation may not work again.

It is also observed by Krenk and Nielsen (1999) that a small variation in parameters of model can cause larger change in experiment than what is predicted by the model. The model is therefore quite sensitive to parameter variation. Although the proposed controller is based on the study of such a sensitive model, it still achieves moderate robustness near the resonant region, despite there are some deficiencies on the control performance when flow condition is far away from the resonant region.

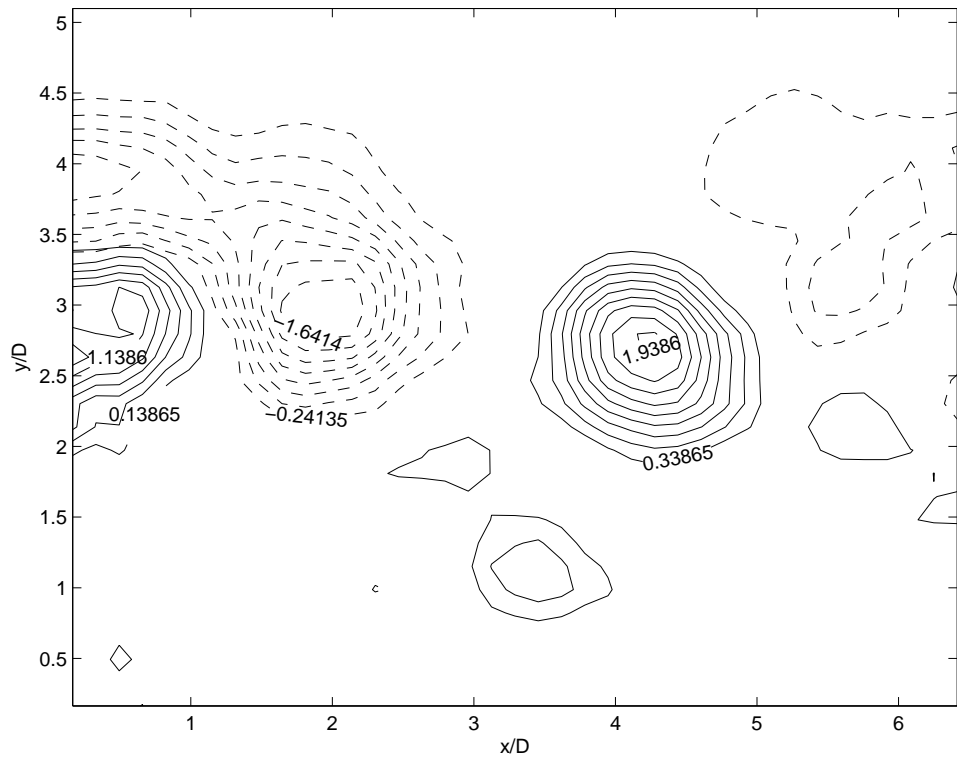


(a) non-controlled contour

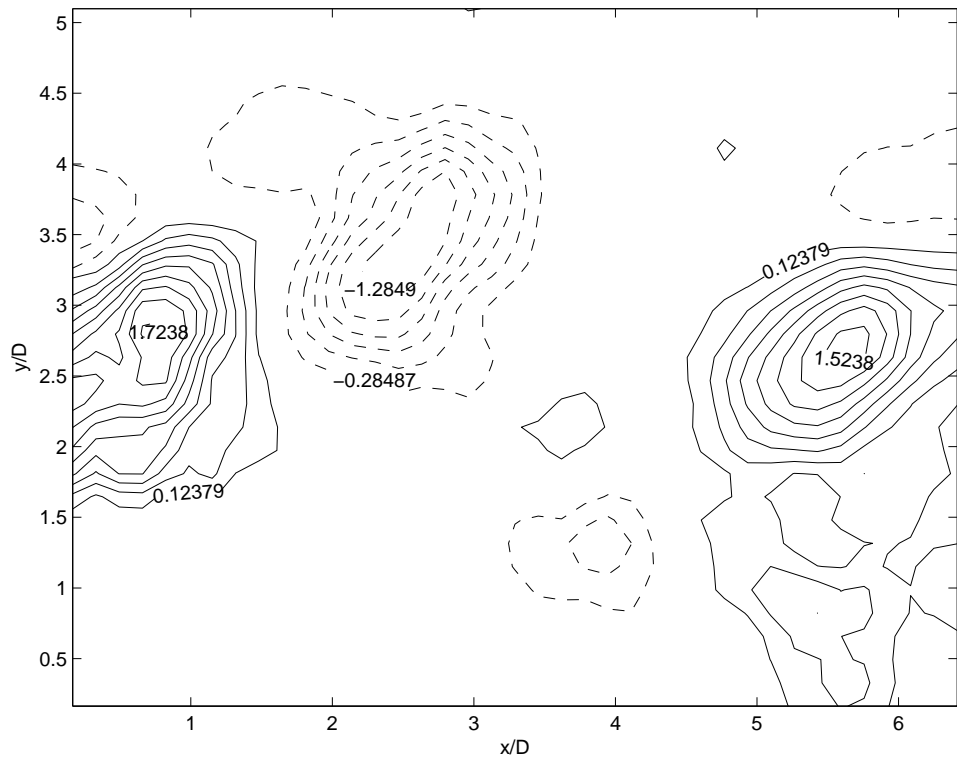


(b) controlled contour

Figure 3.27: Contours of spanwise vorticity from PIV measurement, "-" positive, "--" negative (Re=1000)

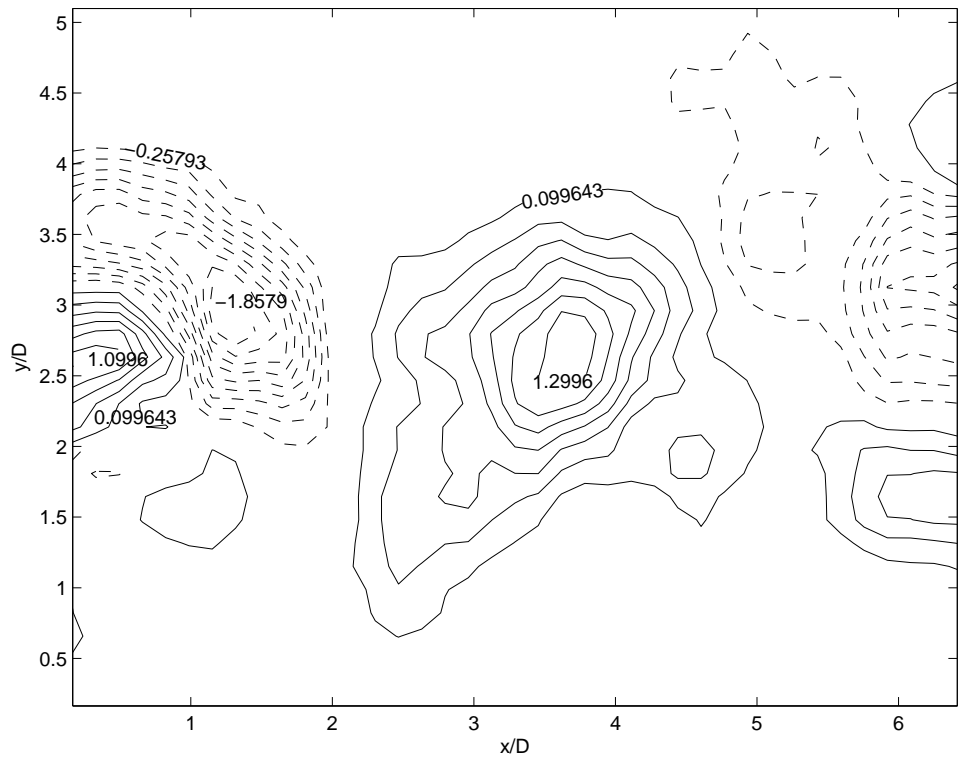


(a) non-controlled contour

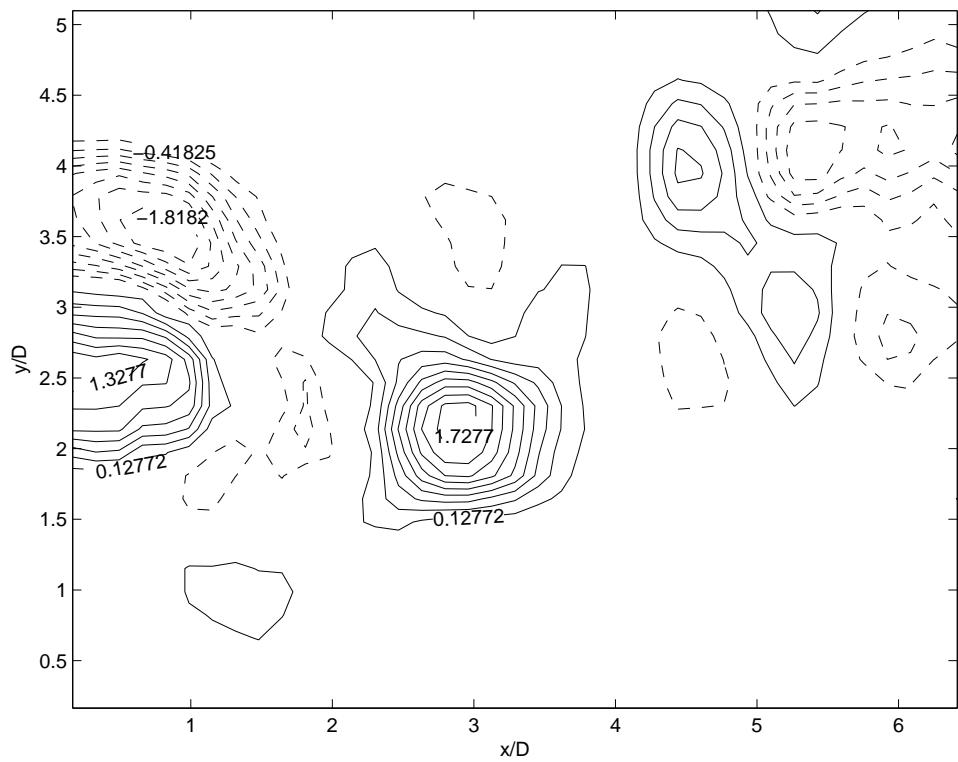


(b) controlled contour

Figure 3.28: Contours of spanwise vorticity from PIV measurement, "-" positive, "--" negative (Re=2500)

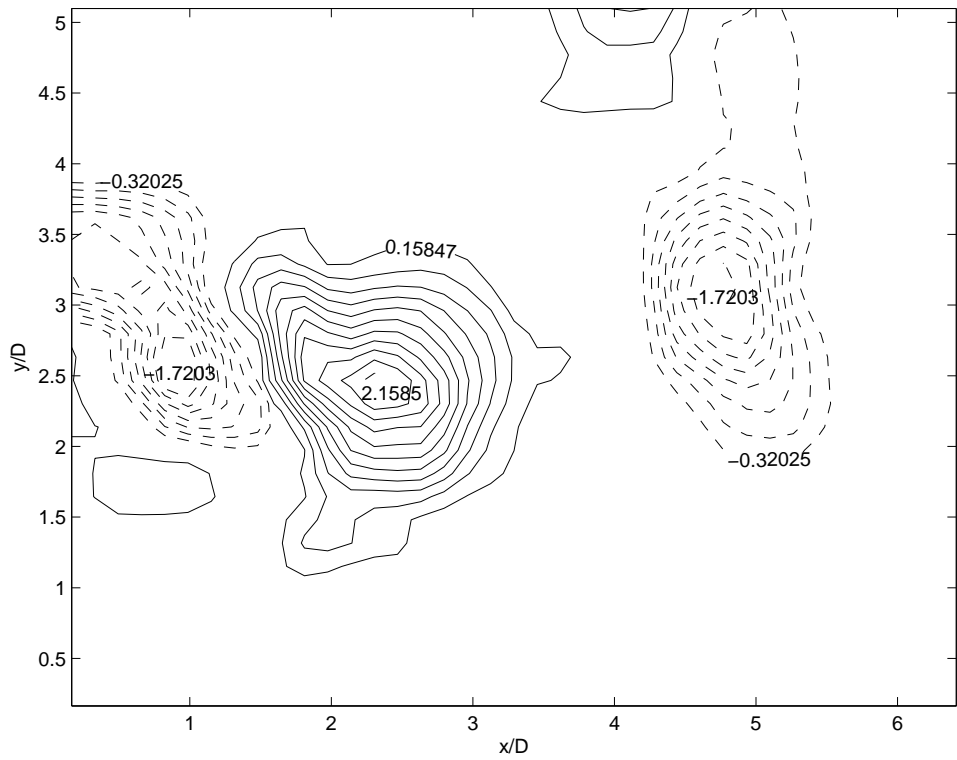


(a) non-controlled contour

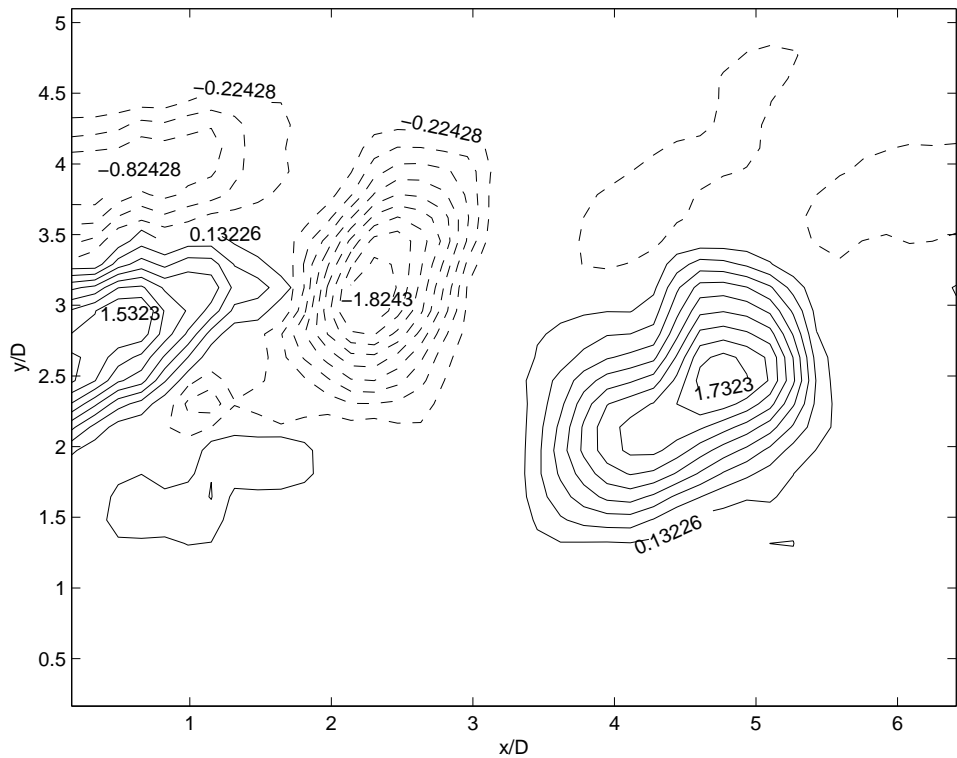


(b) controlled contour

Figure 3.29: Contours of spanwise vorticity from PIV measurement, "-" positive, "--" negative (Re=3400)



(a) non-controlled contour



(b) controlled contour

Figure 3.30: Contours of spanwise vorticity from PIV measurement, "—" positive, " - -" negative ($Re=4100$)

CHAPTER 4

CONCLUSIONS AND FUTURE WORKS

4.1 Controller Development

Considering the difficulty of control problem for uncertain system, this research work makes contributions on the development of the model-independent controller.

4.1.1 Self-Tuning Design

One approach is mathematically based. Basically, the proposed control module consists of two parts: stabilization mechanism and optimization mechanism. The former one is originated from the PID tuning method and further extended to high order versions with the help of singular perturbation tool. One credit for the mechanism is that closed-loop stability can be ensured while the only assumption and requirement is the open-loop stability of the plant. The optimization mechanism is also independent on the plant parameters while only requiring the feedback signal to estimate the controller parameter gradients by simultaneous perturbation algorithm, which can also be regarded as a random-searching scheme. The function of the mechanism is to find the controller that can achieve optimal performance. The validation of this control module has been shown by mathematical proof, numerical simulation, and experiment. Since the control module is model-independent, another credit is that it can be integrated with any other adaptive controller when there is an online identification process for plant parameters.

4.1.2 High-Frequency Perturbation Effect

Another approach is based on the study of FIV control experiment. One perturbation technique developed in the literature is used as the control input. As the testing object, FIV does not have a simple and analytical model for controller design to present knowledge extent. Traditional control methods are tested for FIV, such as variable structure control and active resonator control. However, neither of them produces satisfactory results. One phenomenological model, using two-oscillator idea, is employed to study the controller development. Based on the model, experimental studies at the lock-in condition demonstrate the possibility to suppress the vortex by increasing the damping term of the model through a perturbation input at a high frequency range well-exceeding resonant frequency of structure. This also agrees well with the findings of others who try to control flow by acoustic excitations. Therefore, besides the control module, one additional controller composed by a low-frequency active resonator with a hard limiter is found to have the best performance in the FIV control compared with those traditional control methods. Especially near the lock-in regime, the proposed high-frequency perturbation method even gives moderately robust property.

4.2 Design Rationale: one useful 'model'

Although this thesis concentrates on the model-independent controller design, when discussing the case study of FIV control problem, this work first links a phenomenological model to the issue. From the point of view of controller design, the model makes contributions on finding out an effective control method, a so-called multi-high-frequency perturbation method. On the other hand, from the point of view of

model validation, this study provides evidence that experimental results agree with the predication on high-frequency effects on FIV, which verifies the eligibility to use such a phenomenological model in practical control application. This study leads to a brand new direction to understand and control FIV problem from a useful 'model', even if the model is not physically developed. Compared with traditional modeling approaches, such as solving Navier-Stoke equations, the phenomenological model is much easier to handle.

4.3 Comments on Future Works

Controller Improvement

This research work has already provided a set of applicable control methods for uncertain systems based on the model-independent purpose. Indeed, there are some aspects that can help to improve the performance of those controllers. Having been shown in the section 2.1.4, generalized tuning is possible for the stabilization mechanism design. In other words, more flexible design options can be made using the tuning technique. For example, the pseudo observer tuning can employ another type of filter rather than Butterworth filter in this study. Furthermore, for the optimization mechanism design, other methods of random-searching-based gradient estimation can be developed rather than the simultaneous perturbation, such as genetic algorithm searching.

As for the improvement of control methods for FIV, efforts on both algorithmic and technical aspects can be made. For instance, considering the improvement of variable structure control, how to eliminate the chattering problem can be a good approach. As for the control technique, it is conjectured that if the perturbation

created by actuators is imposed on the four angles of cylinder rather than only on the side surfaces, the performance might be more satisfactory since it interferes with flow separation points. Of course, for the multi-high-frequency perturbation method, other approaches can also be used to generate the desired signal, e.g. different formats of the active resonator in Figure 3.8.

Integration of Control Module

One credit of the control module developed in this study is the compatibility during implementation. One interesting approach for further attempt is to integrate the control module with other adaptive and optimal controllers for uncertain systems, such as backstepping, H_2 control.

FIV Modeling Issue

Based on the findings in this research work, the phenomenological model is useful to guide the controller design. However, we only employ its damping characteristic. It is of interest to explore the coupling characteristics in the model. The merit is that if a simple FIV model is fully revealed and admissible for describing FIV behavior, controller design will be easily accessible by doing model simulation. Although this research work does not provide any modeling information for it is a model-independent control approach, an elementary guide for the modeling issue of the FIV scheme used in the experiment is provided in Appendix.

APPENDIX:

ELEMENTARY FIV MODELING GUIDE

With the increase of perception in controller design, it has become more and more necessary to find out a mathematical model to develop high efficient control scheme. As mentioned in many literatures, a van-der-pol oscillator model can be introduced to describe the flow force behavior of FIV. In the project, the control input is driven by embedded actuators, and detailed analysis needs to be accounted on its mathematical process. Here, some highlights are drawn to give an elementary modeling guide for FIV based on the phenomenological model. It is implemented step by step as follows¹. This modeling section is referred to the physical system as shown below.

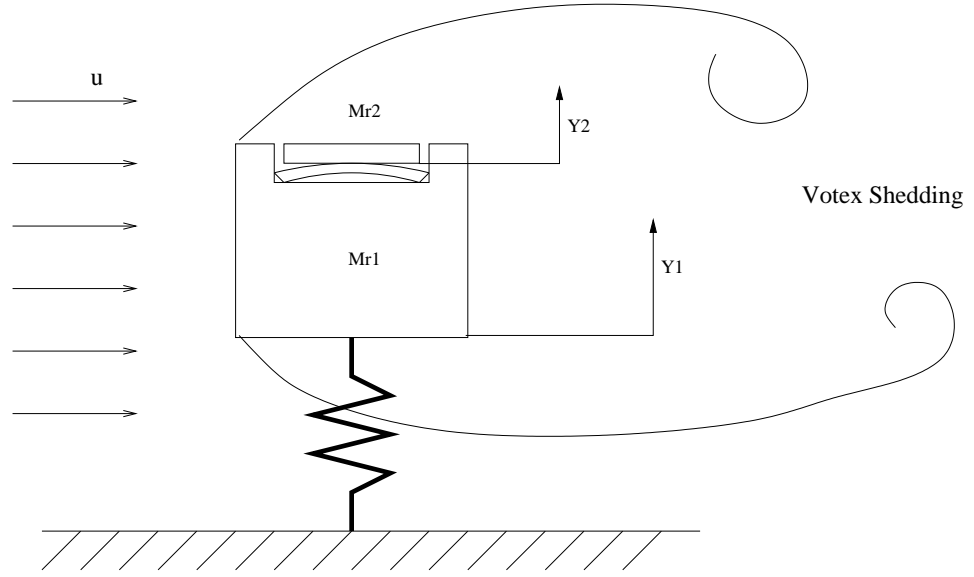
Fixed Cylinder In Cross-flow

wake-oscillator model:

$$\ddot{c}_y + \varepsilon\omega_s(c_y^2 - 1)\dot{c}_y + \omega_s^2 c_y = 0 \quad (\text{A1})$$

where ε is flow damping term, ω_s is the shedding frequency of fluid vortex, and c_y is fluid force exerted on the cylinder. Here, $(c_y^2 - 1)$ is used as the nonlinear damping term and any other option is also possible.

¹The title of each step is the experimental condition, under which the parameters of equations in that step are identified offline.



Cylinder Vibration With Control But No Flow

$$\ddot{Y}_1 + 2\zeta_{s1}\omega_{n1}\dot{Y}_1 + \omega_{n1}^2 Y_1 = -\frac{c_p}{2M_{r1}} \quad (A2)$$

$$\ddot{Y}_2 = \frac{c_p}{2M_{r2}}$$

where c_p is the force generated by the control unit, M_{r1} and M_{r2} are mass ratios

$$\frac{M}{\rho_f H^2 L}.$$

Cylinder Vibration When Flow Is Presented But No Control

$$\ddot{c}_y + \varepsilon\omega_s(c_y^2 - 1)\dot{c}_y + \omega_s^2 c_y = D_1 Y + D_2 \dot{Y} + D_3 \ddot{Y} \quad (A3)$$

$$\ddot{Y} + 2\zeta_s\omega_n\dot{Y} + \omega_n^2 Y = -\frac{c_y}{2M_r}$$

Cylinder Vibration With Both Flow and Control

$$\begin{aligned}
\ddot{c}_y + \varepsilon\omega_s(c_y^2 - 1)\dot{c}_y + \omega_s^2 c_y &= D_1 Y_1 + D_2 \dot{Y}_1 + D_3 \ddot{Y}_1 + f(Y_p, \dot{Y}_p, \ddot{Y}_p) \\
\ddot{Y}_1 + 2\zeta_{s1}\omega_{n1}\dot{Y}_1 + \omega_{n1}^2 Y_1 &= \frac{c_{y1} - c_p}{2M_{r1}} \\
\ddot{Y}_2 + \omega_p^2 Y_2 &= \frac{c_p - c_{y2}}{2M_{r2}} \\
c_y &= c_{y1} - c_{y2}
\end{aligned} \tag{A4}$$

where $f(Y_p, \dot{Y}_p, \ddot{Y}_p)$ is the force that is exerted by the slice onto the fluid, c_{y1} is the fluid force acting on the cylinder and c_{y2} is the fluid force acting on the slice.

Final Mathematical Model

The overall equations are

$$\begin{aligned}
\ddot{c}_y + \varepsilon\omega_s(c_y^2 - 1)\dot{c}_y + \omega_s^2 c_y &= D_1 Y_1 + D_2 \dot{Y}_1 + D_3 \ddot{Y}_1 + f(Y_p, \dot{Y}_p, \ddot{Y}_p) \\
(1 + \frac{M_{r2}}{M_{r1}})\ddot{Y}_1 + 2\zeta_{s1}\omega_{n1}\dot{Y}_1 + (\omega_{n1}^2 + \frac{M_{r2}\omega_p^2}{M_{r1}})Y_1 &= \frac{c_y - 2M_{r2}(\ddot{Y}_p + \omega_p^2 Y_p)}{2M_{r1}}
\end{aligned} \tag{A5}$$

Now we can transfer them into state-space expressions.

$$\dot{x}_1 = x_2$$

$$\begin{aligned}
\dot{x}_2 &= \left(\frac{D_3}{2(M_{r1} + M_{r2})} - \omega_s^2 \right) x_1 + \varepsilon\omega_s(1 - x_1^2)x_2 + \left(D_1 - \frac{D_3(\omega_{n1}^2 M_{r1} + \omega_p^2 M_{r2})}{M_{r1} + M_{r2}} \right) x_3 \\
&+ \left(D_2 - \frac{2\zeta_{s1}\omega_{n1}M_{r1}D_3}{M_{r1} + M_{r2}} \right) x_4 - \frac{\omega_p^2 M_{r2}D_3}{M_{r1} + M_{r2}} x_5 - \frac{M_{r2}D_3}{M_{r1} + M_{r2}} u + f(x_5, x_6, u)
\end{aligned}$$

$$\dot{x}_3 = x_4$$

$$\dot{x}_4 = \frac{1}{2(M_{r1} + M_{r2})} x_1 - \frac{\omega_{n1}^2 M_{r1} + \omega_p^2 M_{r2}}{M_{r1} + M_{r2}} x_3 - \frac{2\zeta_{s1}\omega_{n1}M_{r1}}{M_{r1} + M_{r2}} x_4 - \frac{\omega_p^2 M_{r2}}{M_{r1} + M_{r2}} x_5 - \frac{M_{r2}}{M_{r1} + M_{r2}} u$$

$$\dot{x}_5 = x_6$$

$$\dot{x}_6 = u$$

$$\tag{A6}$$

where $x_1 = c_y$, $x_2 = \dot{c}_y$, $x_3 = Y_1$, $x_4 = \dot{Y}_1$, $x_5 = Y_p$, and $x_6 = \dot{Y}_p$.

Bibliography

- Agrachev, A. and Sarychev, A. (2003). Controllability by low modes forcing of the navier-stokes equation with periodic data. *Proceedings of the 42nd Conference on Decision and Control*, pages 2734–2739.
- Åström, K. J. and Haggglund, T. (1984). Automatic tuning of simple regulators with specifications on phase and amplitude margins. *Automatica*, 20(5):645–651.
- Bands, H. T. and Ito, K. (1994). Structural actuator control of fluid/structure interactions. *Proceedings of the 33rd Conference on Decision and Control*, pages 283–288.
- Bearman, P. W. (1984). Vortex shedding from oscillating bluff bodies. *Annual Reviews of Fluid Mechanics*, 16:195–222.
- Benaskeur, A. R. and Desbiens, A. (2002). Backstepping-based adaptive pid control. *Instruments and Electronics Engineering Proceedings of Control Theory Applications*, 149:54–59.
- Berger, E. (1967). Suppression of vortex shedding and turbulence behind oscillating cylinders. *Physics of Fluids*, 10:191–193.
- Bishop, R. E. D. and Hassan, A. Y. (1964). The lift and drag forces on a circular cylinder oscillating in flowing fluid. *Proceedings of the Royal Society of London*, A277:51–75.
- Blevins, R. D. (1990). *Flow-Induced Vibrations*. Van Nostrand Reinhold, New York, 2nd edition.

- Chang, M. H. and Davison, E. J. (2003). Control of lti systems subject to unanticipated extreme perturbations using self-tuning 3-term switching controllers. *IEEE Transactions on Automatic Control*, 48(11):1975–1985.
- Chang, W. D., Hwang, R. C., and Hsieh, J. G. (2002). A self-tuning pid control for a class of nonlinear systems based on the lyapunov approach. *Journal of Process Control*, 12:233–242.
- Cheng, L., Zhou, Y., and Zhang, M. M. (2003). Perturbed interaction between vortex shedding and induced vibration. *Journal of Fluids and Structures*, 17(7):887–901.
- Christofides, P. D. and Armaou, A. (1998). Nonlinear control of navier-stokes equations. *Proceedings of the American Control Conference*, pages 1355–1359.
- Costa, O. L. V., do Val, J. B. R., and Geromel, J. C. (1999). Continuous-time state-feedback h_2 -control of markovian jump linear systems via contex analysis. *Automatica*, 35:259–268.
- Emelyanov, S. V. and Korovin, S. K. (2000). *Control of Complex and Uncertain Systems*. Springer.
- Facchinetti, M. L., de Langre, E., and Biolley, F. (2004). Coupling of structure and wake oscillators in vortex-induced vibrations. *Journal of Fluids and Structures*, 19:123–140.
- Feuer, A. and Morse, A. S. (1978). Adaptive control of single-input, single-output linear systems. *IEEE Transactions on Automatic Control*, 23:557–569.
- Fujisawa, N., Kawaji, Y., and Ikemoto, K. (2001). Feedback control of vortex shedding from a circular cylinder by rotational oscillations. *Journal of Fluids and Structures*, 15:23–37.

- Guldner, J. and Utkin, V. I. (2000). The chattering problem in sliding mode systems. *Proceedings of the 14th International Symposium of MTNS, Perpignan.*
- Hartlen, R. T. and Currie, I. G. (1970). Lift-oscillator model of vortex-induced vibration. *ASCE Journal of Engineering Mechanics*, 96:577–591.
- Ho, W. K., Hong, Y., Hansson, A., Hjalmarsson, H., and Deng, J. W. (2003). Relay auto-tuning of pid controllers using iterative feedback tuning. *Automatica*, 39. Brief Paper.
- Hsiao, F. B., Liu, C. F., and Shyu, J. Y. (1990). Control of wall-separated flow by internal acoustic excitation. *AIAA Journal*, 28(8):1440–1446.
- Iwan, W. D. and Blevins, R. D. (1974). A model for vortex-induced oscillation of structures. *Journal of Applied Mechanics*, 41:581–586.
- Kawamura, Y., Nakano, M., and Yamamoto, H. (2004). Model-free recursive lq controller design (learning lq control). *Int. Journal of Adaptive Control and Signal Processing*, 18:551–570.
- Khalil, H. K. (1996). Adaptive output feedback control of nonlinear systems represented by input-output models. *IEEE Transactions on Automatic Control*, 41(2).
- Kim, K.-S. and Kim, Y. (2003). Robust backstepping control for slew maneuver using nonlinear tracking function. *IEEE Transactions on Control Systems Technology*, 11(6).
- Kokotović, P. V., Khalil, H. K., and O’Reilly, J. (1986). *Singular Perturbation Methods in Control Analysis and Design*. London, U.K. Academic.
- Krenk, S. and Nielsen, S. R. K. (1999). Energy balanced double oscillator model

- for vortex-induced vibration. *ASCE Journal of Engineering Mechanics*, pages 263–271.
- Krstić, M., Kanellakopoulos, I., and Kokotović, P. (1995). *Nonlinear and Adaptive Control Design*. Wiley-Interscience.
- Lin, F., Wai, R., Chou, W., and Hsu, S. (2002). Adaptive backstepping control using recurrent neural network for linear induction motor drive. *IEEE Transaction on Industrial Electronics*, 49:134–146.
- Liu, W. P. and Brodie, G. H. (2000). A demonstration of mems-based active turbulence transitioning. *International Journal of Heat and Fluid Flow*, 21:297–303.
- Maeda, Y. and Figueiredo, R. J. P. D. (1997). Learning rules for neuro-controller via simultaneous perturbation. *IEEE Transactions on Neural Networks*, 8(5):1119–1130.
- Maeda, Y. and Yoshida, T. (1999). An active noise control without estimation of secondary path. *Proceedings of ACTIVE 99*, pages 985–994.
- Milliken, P., Marsh, C., and Brunt, B. V. (1999). Minimax controller design for a class of uncertain linear systems. *Automatica*, 35:583–590.
- Min, C. H. and Choi, H. C. (1999). Suboptimal feedback control of vortex shedding at low reynolds numbers. *Journal of Fluid Mechanics*, 401:123–156.
- Ogata, K. (1997). *Modern Control Engineering*. Prentice Hall.
- Park, K.-B. and Tsuji, T. (1999). Terminal sliding mode control of second-order nonlinear uncertain systems. *International Journal of Robust and Nonlinear Control*, 9:769–780.

- Park, M. K., Lee, M. C., and Go, S. J. (2001). The design of sliding mode controller with perturbation observer for a 6-dof parallel manipulator. *IEEE International Symposium on Industrial Electronics*.
- Peterka, J. A. and Richardson, P. D. (1969). Effects of sound on separated flows. *Journal of Fluid Mechanics*, 37(2):265–287.
- Petersen, I. R. (1987). A stabilization algorithm for a class of uncertain linear systems. *Systems and Control Letter*, 8:351–357.
- Raffel, M., Willert, C., and Kompenhans, J. (1998). *Particle Image Velocimetry: A Practical Guide*. Springer, Reading.
- Sarpkaya, T. (1979). Vortex-induced oscillations—a selective review. *Journal of Applied Mechanics, ASME Trans.*, 46:241–258.
- Skop, R. A. and Balasubramanian, S. (1997). A new twist on an old model for vortex-excited vibrations. *Journal of Fluids and Structures*, 11:395–412.
- Skop, R. A. and Griffin, O. M. (1973). An heuristic model for determining flow-induced vibrations of offshore structures. *5th Offshore Technology Conference, OTC paper.1843*.
- Slotine, J.-J. E. and Li, W. P. (1991). *Applied Nonlinear Control*. Prentice Hall.
- Spall, J. C. (1992). Multivariate stochastic approximation using a simultaneous perturbation gradient approximation. *IEEE Transactions on Automatic Control*, 37(3):332–341.
- Stotsky, A., Hedrick, J., and Yip, P. (1997). The use of sliding modes to simplify the backstepping control method. *Proceedings of the American Control Conference*.

- Tan, K. K., Huang, S., and Ferdous, R. (2002). Robust self-tuning pid controller for nonlinear systems. *Journal of Process Control*, 12:753–761.
- Utkin, V. I. (1992). *Sliding Modes in Control Optimization*. Springer-Verlag.
- Wai, R., Lin, F., Duan, R., Hsieh, K., and Lee, J. (2002). Robust fuzzy neural network control for linear ceramic motor drive via backstepping design technique. *IEEE Transactions on Fuzzy Systems*, 10:102–112.
- Warui, H. M. and Fujisawa, N. (1996). Feedback control of vortex shedding from a circular cylinder by cross-flow cylinder oscillations. *Experiments in Fluids*, 21:49–56.
- Williamson, C. H. K. and Govardhan, R. (2004). Vortex-induced vibrations. *Annual Reviews of Fluid Mechanics*, 36:413–455.
- Wu, W. and Chou, Y. S. (1999). Adaptive feedforward and feedback control of non-linear time-varying uncertain systems. *International Journal of Control*.
- Wu, W., Yuan, J., and Cheng, L. (2005). Self-tuning sub-optimal control for time-invariant systems with bounded disturbance. *Proceedings of the American Control Conference*.
- Yeh, T. J. and Youcef-Toumi, K. (1995). Adaptive control of nonlinear, uncertain systems using local function estimation. *Proceedings of the American Control Conference*.
- Zhang, M. M., Cheng, L., and Zhou, Y. (2003). Closed-loop control of fluid-structure interactions on a flexibly supported cylinder. *European Journal of Mechanics*, 23(1):189–197.

Zhang, M. M., Cheng, L., and Zhou, Y. (2004). Closed-loop-controlled vortex shedding and vibration of a flexibly supported square cylinder under different schemes. *Physics of Fluids*, 16:1439–1448.